# NEW SKYRME NUCLEON-NUCLEON INTERACTION FOR THE MEAN-FIELD APPROXIMATION

A Dissertation

by

AU KIM VUONG

Submitted to the Office of Graduate Studies of
Texas A&M University
in partial fulfillment of the requirements for the degree of

DOCTOR OF PHILOSOPHY

May 2007

Major Subject: Physics

# NEW SKYRME NUCLEON-NUCLEON INTERACTION FOR THE MEAN-FIELD APPROXIMATION

A Dissertation

by

AU KIM VUONG

Submitted to the Office of Graduate Studies of
Texas A&M University
in partial fulfillment of the requirements for the degree of

DOCTOR OF PHILOSOPHY

Approved by:

| | |
|---|---|
| Chair of Committee, | Shalom Shlomo |
| Committee Members, | Rand Watson |
| | Ronald Bryan |
| | Dave Youngblood |
| Head of Department, | Edward S. Fry |

May 2007

Major Subject: Physics

# ABSTRACT

New Skyrme Nucleon-Nucleon Interaction
for the Mean-Field Approximation. (May 2007)
Au Kim Vuong, B.S., Hue University, Viet Nam
Chair of Advisory Committee: Dr. Shalom Shlomo

The effective Skyrme type interactions have been used in the mean-field models for several decades, and many different parameterizations of the interaction have been realized to better reproduce nuclear masses, radii, and various other data. Today, there are more experimental data of nuclei far from the $\beta$ stability line. It is time to improve the prediction power of the Skyrme type effective nucleon-nucleon interactions. In this dissertation, we present the procedure of the fitting of the mean-field results to an extensive set of experimental data with some constraints on the Skyrme parameters and some approximations in the Hartree-Fock mean-field to obtain the parameters of the new Skyrme type effective interactions, namely, KDE and KDE0. We investigate the long-standing discrepancy of more than 20% between the values of the incompressibility coefficient $K_{\rm n.m.}$ obtained within relativistic and non-relativistic models. We show that this difference is basically due to the differences in values of the symmetry energy coefficient $J$ and its slope $L$ associated with the relativistic and non-relativistic models. We also present the results of fully self-consistent Hartree-Fock based Random Phase Approximation calculations for the centroid energies of the breathing modes in four nuclei, namely, $^{90}$Zr, $^{116}$Sn, $^{144}$Sm, $^{208}$Pb, obtained with our new Skyrme interaction KDE0. A good agreement with the experimental data is achieved.

To my parents, my sisters, my brothers, my nephews, my niece, and my love.

# ACKNOWLEDGMENTS

I would like to thank my research advisor, Dr. Shalom Shlomo, for his guidance, enthusiasm and endless encouragement over the past years. I was very lucky to meet him in the research center RIKEN, Wako, Japan. He is the person who led me to get a United States' education and guided me during the critical point of my academic career.

Dr. Nguyen Dinh Dang was the first person who introduced me to nuclear physics. He had faith in me by taking me to RIKEN, Japan, for over one year to carry out research in nuclear physics. I want to extend my gratitude to him for his mentoring and his enthusiasm. He not only taught me some physics but also showed me the real world. He is the person who changed my life.

During my years at Texas A&M University, I had the opportunity to work with Dr. Bijay K. Agrawal and Dr. Tapas Sil. They helped me alot in my research.

I also express my gratitude to my committee members: Professor Rand Watson, Professor Dave Youngblood, and Professor Ronald Bryan. I also would like to thank Professor Sherry Yennello for attending my final exam.

TABLE OF CONTENTS

# LIST OF TABLES

TABLE Page

TABLE Page

# LIST OF FIGURES

FIGURE Page

# CHAPTER I

## INTRODUCTION

In nuclear physics, the knowledge of the nucleon-nucleon interaction inside the nucleus is very important for describing the nuclear structure properties. Our understanding of the nucleon-nucleon potential is still not clear. Basically, the effective nucleon-nucleon potential can be identified using two approaches. The first one is that the nucleon-nucleon interaction in nuclear matter is constructed from free nucleon-nucleon interaction [15, 16, 17]. The second approach which is called the phenomenological model begins with a parametrized effective interaction. The effective nucleon-nucleon interactions in case of relativistic mean-field models are generated through the exchange of mesons. The parameters of the Lagrangian which represent a system of interacting nucleons are obtained by fitting procedure to some bulk properties of a set of spherical nuclei [18]. In the non-relativistic approach, the parameters of the effective nucleon-nucleon interaction are obtained by fitting the Hartree-Fock mean-field results to the experimental data. In this dissertation, we concentrate on the non-relativistic models to study nuclear properties.

Since the first work of Vautherin and Brink [19], who performed fully microscopic self-consistent mean-field Hartree-Fock calculations with the Skyrme type effective nucleon-nucleon interaction [20, 21, 22], many different parameterizations of the Skyrme interaction have been realized to better reproduce data on nuclear masses, radii and other physical quantities. The reason why the effective Skyrme interaction is popular is due to its simple expression in term of the $\delta(\mathbf{r}_1 - \mathbf{r}_2)$ interaction, which makes the calculations in the Hartree-Fock mean-field much simpler. Most of the

---

The journal model is Physical Review C.

parameter sets of the Skyrme interaction available in the literature are obtained by fitting Hartree-Fock results to experimental data on the ground state properties, such as charge radii and binding energies of a few closed shell nuclei. We point out that the values obtained for some of the parameters of the Skyrme interaction depend on the selected set of nuclear data used in the fit. In 1972, Vautherin and Brink produced two sets of parameters SI and SII [19] by fitting the ground state properties, such as binding energies and radii, to experimental data for two spherical nuclei $^{16}$O and $^{208}$Pb. In 1975, Beiner et al. generated SIII, SIV, SV, and SVI parameter sets [23], using more experimental data, the binding energies and charge radii for $^{40}$Ca, $^{48}$Ca, $^{56}$Ni, $^{90}$Zr and $^{140}$Ce. The SIII interaction, with its density dependence ($\alpha = 1$), is associated with a very high value of the incompressibility coefficient ($K_{\text{n.m.}} = 356$ MeV). At this time, experimental information about isoscalar giant monopole resonance (ISGMR) was not available. The first experimental measurement of the ISGMR on $^{208}$Pb [24, 25] provided information on the nuclear matter incompressibility coefficient $K_{\text{n.m.}}$. The SkM interaction [26], with $\alpha \leq 1/3$, was obtained by including this new experimental data on the monopole energy in the fit. The SkM* [27] which is a modified interaction of the SkM interaction was generated by also studying the fission barriers [28] of $^{240}$Pu. The self-consistent Hartree-Fock and Random Phase Approximation formalism describe very well the ground state of nuclei and also the giant resonances states. The incompressibility coefficient $K_{\text{n.m.}}$ which is one of the important nuclear matter properties is extracted from the centroid energy of the ISGMR. With different Skyrme interactions, we have a wide range of values for the incompressibility coefficient $K_{\text{n.m.}}$. In 1981, Nguyen Van Giai and Sagawa produced two Skyrme interactions, namely, SGI and SGII [8], by including additional constraints on the Landau parameters $G_0$ and $G'_0$. These interactions reproduced quite well the values of the incompressibility coefficient $K_{\text{n.m.}}$ and of $G'_O$ ($K_{\text{n.m.}} = 215$ MeV and

$G'_0 = 0.503$ for SGII). However, the term $t_3\rho^\alpha\delta(\mathbf{r}-\mathbf{r}')$, leading to the particle-hole interaction, is not fully anti-symmetric. In 1984, the Skyrme interactions E, Es, Z, Zs [29] were introduced. These interactions yield values of $K_{\text{n.m.}}$ which are quite high.

More recently, many sets of the Skyrme parameters have been generated, such as, SkI1-5 [30], SLy4-7,10 [2, 31], SKX [32] and SkO [33], to reproduce the nuclear matter properties, properties of nuclei at the $\beta$-line and of nuclei near the proton/neutron drip line. For the SKX interaction, the exchange term of the Coulomb energy is neglected, and the direct term is determined by replacing the point-proton distribution by the charge distribution. This interaction reproduces well the values for the Coulomb displacement energy (CDE), which is the binding energy differences between mirror nuclei. A systematic investigation of Skyrme parameterizations by Stone et al [34] showed that only 27 out of 87 different sets of Skyrme parameters are appropriate for the study of the properties of neutron stars. The symmetry energy coefficient $J$ (at $\rho = \rho_0$) is very important in the study of properties of neutron star. The SKX interaction is not suitable for the study of neutron stars. The reason is that the quantity $P = 3\rho\frac{dS}{d\rho}$, which is directly related to the slope of the symmetry energy coefficient $S$, is negative for nuclear matter densities $\rho$ below $3\rho_0$ ($\rho_0 = 0.16$ fm$^{-3}$). The SkI1-6, SLy1-10 and SkO Skyrme interactions are suitable for the study of the properties of neutron stars [34]. However, these sets of Skyrme parameters give very low values for the CDE because the Coulomb exchange term was included. The family of Skyrme interactions Skz0-4 [35] were obtained with stability requirements for the equation of state.

Although the Skyrme type effective nucleon-nucleon interactions have been introduced by parameterizing the interaction as a whole, it is not fully fundamental. However, the Hartree-Fock mean-field calculations with using Skyrme interaction have been very successful in studying the ground state properties of nuclei. Today there

are more experimental data available for nuclei at and far from $\beta$-line. Therefore, it is desirable to generate a new Skyrme type interaction which includes the merits of many sets of existing Skyrme parameters, as we discussed earlier. In our HF mean-field formalism, there are approximations for the Coulomb interaction and the center of mass corrections not only to the binding energy and but also to charge radii. The details of these approximations will be given in Chapter II. We also include the constraints on the Skyrme parameters by using the stability conditions of the Landau parameters for symmetric nuclear matter and pure neutron matter. In Landau theory for the Fermi liquid model, the particle-hole interaction is characterized by the Landau parameters. The Landau parameters, which are written in terms of the Skyrme parameters [35, 36], have to satisfy the stability conditions. We also use an extensive set of experimental data for the fitting. For the first time the experimental data include the breathing mode energies of the isoscalar giant monopole resonances, the spin orbit splittings, and the root mean square radii for the valence neutron. The details of selection of the available experimental data will be given in Chapter II.

The procedure of fitting the HF mean-field results to the a set of experimental data is very important for the quality of the Skyrme parameters. We introduce for the first time the simulated annealing method (SAM), which is a generalization of a Monte Carlo simulation based on the Metropolis algorithm [37], initially developed for studying the equation of state (EOS). The SAM is a popular method for the optimization problems of large scale, especially for searching the global extrema hidden among many local extrema. It has been used in many different area of science. The SAM is very close to the the thermodynamics processes. In this process, the liquid is initially at high temperature and the molecules inside the liquid move freely. If the temperature decreases slowly, the thermal motion of molecules is lost and they form an ideal crystal. In other word, the liquid reaches the state of minimum energy. We

use the SAM to obtain the parameters of the Skyrme type effective nucleon-nucleon interaction by searching the global minimum in the hyper-surface of the $\chi^2$ function. The detail of the $\chi^2$ function will be discussed in Chapter III.

It is well known that the HF mean-field model describes well the ground-state properties of nuclei. The existence of collective motion is a common feature of quantum many-body system. Studies of collective modes in nuclei improve our knowledge on the nuclear matter properties, excited states, and nuclear forces. The giant resonance states are the elementary vibrational collective modes which are described as the resonance peaks in the transition strength distribution of a weak external field that excites the nucleus. The giant resonance states are classified by the the amount of total angular momentum $J$, spin $\Delta S$, and isospin $\Delta T$ transferred to the nuclear ground state as a result of the excitation. In this dissertation, we study only the case of electric isoscalar resonance, where $\Delta S = 0$, and $\Delta T = 0$. One of the theoretical models providing a good microscopic description of nuclear collective giant resonance is the Random Phase Approximation (RPA). In the RPA, the excited states of nuclei are considered as a superposition of one particle - one hole excitations of a correlated ground state. All properties of the ground states of nuclei are well described by the self-consistent mean-field, therefore it is obvious to build a formulation of RPA on the single particle wave function basis of the HF model. The HF-RPA has been extensively studied for many years and has been a successful formalism for describing the properties of the ground state and the excitation states, especially the giant resonances. The study of collective modes gives important information on properties of the nuclear system. Among different collective modes, the isoscalar giant monopole resonance (ISGMR) and isoscalar giant dipole resonance (ISGDR) are very important in the study of the nuclear matter incompressibility coefficient $K_{\text{n.m.}}$. It is very desirable to know an accurate value of $K_{\text{n.m.}}$, which is mainly extracted from the centroid

energy of the ISGMR, in order to improve our knowledge of the nuclear matter equation of state (EOS) around the saturation point. There have been many experimental works carried out in order to determine an accurate value of the centroid energy $E_0$ of ISGMR. The recent very accurate experimental results [11, 12, 38] for $E_0$ allow us to pin down the value of the incompressibility coefficient $K_{\text{n.m.}}$. There are many theoretical approaches for determining the value of $K_{\text{n.m.}}$ in relativistic and non-relativistic models. In the relativistic models based RPA [39, 40], the value of $K_{\text{n.m.}}$ is in the range of $250 - 270$ MeV. The recent non-relativistic HF-RPA calculations using the Skyrme interaction [41, 42] gives the value of $K_{\text{n.m.}}$ about $210 - 220$ MeV. We analyze this discrepancy in the value of $K_{\text{n.m.}}$ between these models in Chapter IV and provide a simple explanation. We also carry out the fully self-consistent HF-RPA calculation, using our new set of Skyrme parameters, for the centroid energy of the ISGMR for $^{90}$Zr, $^{116}$Sn, $^{144}$Sm, and $^{208}$Pb, and compare our results to experimental data and to the values obtained using the NL3 and SGII interactions.

The structure of this dissertation is the following. In Chapter II we present the Hartree-Fock method with Skyrme interaction and describe some approximations in the mean-field and constraints that will be used in the next chapter. In Chapter III the simulated annealing method, which is used to obtain the new set of Skyrme parameters, is described. In Chapter IV the Random Phase Approximation is summarized briefly and the results of fully self-consistent of HF-RPA calculations of strength functions for four nuclei are presented. The conclusions are given in Chapter V.

# CHAPTER II

## HARTREE-FOCK WITH SKYRME INTERACTION

### A. Hartree-Fock formalism

The basic idea of the Hartree-Fock method is that the mutual interactions among nucleons leads to an average potential felt by each one of the nucleons. The nucleus is a many-body system of fermions so the wave function of the nucleus of any state must be antisymmetric under the interchange of the coordinates of any two nucleons. In the Hartree-Fock (HF) approximation the ground state wave function $\Phi$ of the nucleus with A nucleons is a Slater determinant built from the single-particle wave function $\phi_i(\mathbf{r}_i, \sigma_i, q_i)$, where $\mathbf{r}_i$, $\sigma_i$, $q_i$ are the spacial, spin, and isospin coordinates of the $i$-th nucleon, respectively. For a proton $q_i = \frac{1}{2}$ and for a neutron $q_i = -\frac{1}{2}$.

$$\Phi = \frac{1}{\sqrt{A!}} \begin{vmatrix} \phi_1(\mathbf{r}_1, \sigma_1, q_1) & \phi_2(\mathbf{r}_1, \sigma_1, q_1) & \dots & \phi_A(\mathbf{r}_1, \sigma_1 q_1) \\ \phi_1(\mathbf{r}_2, \sigma_2, q_2) & \phi_2(\mathbf{r}_2, \sigma_2, q_2) & \dots & \phi_A(\mathbf{r}_2, \sigma_2, q_2) \\ \vdots & \vdots & \vdots & \vdots \\ \phi_1(\mathbf{r}_A, \sigma_A, q_A) & \phi_2(\mathbf{r}_A, \sigma_A, q_A) & \dots & \phi_A(\mathbf{r}_A, \sigma_A, q_A) \end{vmatrix} \tag{2.1}$$

The ground state wave function $\Phi$ gives the lowest possible expectation value of the total Hamiltonian. The total Hamiltonian of the nucleus is:

$$H = T + V \tag{2.2}$$

where the kinetic energy operator

$$T = -\frac{\hbar^2}{2} \sum_{i=1}^{A} \frac{\overrightarrow{\nabla}_i^2}{m_{q_i}} \tag{2.3}$$

and the two-body interaction $V(\mathbf{r}_i, \mathbf{r}_j)$ is written in term of the effective nucleon-nucleon interaction $V_{ij}^{NN}$ and the Coulomb nucleon-nucleon interaction $V_{\text{Coulomb}}^{NN}$

$$V = \frac{1}{2}\sum_{i\neq j} V(\mathbf{r}_i, \mathbf{r}_j) = \frac{1}{2}\sum_{i\neq j}(V_{ij}^{NN} + V_{\text{Coulomb}}^{NN}), \tag{2.4}$$

where the Coulomb nucleon-nucleon interaction is written as

$$V_{\text{Coulomb}}^{NN} = \frac{e^2}{4}\sum_{i,j=1}^{A}\frac{q_{ij}^2 - q_{ij}}{|\mathbf{r}_i - \mathbf{r}_j|}, \qquad q_{ij} = q_i + q_j. \tag{2.5}$$

The total energy $E$ is obtained as the expectation of the total Hamiltonian with the total wave function $\Phi$

$$\begin{aligned} E &= \langle\Phi|H|\Phi\rangle \\ &= -\frac{\hbar^2}{2m}\sum_{i=1}^{A}\int \phi_{\alpha_i}^*(\mathbf{r})\triangle\phi_{\alpha_i}(\mathbf{r})d\mathbf{r} + \sum_{i<j}^{A}\int \phi_{\alpha_i}^*(\mathbf{r})\phi_{\alpha_j}^*(\mathbf{r}')V(\mathbf{r},\mathbf{r}')\phi_{\alpha_i}(\mathbf{r})\phi_{\alpha_j}(\mathbf{r}')d\mathbf{r}d\mathbf{r}' \\ &\quad -\sum_{i<j}^{A}\int \phi_{\alpha_i}^*(\mathbf{r})\phi_{\alpha_j}^*(\mathbf{r}')V(\mathbf{r},\mathbf{r}')\phi_{\alpha_i}(\mathbf{r}')\phi_{\alpha_j}(\mathbf{r})d\mathbf{r}d\mathbf{r}'. \end{aligned} \tag{2.6}$$

Now we apply the variation principle to derive the Hartree-Fock equations with the constraint that the number of nucleons is conserved.

$$\sum_{i=1}^{A}\int |\phi_i(\mathbf{r})|^2 d\mathbf{r} = \sum_{\sigma,q}\int \rho_{\sigma,q}(\mathbf{r})d\mathbf{r} = A. \tag{2.7}$$

We have

$$\delta[E - \sum_i \varepsilon_{\alpha_i}\int \phi_{\alpha_i}^*(\mathbf{r})\phi_{\alpha_i}(\mathbf{r})d\mathbf{r}] = 0, \tag{2.8}$$

where $\varepsilon_{\alpha_i}$ is the Lagrangian. We carry out the variation with respect to the single-particle function,

$$\delta = \frac{\partial}{\partial\phi_{\alpha_i}^*(\mathbf{r})}\delta(\phi_{\alpha_i}^*(\mathbf{r})). \tag{2.9}$$

We obtain the Hartree-Fock equations for the single-particle wave functions,

$$-\frac{\hbar^2}{2m}\triangle\phi_{\alpha_i}(\mathbf{r}) + \sum_{j}^{A}\int \phi_{\alpha_j}^*(\mathbf{r}')V(\mathbf{r},\mathbf{r}')\phi_{\alpha_i}(\mathbf{r})\phi_{\alpha_j}(\mathbf{r}')d\mathbf{r}'$$

$$- \sum_{j}^{A} \int \phi^*_{\alpha_j}(\mathbf{r}')V(\mathbf{r},\mathbf{r}')\phi_{\alpha_i}(\mathbf{r}')\phi_{\alpha_j}(\mathbf{r})d\mathbf{r}' = \varepsilon_{\alpha_i}\phi_{\alpha_i}(\mathbf{r}). \tag{2.10}$$

The Lagrangian turn out to be the single-particle energies. The above Hartree-Fock equations (2.10) can be rewritten in the form,

$$-\frac{\hbar^2}{2m}\triangle\phi_{\alpha_i}(\mathbf{r}) + U_H(\mathbf{r})\phi_i(\mathbf{r}) - \int U_F(\mathbf{r},\mathbf{r}')\phi_i(\mathbf{r}')d\mathbf{r}' = \varepsilon_i\phi_i(\mathbf{r}), \tag{2.11}$$

with the direct potential affecting the nucleon motion in the nucleus, $U_H(\mathbf{r})$,

$$U_H(\mathbf{r}) = \sum_{i\in F}\int \phi^*_i(\mathbf{r}')V(\mathbf{r},\mathbf{r}')\phi_i(\mathbf{r}')d\mathbf{r}', \tag{2.12}$$

and the exchange potential $U_F(\mathbf{r},\mathbf{r}')$,

$$U_F(\mathbf{r},\mathbf{r}') = \sum_{i\in F}\phi^*_i(\mathbf{r}')V(\mathbf{r},\mathbf{r}')\phi_i(\mathbf{r}). \tag{2.13}$$

The iterative Hartree-Fock method is that for a given effective potential $V(\mathbf{r},\mathbf{r}')$, we start from an initial guess for the single-particle wave functions $\phi_i(\mathbf{r})$, we calculate $U_H(\mathbf{r})$, $U_F(\mathbf{r},\mathbf{r}')$ and solve the Hartree-Fock equations to get the new values of the single-particle wave functions and the single particle energies. One can proceed in this way until reaching convergence with a given certain accuracy. At the end, we obtain the single-particle wave functions $\phi_i(\mathbf{r})$, the single-particle energies $\varepsilon_i$, and the minimal value of the total energy. In the next section we will derive the Hartree-Fock equations for the Skyrme type effective nucleon-nucleon interaction.

## B. Hartree-Fock with Skyrme interaction

In this thesis we adopt the following standard form for the Skyrme type effective $NN$ interaction [19, 31]:

$$V^{NN}_{ij} = t_0\left(1 + x_0P^{\sigma}_{ij}\right)\delta(\mathbf{r}_i - \mathbf{r}_j)$$

$$
\begin{aligned}
&+\frac{1}{2}t_1\left(1+x_1P_{ij}^{\sigma}\right)\times\left[\overleftarrow{k}_{ij}^{2}\delta(\mathbf{r}_i-\mathbf{r}_j)+\delta(\mathbf{r}_i-\mathbf{r}_j)\overrightarrow{k}_{ij}^{2}\right]\\
&+t_2\left(1+x_2P_{ij}^{\sigma}\right)\overleftarrow{k}_{ij}\delta(\mathbf{r}_i-\mathbf{r}_j)\overrightarrow{k}_{ij}\\
&+\frac{1}{6}t_3\left(1+x_3P_{ij}^{\sigma}\right)\rho^{\alpha}\left(\frac{\mathbf{r}_i+\mathbf{r}_j}{2}\right)\delta(\mathbf{r}_i-\mathbf{r}_j)\\
&+iW_0\overleftarrow{k}_{ij}\delta(\mathbf{r}_i-\mathbf{r}_j)(\overrightarrow{\sigma_1}+\overrightarrow{\sigma_2})\times\overrightarrow{k}_{ij},
\end{aligned}
\tag{2.14}
$$

where $t_i$, $x_i$, $\alpha$ and $W_0$ are the parameters of the Skyrme interaction; $P_{ij}^{\sigma}=\frac{1}{2}\left(1+\vec{\sigma}_i\vec{\sigma}_j\right)$ is the spin exchange operator; $\vec{\sigma}_i$ is the Pauli spin operator; $\overrightarrow{k}_{ij}=-i(\overrightarrow{\nabla}_i-\overrightarrow{\nabla}_j)/2$ and $\overleftarrow{k}_{ij}=i(\overleftarrow{\nabla}_i-\overleftarrow{\nabla}_j)/2$ are the momentum operators acting on the right and on the left, respectively. The parameters of the Skyrme interaction are obtained by fitting the Hartree-Fock results to the experimental data. In Table I, we give some of the existing sets of the Skyrme parameters. The total energy $E$ of the nucleus is given by

$$
\begin{aligned}
E &= \langle\Phi|H|\Phi\rangle=\langle\Phi|T+\frac{1}{2}\sum_{ij}(V_{ij}^{NN}+V_{\text{Coulomb}}^{NN})|\Phi\rangle\\
&= \int\left[\mathcal{K}(r)+\mathcal{H}_{\text{Skyrme}}(r)+\mathcal{H}_{\text{Coulomb}}(r)\right]d\mathbf{r}=\int\mathcal{H}(r)d\mathbf{r}.
\end{aligned}
\tag{2.15}
$$

The kinetic energy density is

$$
\mathcal{K}(r)=\frac{\hbar^2}{2m_p}\tau_p(r)+\frac{\hbar^2}{2m_n}\tau_n(r). \tag{2.16}
$$

The expression for the local energy density $\mathcal{H}_{\text{Skyrme}}$ is derived in details in Appendix A and [19].

$$
\mathcal{H}_{\text{Skyrme}}=\mathcal{H}_0+\mathcal{H}_3+\mathcal{H}_{\text{eff}}+\mathcal{H}_{\text{fin}}+\mathcal{H}_{\text{so}}+\mathcal{H}_{\text{sg}}, \tag{2.17}
$$

where $\mathcal{H}_0$ is the zero-range term, $\mathcal{H}_3$ the density-dependent term, $\mathcal{H}_{\text{eff}}$ an effective-mass term, $\mathcal{H}_{\text{fin}}$ a finite-range term, $\mathcal{H}_{\text{so}}$ a spin-orbit term, and $\mathcal{H}_{\text{sg}}$ is a term that is due to tensor coupling with spin and gradient. For the Skyrme interaction of Eq.

(2.14), we have,

$$\mathcal{H}_0 = \frac{1}{4}t_0\left[(2+x_0)\rho^2 - (2x_0+1)(\rho_p^2+\rho_n^2)\right], \tag{2.18}$$

$$\mathcal{H}_3 = \frac{1}{24}t_3\rho^\alpha\left[(2+x_3)\rho^2 - (2x_3+1)(\rho_p^2+\rho_n^2)\right], \tag{2.19}$$

$$\mathcal{H}_{\text{eff}} = \frac{1}{8}\left[t_1(2+x_1)+t_2(2+x_2)\right]\tau\rho + \frac{1}{8}\left[t_2(2x_2+1)-t_1(2x_1+1)\right](\tau_p\rho_p+\tau_n\rho_n), \tag{2.20}$$

$$\begin{aligned}\mathcal{H}_{\text{fin}} &= \frac{1}{32}\left[3t_1(2+x_1)-t_2(2+x_2)\right](\nabla\rho)^2 \\ &\quad -\frac{1}{32}\left[3t_1(2x_1+1)+t_2(2x_2+1)\right]\left[(\overrightarrow{\nabla}\rho_p)^2+(\overrightarrow{\nabla}\rho_n)^2\right], \qquad (2.21)\\ \mathcal{H}_{\text{so}} &= \frac{W_0}{2}\left[\mathbf{J}\cdot\nabla\rho+\mathbf{J}_p\cdot\nabla\rho_p+\mathbf{J}_n\cdot\nabla\rho_n\right], \qquad (2.22)\\ \mathcal{H}_{\text{sg}} &= -\frac{1}{16}(t_1x_1+t_2x_2)\mathbf{J}^2+\frac{1}{16}(t_1-t_2)\left[\mathbf{J}_p^2+\mathbf{J}_n^2\right]. \qquad (2.23)\end{aligned}$$

where the nucleon $\rho_q(\mathbf{r})$, the kinetic energy $\tau_q(\mathbf{r})$, and the current $\mathbf{J}_q(\mathbf{r})$ densities are obtained from the single-particle wave function $\phi_i(\mathbf{r}_i,\sigma_i,q_i)$;

$$\rho_q(\mathbf{r}) = \sum_{i\sigma}\phi_i^*(\mathbf{r},\sigma,q)\phi_i(\mathbf{r},\sigma,q), \qquad \rho(\mathbf{r}) = \sum_q\rho_q(\mathbf{r}), \tag{2.24}$$

$$\tau_q(\mathbf{r}) = \sum_{i\sigma}\overrightarrow{\nabla}\phi_i^*(\mathbf{r},\sigma,q)\overrightarrow{\nabla}\phi_i(\mathbf{r},\sigma,q), \qquad \tau(\mathbf{r}) = \sum_q\tau_q(\mathbf{r}), \tag{2.25}$$

$$\mathbf{J}_q(\mathbf{r}) = -i\sum_{i\sigma\sigma'}\phi_i^*(\mathbf{r},\sigma,q)\left[\overrightarrow{\nabla}\phi_i(\mathbf{r},\sigma',q)\times\langle\sigma|\vec{\sigma}|\sigma'\rangle\right], \qquad \mathbf{J}(\mathbf{r}) = \sum_q\mathbf{J}_q(\mathbf{r}). \tag{2.26}$$

The total energy density $\mathcal{H}(r)$ is

$$\mathcal{H}(r) = \frac{\hbar^2}{2m_p}\tau_p(r) + \frac{\hbar^2}{2m_n}\tau_n(r) + \mathcal{H}_{\text{Skyrme}}(r) + \mathcal{H}_{\text{Coulomb}}(r). \tag{2.27}$$

The symmetric infinite nuclear matter is considered as a Fermi gas in a volume $V$ large enough so that the surface effects can be neglected, and the ground state wave function is a Slater determinant built from plane wave states with the momentum $\vec{k}$, which has a range from 0 to the Fermi momentum $\vec{k}_f$. We have $Z = N$, no Coulomb field, $\rho_p(r) = \rho_n(r) = \frac{1}{2}\rho(r)$, $\tau_p(r) = \tau_n(r) = \frac{1}{2}\tau(r)$, spin current densities vanish, and

TABLE I. Some of the existing sets of the Skyrme parameters.

| Parameter | SI | SII | SkM | SGII |
|---|---|---|---|---|
| $t_0$(MeV·fm$^3$) | -1057.3000 | -1169.9000 | -2645.0000 | -2645.0000 |
| $t_1$ (MeV·fm$^5$) | 235.9000 | 585.6000 | 385.0000 | 340.0000 |
| $t_2$ (MeV·fm$^5$) | -100.0000 | -27.1000 | -120.0000 | -41.9000 |
| $t_3$(MeV·fm$^{3(1+\alpha)}$) | 14463.5000 | 9331.1000 | 15595.0000 | 15595.000 |
| $x_0$ | 0.5600 | 0.3400 | 0.0900 | 0.0900 |
| $x_1$ | | | | -0.0588 |
| $x_2$ | | | | 1.4250 |
| $x_3$ | | | 0 | 0.06044 |
| $W_0$ (MeV·fm$^5$) | 120.0000 | 105.0000 | 130.00 | 105.0000 |
| $\alpha$ | 1.0 | 1.0 | 0.16667 | 0.16667 |

with assumption $m_p = m_n = m$. The total energy density becomes

$$\mathcal{H}(r) = \frac{\hbar^2}{2m}\tau(r) + \frac{3}{8}t_0\rho^2 + \frac{1}{16}t_3\rho^{\alpha+2} + \frac{1}{16}\rho\tau\Theta, \tag{2.28}$$

with

$$\tau(r) = \frac{3}{5}k_f^2\rho, \quad \rho(r) = \frac{2}{3\pi^2}k_f^3, \quad \Theta = 3t_1 + t_2(5 + 4x_2). \tag{2.29}$$

So the total binding energy per nucleon in nuclear matter is

$$\frac{E}{A} = \frac{\mathcal{H}(r)}{\rho} = \frac{3\hbar^2}{10m}\left(\frac{3\pi^2}{2}\right)^{2/3}\rho^{2/3} + \frac{3}{8}t_0\rho + \frac{1}{16}t_3\rho^{\alpha+1} + \frac{3}{80}\left(\frac{3\pi^2}{2}\right)^{2/3}\Theta\rho^{5/3}. \tag{2.30}$$

The saturation point of the symmetric infinite nuclear matter is very important for the construction of the Skyrme type effective interaction. The saturation density $\rho_0$ is obtained from the saturation condition

$$\rho_0^2\left(\frac{dE/A}{d\rho}\right)_{\rho=\rho_0} = 0, \tag{2.31}$$

or

$$\frac{\hbar^2}{5m}\left(\frac{3\pi^2}{2}\right)^{2/3}\rho_0^{5/3} + \frac{3}{8}t_0\rho_0^2 + \frac{\alpha+1}{16}t_3\rho_0^{\alpha+2} + \frac{1}{16}\left(\frac{3\pi^2}{2}\right)^{2/3}\Theta\rho_0^{8/3} = 0. \tag{2.32}$$

The experimental value of the saturation density is $\rho_0 = 0.16 \pm 0.005$ fm$^{-3}$. From this value we can determine the value of the Fermi momentum $k_f$ using (2.29). The incompressibility coefficient $K_{\text{n.m.}}$ of nuclear matter is defined as,

$$K_{\text{n.m.}} = k_f^2\frac{\partial^2\left(\frac{E}{A}\right)_{\rho_0}}{\partial k_f^2} = 9\rho_0^2\left(\frac{\partial^2\frac{E}{A}}{\partial\rho^2}\right)_{\rho_0}. \tag{2.33}$$

In term of the Skyrme parameters

$$K_{\text{n.m.}} = -\frac{3\hbar^2}{5m}\left(\frac{3\pi^2}{2}\right)^{2/3}\rho_0^{2/3} + \frac{9\alpha(\alpha+1)}{16}t_3\rho_0^{\alpha+1} + \frac{3}{8}\left(\frac{3\pi^2}{2}\right)^{2/3}\Theta\rho_0^{5/3}. \tag{2.34}$$

The experimental results of the giant breathing mode in nuclei allow us to estimate

the value of the compressibility coefficient $K_{\text{n.m.}}$. Detail discussion on the incompressibility coefficient $K_{\text{n.m.}}$ will be given in the next section. The isoscalar effective mass is defined as (from the total binding energy per nucleon Eq. (2.30))

$$m^* = m\Big(1 + \frac{m}{8\hbar^2}\rho_0\Theta\Big)^{-1}. \tag{2.35}$$

The total binding energy per nucleon is rewritten as

$$\frac{E}{A} = \frac{3\hbar^2}{10m^*}\left(\frac{3\pi^2}{2}\right)^{2/3}\rho^{2/3} + \frac{3}{8}t_0\rho + \frac{1}{16}t_3\rho^{\alpha+1}. \tag{2.36}$$

For the nuclear matter with $Z \neq N$, we expand the proton, neutron densities $\rho_q(r) = \frac{2}{3\pi^2}{k_f}_q^3$ and the kinetic density $\tau(r) = \frac{3}{5}k_f^2\rho_q = \frac{3}{5}(\frac{3\pi^2}{2})^{2/3}{\rho_q}^{5/3}$ around the saturation density $\rho_0 = \rho_p + \rho_n$. We limit ourself to the second order term

$$\frac{E}{A} = \Big(\frac{E}{A}\Big)_{\rho_0} + J\Big(\frac{N-Z}{A}\Big)^2, \tag{2.37}$$

where $\left(\frac{E}{A}\right)_{\rho_0}$ is given in Eq. (2.36), and $J$ is the symmetry energy coefficient

$$\begin{aligned} J &= \frac{\hbar^2}{6m}\left(\frac{3\hbar^2}{2}\right)^{2/3}\rho^{2/3} - \frac{1}{8}t_0(2x_0+1)\rho + \frac{1}{24}\left(\frac{3\pi^2}{2}\right)^{2/3}\left[t_2(5+4x_2) - 3t_1x_1\right]\rho^{5/3} \\ &\quad -\frac{1}{48}t_3(2x_3+1)\rho^{\alpha+1}. \end{aligned} \tag{2.38}$$

The Hartree-Fock equations for the Skyrme interaction are obtained from the fact that the total energy is stationary with respect to the normalized single-particle wave-function $\phi_i(\mathbf{r})$. It requires that

$$\frac{\delta}{\delta\rho_{\sigma,q}}\left[E - \sum_i \epsilon_i \int \rho_{\sigma,q} d\mathbf{r}\right] = 0. \tag{2.39}$$

We have

$$\delta E = \sum_{\sigma,q}\int\left[\frac{\hbar^2}{2m_q^*(\mathbf{r})}\delta\tau_{\sigma q}(\mathbf{r}) + U_q(\mathbf{r})\delta\rho_{\sigma q}(\mathbf{r}) + W_q(\mathbf{r})\delta\mathbf{J}_{\sigma q}(\mathbf{r})\right]d\mathbf{r}, \tag{2.40}$$

where $\delta\tau_{\sigma q}(\mathbf{r})$, $\delta\rho_{\sigma q}(\mathbf{r})$, $\delta\mathbf{J}_{\sigma q}(\mathbf{r})$ are the variations of spin-isospin kinetic energy, matter, and the spin current densities. The effective mass $m_q^*(\mathbf{r})$, the central potential $U_q(\mathbf{r})$, and the spin-orbit potential $W_q(\mathbf{r})$ are expressed in terms of Skyrme parameters, matter density, charge density and the current density as,

$$\begin{aligned}\frac{\hbar^2}{2m_q^*(\mathbf{r})} &= \frac{\hbar^2}{2m_q}+\frac{1}{4}\left[t_1(1+\frac{x_1}{2})+t_2(1+\frac{x_2}{2})\right]\rho(\mathbf{r})\\ &\quad -\frac{1}{4}\left[t_1(\frac{1}{2}+x_1)-t_2(\frac{1}{2}+x_2)\right]\rho_q(\mathbf{r}),\end{aligned} \tag{2.41}$$

$$\begin{aligned}U_q(\mathbf{r}) &= t_0\left(1+\frac{x_0}{2}\right)\rho(\mathbf{r})-t_0\left(\frac{1}{2}+x_0\right)\rho_q(\mathbf{r})+\frac{1}{4}\left[t_1\left(1+\frac{x_1}{2}\right)+t_2\left(1+\frac{x_2}{2}\right)\right]\tau(\mathbf{r})\\ &\quad -\frac{1}{4}\left[t_1\left(\frac{1}{2}+x_1\right)+t_2\left(\frac{1}{2}+x_2\right)\right]\tau_q(\mathbf{r})+\frac{\alpha+2}{12}t_3\left(1+\frac{x_3}{2}\right)\rho^{\alpha+1}(\mathbf{r})\\ &\quad -\frac{\alpha}{12}t_3\left(\frac{1}{2}+x_3\right)\rho^{\alpha-1}(\mathbf{r})\left(\rho_p^2(\mathbf{r})+\rho_n^2(\mathbf{r})\right)-\frac{1}{6}t_3\left(\frac{1}{2}+x_3\right)\rho^{\alpha}(\mathbf{r})\rho_q(\mathbf{r})\\ &\quad -\frac{1}{8}\left[3t_1\left(1+\frac{x_1}{2}\right)-t_2\left(1+\frac{x_2}{2}\right)\right]\overrightarrow{\nabla}^2\rho(\mathbf{r})\\ &\quad +\frac{1}{8}\left[3t_1\left(\frac{1}{2}+x_1\right)+t_2\left(\frac{1}{2}+x_2\right)\right]\overrightarrow{\nabla}^2\rho_q(\mathbf{r})\\ &\quad -\frac{1}{2}W_0\left[\overrightarrow{\nabla}\mathbf{J}(\mathbf{r})+\overrightarrow{\nabla}\mathbf{J}_q(\mathbf{r})\right]+\delta_{q,\frac{1}{2}}e^2\int\frac{\rho_{\text{ch.}}(\mathbf{r})}{\mid\mathbf{r}-\mathbf{r}'\mid}d\mathbf{r}',\end{aligned} \tag{2.42}$$

$$W_q(\mathbf{r})=\frac{1}{2}W_0\left[\overrightarrow{\nabla}\rho(\mathbf{r})+\overrightarrow{\nabla}\rho_q(\mathbf{r})\right]+\frac{1}{8}(t_1-t_2)\mathbf{J}_q(\mathbf{r})-\frac{1}{8}(t_1x_1-t_2x_2)\mathbf{J}(\mathbf{r}). \tag{2.43}$$

Because of the time reversal invariance, the variations $\delta\tau_{\sigma q}(\mathbf{r})$, $\delta\rho_{\sigma q}(\mathbf{r})$, and $\delta\mathbf{J}_{\sigma q}(\mathbf{r})$ are written as

$$\delta\tau_{\sigma q}(\mathbf{r})=\delta\sum_i\overrightarrow{\nabla}\phi_i^*(\mathbf{r},\sigma,q)\overrightarrow{\nabla}\phi_i(\mathbf{r},\sigma,q)=\sum_{i\sigma'}\overrightarrow{\nabla}\phi_i(\mathbf{r},\sigma',q)\overrightarrow{\nabla}\delta\phi_i^*(\mathbf{r},\sigma',q), \tag{2.44}$$

$$\begin{aligned}\delta\rho_{\sigma q}(\mathbf{r}) &= \sum_i\left[\delta\phi_i^*(\mathbf{r},\sigma,q)\phi_i(\mathbf{r},\sigma,q)+\phi_i^*(\mathbf{r},\sigma,q)\delta\phi_i(\mathbf{r},\sigma,q)\right]\\ &= \sum_i\left[\delta\phi_i^*(\mathbf{r},\sigma,q)\phi_i(\mathbf{r},\sigma,q)+\phi_{\bar{i}}^*(\mathbf{r},\sigma,q)\delta\phi_{\bar{i}}(\mathbf{r},\sigma,q)\right]\\ &= \sum_i\left[\delta\phi_i^*(\mathbf{r},\sigma,q)\phi_i(\mathbf{r},\sigma,q)+\phi_i(\mathbf{r},-\sigma,q)\delta\phi_i^*(\mathbf{r},-\sigma,q)\right]\end{aligned}$$

$$= \sum_{i,\sigma'} \phi_i(\mathbf{r},\sigma',q)\delta\phi_i^*(\mathbf{r},\sigma',q), \tag{2.45}$$

$$\begin{aligned}\delta\mathbf{J}_{\sigma q}(\mathbf{r}) &= -i\delta\sum_{i\sigma''}\phi_i^*(\mathbf{r},\sigma,q)\left[\overrightarrow{\nabla}\phi_i(\mathbf{r},\sigma'',q)\langle\sigma|\vec{\sigma}|\sigma''\rangle\right] \\ &= -i\sum_{i\sigma'\sigma''}\delta\phi_i^*(\mathbf{r},\sigma',q)\left[\overrightarrow{\nabla}\phi_i(\mathbf{r},\sigma'',q)\langle\sigma|\vec{\sigma}|\sigma''\rangle\right].\end{aligned} \tag{2.46}$$

Substituting all variations in Eq. (2.40), we obtain

$$\begin{aligned}&\sum_{i,\sigma'}\int d\mathbf{r}\delta\phi_i^*(\mathbf{r},\sigma',q)\left[\frac{\hbar^2}{2m_q^*(\mathbf{r})}\overrightarrow{\nabla}\phi_i(\mathbf{r},\sigma',q)\overrightarrow{\nabla}+U_q(\mathbf{r})\phi_i(\mathbf{r},\sigma',q)\right. \\ &\left.-iW_q(\mathbf{r})\sum_{\sigma''}\left(\overrightarrow{\nabla}\times\langle\sigma'|\vec{\sigma}|\sigma''\rangle\right)\phi_i(\mathbf{r},\sigma'',q)-\epsilon_i\phi_i(\mathbf{r},\sigma',q)\right]=0.\end{aligned} \tag{2.47}$$

Since all the coefficients of the variation $\delta\phi_i^*(\mathbf{r},\sigma',q)$ vanish, we have

$$\begin{aligned}&\sum_{i,\sigma'}\int d\mathbf{r}\left[\frac{\hbar^2}{2m_q^*(\mathbf{r})}\overrightarrow{\nabla}\phi_i(\mathbf{r},\sigma',q)\overrightarrow{\nabla}+U_q(\mathbf{r})\phi_i(\mathbf{r},\sigma',q)\right. \\ &\left.-iW_q(\mathbf{r})\sum_{\sigma''}\left(\overrightarrow{\nabla}\times\langle\sigma'|\vec{\sigma}|\sigma''\rangle\right)\phi_i(\mathbf{r},\sigma'',q)-\epsilon_i\phi_i(\mathbf{r},\sigma',q)\right]=0.\end{aligned} \tag{2.48}$$

Integrating by parts, we finally obtain the equations:

$$\left[-\overrightarrow{\nabla}\frac{\hbar^2}{2m_q^*(\mathbf{r})}\overrightarrow{\nabla}+U_q(\mathbf{r})-iW_q(\mathbf{r})\left(\overrightarrow{\nabla}\times\vec{\sigma}\right)\right]\phi_i(\mathbf{r},q)=\epsilon_i\phi_i(\mathbf{r},q). \tag{2.49}$$

These equations are known as Hartree-Fock equations, by solving these equation we can obtain the single-particle wave functions $\phi_i(\mathbf{r},\sigma,q)$ with the single-particle energies $\epsilon_i$. From here we can build the total wave function $\Phi$ and know the properties of the ground state nucleus. All the nuclei considered in this dissertation are spherical closed shell nuclei. The single-particle wave function $\phi_i(\mathbf{r}_i,\sigma_i,q)$ is written in term of the radial function $R_\alpha(r)$, spherical harmonic function $Y_{jlm}(\mathbf{r},\sigma)$, and isospin function $\chi_{m_q}(q)$, as

$$\phi(\mathbf{r},\sigma,q)=\frac{R_\alpha(r)}{r}Y_{jlm}(\mathbf{r},\sigma)\chi_{m_q}(q), \tag{2.50}$$

where $\alpha$ stands for quantum numbers $n$, $j$, $l$, $m_q$, and

$$Y_{jlm}(\mathbf{r},\sigma) = \sum_{m_l,m_s} \langle l\frac{1}{2}m_l m_s|jm\rangle Y_{lm_l}(\mathbf{r})\mu_{m_s}(\sigma), \tag{2.51}$$

with

$$\chi_{m_q} = \delta_{q,m_q}; \qquad \mu_{m_s}(\sigma) = \delta_{\delta,m_s}. \tag{2.52}$$

We also have

$$\sum_m Y^*_{jlm}(\mathbf{r},\sigma)Y_{jlm}(\mathbf{r},\sigma) = \frac{2j+1}{4\pi}, \tag{2.53}$$

$$\tau(r) = \frac{1}{4\pi}\sum_{n,j_\alpha,l_\alpha}(2j_\alpha+1)\left[\left(\frac{dR_\alpha(r)}{dr}\right)^2 + \frac{l_\alpha(l_\alpha+1)}{r^2}R^2_\alpha(r)\right], \tag{2.54}$$

$$\mathbf{J}_q(\mathbf{r}) = J_q(r)\mathbf{r} = -i\sum_{i=1}^{A}\phi^*_i(\mathbf{r},q)\frac{\mathbf{r}}{r}\left(\overrightarrow{\nabla}\times\vec{\sigma}\right)\phi_i(\mathbf{r},q)\frac{\mathbf{r}}{r}, \tag{2.55}$$

with

$$J_q(r) = \frac{1}{4\pi r^2}\sum_{n,j_\alpha,l_\alpha}(2j_\alpha+1)\left[j_\alpha(j_\alpha+1) - l_\alpha(l_\alpha+1) - \frac{3}{4}\right]R^2_\alpha(r). \tag{2.56}$$

The Hartree-Fock equations become

$$\begin{aligned} &\frac{\hbar^2}{2m^*_q(r)}\left[-R''_\alpha(r) + \frac{l_\alpha(l_\alpha+1)}{r^2}R_\alpha(r)\right] - \frac{d}{dr}\left(\frac{\hbar^2}{2m^*_q(r)}\right)R'_\alpha(r) \\ + &\left[U_q(r) + \frac{1}{r}\frac{d}{dr}\left(\frac{\hbar^2}{2m^*_q(r)}\right) + \frac{\left[j_\alpha(j_\alpha+1) - l_\alpha(l_\alpha+1) - \frac{3}{4}\right]}{r}W_q(r)\right]R_\alpha(r) \\ = &\ \epsilon_\alpha R_\alpha(r). \end{aligned} \tag{2.57}$$

Using iteration to solve these equations, we can find the radial part of the single-particle wave functions of the states $\alpha$.

## C. Approximations and constraints

### 1. Coulomb energy

The Coulomb energy can be written as a sum of a direct and an exchange terms

$$\begin{aligned}\langle\Phi|\frac{1}{2}\sum_{i\neq j}V^{NN}_{\text{Coulomb}}|\Phi\rangle &= \frac{e^2}{2}\int d\mathbf{r}d\mathbf{r}'\left[\frac{\rho_{\text{ch.}}(\mathbf{r})\rho_{\text{ch.}}(\mathbf{r}')-|\rho_{\text{ch.}}(\mathbf{r},\mathbf{r}')|^2}{|\mathbf{r}-\mathbf{r}'|}\right]\\ &= \int\mathcal{H}_{\text{Coulomb}}(\mathbf{r})d\mathbf{r},\end{aligned} \tag{2.58}$$

$$\mathcal{H}_{\text{Coulomb}}(r)=\mathcal{H}^{\text{dir.}}_{\text{Coulomb}}(r)+\mathcal{H}^{\text{ex.}}_{\text{Coulomb}}(r). \tag{2.59}$$

where $\rho_{\text{ch.}}(\mathbf{r})$ is the local charge density, in the case of the proton is treated as a point charge, we have $\rho_{\text{ch.}}(\mathbf{r})=\rho_p(\mathbf{r})$, and the $\rho_{\text{ch.}}(\mathbf{r},\mathbf{r}')$ is the non-local charge density

$$\rho_{\text{ch.}}(\mathbf{r},\mathbf{r}')=\sum_{i,\sigma,\sigma'}\phi^*_i(\mathbf{r},\sigma,\frac{1}{2})\phi_i(\mathbf{r}',\sigma',\frac{1}{2}). \tag{2.60}$$

The direct term of the Coulomb energy density is written as

$$\mathcal{H}^{\text{dir.}}_{\text{Coulomb}}(r)=\frac{1}{2}e^2\rho_p(r)\int\frac{\rho_p(r')d^3r'}{\mid\mathbf{r}-\mathbf{r}'\mid}, \tag{2.61}$$

and with the Slater approximation [43], the exchange term is given as

$$\mathcal{H}^{\text{ex.}}_{\text{Coulomb}}(r)=-\frac{3}{4}e^2\rho_p(r)\left[\frac{3\rho_p(r)}{\pi}\right]^{1/3}. \tag{2.62}$$

The contributions of the Coulomb self-interaction in both Eqs. (2.61) and (2.62) have opposite signs and will cancel out in Eq. (2.59). It is obvious that if one ignores the exchange term in Eq. (2.59), the direct term has the contribution of self interaction which has to be removed. The direct term of the Coulomb interaction given by Eq. (2.61) is proportional to $Z^2$ and not to $Z(Z-1)$, as it should be for a direct term [44, 45]. For the Coulomb displacement energy (CDE) of mirror nuclei, the magnitude of the self-interaction term is CDE/$(2Z)$, this means that one has a spurious increase

in the calculated CDE of about 6.3% and 2.5% for the A=17 and 41 systems of mirror nuclei, respectively.

It was first shown in Ref. [45, 46] that within the mean-field approximation, adjusted to reproduce the experimental values of the charge rms radii, the calculated CDE of analog states which is obtained by using Eq. (2.59) are smaller than the corresponding experimental values by about 7%. This discrepancy which is referred to as the Nolen-Schiffer anomaly [46] can be understood when the contributions that are due to long-range correlations (LRC) and the charge symmetry breaking (CSB) in the $NN$ interaction are taken into account (Refs. [45, 47]). The CSB is due to the fact that the $NN$ interaction is not charge independent. In fact the neutron-neutron $(n-n)$ interaction is more attractive than the proton-proton $(p-p)$ interaction. We know that for the mirror nuclei with A=17 and A=41, the contribution of each the LRC and the CSB is about half of the discrepancy between theory and experiment [45]. The magnitude of the bona fide exchange Coulomb term is about the same as that due to LRC, but with opposite sign. So, if one neglects the bona fide Coulomb exchange term, although this way does not solve the discrepancy between theory and experiment, one can account for the contribution of LRC. And it was also shown in Ref. [48] that by dropping the Coulomb exchange term in the form of Eq. (2.62) from the Coulomb interaction density Eq. (2.59), (as is the case for the SKX interaction), one could reproduce the experimental values of the CDE. We have to emphasize that by accepting the form of Eq. (2.61) for the Coulomb direct term one not only neglects the bona fide Coulomb exchange term, but also adds the spurious contribution of the self-interaction term in the Coulomb interaction Eq. (2.59). Therefore, the unphysical neglect of the bona fide Coulomb exchange term together with the spurious contribution of the self-interaction term results in a contribution to CDE that is similar in magnitude to that obtained from the LRC and CSB terms. Therefore,

in this dissertation, only the direct term of the Coulomb energy density given in Eq. (2.61) is used.

### 2. Center of mass corrections to the binding energy and charge radii

The expectation value of the mean-field Hamiltonian with respect to the total wave function $\Phi$ gives us not only the ground state energy but also the energy of the nucleus moving around its center of mass (CM) and the rotation energy of the nucleus as a whole. All the nuclei in this dissertation are spherical nuclei, so the rotation energy is zero. Calculating the exact value of the ground state energy as the expectation value of the Hamiltonian is very difficult because the contribution from the motion of the nucleons around the center of mass and the motion of the center of mass in the total wave function $\Phi$ is not clearly separated. An exact way which can restore the translational invariance is to use the projection method, but it is extremely difficult. The HF method applied to finite nuclei violates the translational invariance, because the center of mass motion is not separated and thus introduces the spurious states. Thus, one has to extract the contributions of the CM motion to the total binding energy $B$, radii and other observables. Therefore, the purpose of our work is to develop simple schemes for the CM corrections to various observables. In the literature, one usually makes the CM corrections only to the binding energy and not to the radii. However, the CM corrections to the rms radii for light nuclei may be as large as 2% [44]. In this dissertation we carry out the CM corrections not only to the binding energy but also to charge rms radii used in the fit for determining the Skyrme parameters.

For the CM correction to the total binding energy, one must subtract from it the

so-called CM energy, given as,

$$E_{\rm CM} = \frac{1}{2mA}\langle \mathbf{P}^2 \rangle. \tag{2.63}$$

One good approximation is that the ground state energy is calculated by subtracting the expectation value of the center of mass kinetic energy from the expectation value of the total Hamiltonian,

$$E = \langle \Phi | T + \frac{1}{2}\sum_{ij}(V_{ij}^{NN} + V_{\rm Coulomb}^{NN})|\Phi\rangle - \langle \Phi | \frac{\mathbf{P}_{cm}^2}{2M}|\Phi\rangle, \tag{2.64}$$

with $M = mA$ is the total mass of nucleus and the total linear momentum operator $\mathbf{P}$ is given as

$$\mathbf{P} = -i\hbar \sum_i^A \overrightarrow{\nabla}_i. \tag{2.65}$$

We have

$$\begin{aligned} \mathbf{K} - \frac{\mathbf{P}^2}{2mA} &= \sum_i^A \frac{\mathbf{p}_i^2}{2m} - \frac{\left(\sum_i^A \mathbf{p}_i\right)^2}{2mA} = \sum_i^A \frac{\mathbf{p}_i^2}{2m} - \frac{1}{2mA}\left[\sum_i^A \mathbf{p}_i^2 - \sum_{i\neq j}^A \mathbf{p}_i\mathbf{p}_j\right] \\ &= \frac{1}{2m}\left(1 - \frac{1}{A}\right)\sum_i^A \mathbf{p}_i^2 - \frac{1}{2mA}\sum_{i\neq j}^A \mathbf{p}_i\mathbf{p}_j. \end{aligned} \tag{2.66}$$

Traditionally, one simplifies the calculation by taking into account only the one-body terms. It means that in the kinetic energy term, the factor $\frac{1}{m}$ is replaced by $\frac{1}{m}\left(1 - \frac{1}{A}\right)$. The second term in Eq. (2.66) is the two-body term, which is difficult to calculate. The effects of neglecting the two-body term of Eq. (2.66) are compensated by renormalization of the force parameters, and thus induce some correlations in the values of the parameters. This approach may induce in the forces an incorrect trend with respect to $A$ that becomes visible in the nuclear matter properties. It was shown in Ref. [49] that this approximation which is an oversimplified treatment of $E_{\rm CM}$ obtained by re-normalizing the nucleon mass appearing in the kinetic-energy term gives a larger value of the surface-energy coefficient than those obtained using

the full CM correction. For the case of the super deformed states, this approach also increases the differences in the deformation energy that becomes quite large. Very recently, it was also found [50] that a large value of the surface-energy coefficient will give a smaller value for the critical density. Therefore an appropriate and simple scheme to evaluate Eq. (2.63) is very much needed.

We note that it was shown in Ref. [2] that the SLy6, SLy7 and SLy10 interactions were obtained by including the one- and two-body terms of Eq. (2.63). In the harmonic oscillator (HO) approximation, which means that the single-particle wave function is treated as the HO wave function, the center of mass energy $E_{\rm CM}$ of Eq. (2.63) is given as

$$E_{\rm CM}^{\rm HO} = \frac{3}{4}\hbar\omega. \tag{2.67}$$

A value of $\hbar\omega = 41A^{-1/3}$ MeV is used in many relativistic mean-field calculations [10, 51]. The SKX interaction was obtained in in Ref. [32] by modifying the oscillator frequency as $\hbar\omega = 45A^{-1/3} - 25A^{-2/3}$ MeV. However, this modification gives an overestimated value for the binding energy of light nuclei (e.g., $^{16}$O and $^{40}$Ca) by about $1-2$ MeV, which is very significant.

We also use the HO approximation but give a simple and consistent scheme to evaluate the $E_{\rm CM}$. We calculated the oscillator frequency $\hbar\omega$ in Eq. (2.67) by using the mean-square mass radii $\langle r^2\rangle$ obtained in the HF approach as

$$\hbar\omega = \frac{\hbar^2}{mA\langle r^2\rangle}\sum_i[\mathcal{N}_i + \frac{3}{2}], \tag{2.68}$$

where the sum runs over all the occupied single-particle states for the protons and neutrons and $\mathcal{N}_i$ is the oscillator quantum number. We would like to emphasize that this approach is very reliable even for the nuclei away from the $\beta$-stable line, where the values of the rms radii deviate from the $A^{1/3}$ law.

In order to compare the full CM correction to that evaluated in this scheme, we calculated the total binding energy for the SLy7 interaction using our simple approximation for the CM correction, Eq. (2.68), and compare them with those given in Ref. [2], obtained by using one- and two-body terms of the Eq. (2.63). We found that for the $^{16}$O, $^{40}$Ca, $^{132}$Sn and $^{208}$Pb nuclei the total binding energy $B = 128.65$ (128.55), 344.98 (344.90), 1102.38 (1102.77), and 1636.29 (1636.76) MeV, respectively, where the values in parenthesis are taken from Ref. [2]. These results clearly show that the CM correction to the binding energy can be reliably estimated using Eqs. (2.67) and (2.68).

We now consider the CM correction to the charge rms radii. The mean-square radius for the point-proton distribution corrected for the CM motion was obtained in Ref. [44], and is given as

$$\langle r_p^2 \rangle = \langle r_p^2 \rangle_{\rm HF} - \frac{3}{2\nu A}, \tag{2.69}$$

where, $\nu = m\omega/\hbar$ is the size parameter. Therefore the corresponding mean-square charge radius to be fitted to the experimental data is obtained as

$$\langle r_{\rm ch.}^2 \rangle = \langle r_p^2 \rangle_{\rm HF} - \frac{3}{2\nu A} + \langle r^2 \rangle_p + \frac{N}{Z}\langle r^2 \rangle_n + \frac{1}{Z}\left(\frac{\hbar}{mc}\right) \sum_{nlj\tau} (2j+1)\mu_\tau \langle \vec{\sigma} \cdot \vec{l} \rangle_{lj}, \tag{2.70}$$

where, $\langle r^2 \rangle_p$ and $\langle r^2 \rangle_n$ are the mean-squared radii of the proton and neutron charge distributions, respectively. The last term in Eq. (2.70) is due to the spin-orbit effect [52]. We use, $\langle r^2 \rangle_n = -0.12$ fm$^2$ and the recent [53] value of $\langle r^2 \rangle_p = 0.801$ fm$^2$.

### 3. Critical density

In this section we estimate the value of the critical density $\rho_{\rm cr.}$ which will be included in the fit to determine the parameters of Skyrme interaction by using the stability conditions of the Landau parameters for the symmetric nuclear matter and pure

neutron matter. In the Landau's theory for an infinite nuclear matter, the particle-hole interaction is given by [54]

$$V_{\rm p-h} = \delta(\mathbf{r}_1 - \mathbf{r}_2) N_0^{-1} \sum_l \left[ F_l + F_l' \mathbf{q}_1 \mathbf{q}_2 + G_l \vec{\sigma}_1 \vec{\sigma}_2 + G_l' (\vec{\sigma}_1 \vec{\sigma}_2)(\mathbf{q}_1 \mathbf{q}_2) \right] P_l(cos\theta), \quad (2.71)$$

with

$$N_0^{-1} = \frac{\hbar^2}{2m^*} \frac{\pi^2}{k_f}, \quad (2.72)$$

where $F_l$, $F_l'$, $G_l$ and $G_l'$ are Landau parameters, $l$ is a multi-polarity, $N_0$ is the number of state per unit volume. The stability condition are given as [54],

$$\mathcal{X}_l > -(2l+1), \quad (2.73)$$

where, $\mathcal{X}_l$ are the Landau parameters.

We know that the Skyrme interaction only contains mono-polar and dipolar contributions to the particle-hole ($ph$) interaction then $\mathcal{X}_l = 0$ for $l > 1$. Therefore, we have 12 different Landau parameters, 8 parameters $F_l$, $F_l'$, $G_l$ and $G_l'$ ($l = 0, 1$) for the symmetric nuclear matter and 4 parameters $F_l^{(n)}$, $G_l^{(n)}$ ($l = 0, 1$) for the pure neutron matter. These Landau parameters $\mathcal{X}_l$ have to satisfy the inequality condition given by Eq. (2.73). All the Landau parameters can be written in terms of the Skyrme parameters, see Refs. [35, 36]. The Landau parameters for the symmetric nuclear matter are:

$$F_0 = \left[ \frac{3}{4} t_0 + \frac{1}{16} (\alpha+1)(\alpha+2) t_3 \rho^\alpha \right] \frac{2m^* k_f}{\pi^2 \hbar^2} - F_1, \quad (2.74)$$

$$G_0 = \left[ \frac{1}{4} t_0 (2x_0 - 1) + \frac{1}{24} t_3 \rho^\alpha (2x_3 - 1) \right] \frac{2m^* k_f}{\pi^2 \hbar^2} - G_1, \quad (2.75)$$

$$F_0' = \left[ -\frac{1}{4} t_0 (2x_0 + 1) - \frac{1}{24} t_3 \rho^\alpha (2x_3 - 1) \right] \frac{2m^* k_f}{\pi^2 \hbar^2} - F_1', \quad (2.76)$$

$$G_0' = \left[ -\frac{1}{4} t_0 - \frac{1}{24} t_3 \rho^\alpha \right] \frac{2m^* k_f}{\pi^2 \hbar^2} - G_1', \quad (2.77)$$

$$F_1 = -3T_0\frac{m^*}{\hbar^2}\rho, \tag{2.78}$$

$$G_1 = -3T_1\frac{m^*}{\hbar^2}\rho, \tag{2.79}$$

$$F_1' = 3T_2\frac{m^*}{\hbar^2}\rho, \tag{2.80}$$

$$G_1' = 3T_3\frac{m^*}{\hbar^2}\rho. \tag{2.81}$$

The Landau parameters for the pure neutron matter are:

$$F_0^{(n)} = \left[\frac{1}{2}t_0(1-x_0) + \frac{1}{24}(\alpha+1)(\alpha+2)t_3\rho^\alpha(1-x_3)\right]\frac{2m^*k_f}{\pi^2\hbar^2} - F_1^{(n)}, \tag{2.82}$$

$$G_0^{(n)} = \left[\frac{1}{2}t_0(x_0-1) + \frac{1}{12}t_3\rho^\alpha(x_3-1)\right]\frac{2m^*k_f}{\pi^2\hbar^2} - G_1^{(n)}, \tag{2.83}$$

$$F_1^{(n)} = -3(T_0-T_2)\frac{m_n^*}{\hbar^2}\rho, \tag{2.84}$$

$$G_1^{(n)} = -3(T_1-T_3)\frac{m_n^*}{\hbar^2}\rho. \tag{2.85}$$

Here we have defined,

$$T_0 = \frac{1}{8}\left[3t_1 + t_2(5+4x_2)\right], \tag{2.86}$$

$$T_1 = \frac{1}{8}\left[t_1(x_1-1) + t_2(2x_2+1)\right], \tag{2.87}$$

$$T_2 = \frac{1}{8}\left[t_1(2x_1+1) - t_2(2x_2+1)\right], \tag{2.88}$$

$$T_3 = t_1 - t_2, \tag{2.89}$$

$$\frac{\hbar^2}{m_n^*} = \frac{\hbar^2}{m} + (T_0-T_2)\rho. \tag{2.90}$$

We can obtain the values of the Landau parameters at any density for a given set of the Skyrme parameters. Therefore, the critical density is the maximum density up to which all the stability (inequality) conditions are met can be easily determined.

There are many approximations and improvements that have been made to achieve more realistic Skyrme parameters. In Ref. [35], the stability requirements of the equation of state (EOS) defined by the inequality conditions for the Landau pa-

rameters for symmetric nuclear matter and pure neutron matter was used to constrain the Skyrme parameters. It means that the Skyrme parameters which are not well determined by fitting the results of Hartree-Fock calculations to a set of experimental data can be restricted with a condition that the inequality conditions are satisfied up to a maximum value of the nuclear matter density, called as the critical nuclear matter density $\rho_{\rm cr.}$. In Ref. [34], a first systematic study using many different parameters of the Skyrme interactions shows that there are only 27 out of 87 different parameters of the Skyrme interaction, having a positive slope for the symmetry energy coefficient at nuclear matter densities $\rho$ up to $3\rho_0$ ($\rho_0 = 0.16$ fm$^{-3}$), are suitable for the study of the neutron star model. It means that the symmetry energy coefficient $J$ has very important role in determining the properties of neutron star.

Therefore, the combination of the results of Ref. [35] and of Ref. [34] for determining the parameters of the Skyrme interactions will be taken into account. We study the dependence of the critical density $\rho_{\rm cr.}$ on the nuclear matter saturation density $\rho_{\rm n.m.}$, binding energy coefficient $B/A$, isoscalar effective mass $m^*/m$, incompressibility coefficient $K_{\rm n.m.}$, surface energy $E_s$, and the symmetry energy coefficient $J$.

The difference between our calculation and that carried out in Ref. [35] is that we calculate the critical density $\rho_{\rm cr.}$ in terms of the enhancement factor $\kappa$, the coefficient $L = 3\rho dJ/d\rho$ and the Landau parameter $G_0'$ (at $\rho_{\rm n.m.}$) instead of the combinations $t_i x_i$ ($i = 1, 2,$ and 3) of the Skyrme parameters used in Ref. [35]. We note that the quantities $\kappa$, $L$ and $G_0'$, which can be expressed in terms of the Skyrme parameters, are related to some physical processes. The enhancement factor $\kappa$ [31],

$$\kappa = \frac{m}{4\hbar^2}\left[t_1(2+x_1) + t_2(2+x_2)\right]\rho, \tag{2.91}$$

which accounts for the deviations from the Thomas-Reiche-Kuhn (TRK) sum rule in

the case of the isovector giant dipole resonance [31] has the value of about 0.5 at the $\rho_{\text{n.m.}}$ [31, 55]. From Eq. (2.38), the slope of symmetry energy coefficient is written as

$$\begin{aligned} L &= \frac{\hbar^2}{2m}k_f^2 - \frac{3}{4}t_0\left(x_0+\frac{1}{2}\right)\rho - \frac{1}{8}t_3(\alpha+1)\left(x_3+\frac{1}{2}\right)\rho^{\alpha+1} \\ &+ \frac{5}{24}\left(t_2(4+5x_2)-3t_1x_1\right)\rho k_f^2. \end{aligned} \tag{2.92}$$

The slope of the symmetry energy coefficient at $\rho \leq \rho_0$ determines the neutron skin thickness [56, 57] in nuclei and it must be positive for $\rho$ up to $3\rho_0$; a condition necessary for Skyrme interaction to be suitable for the study of the properties of neutron stars [34]. The Landau parameter $G_0'$ given in Eq. (2.77) has to be positive at $\rho \leq \rho_{\text{n.m.}}$ in order to reproduce the position of the isovector $M1$ and Gamow-Teller states [55, 58].

The Skyrme parameters $t_i$, $x_i$ and $\alpha$ for a fixed value of $W_0$ can be expressed in terms of the quantities associated with the symmetric nuclear matter as follows [9, 31, 35, 59].

$$\begin{aligned} t_0 &= \frac{8}{\rho_{\text{n.m.}}}\left[\frac{\left(-B/A+\left(2\frac{m}{m^*}-3\right)\frac{\hbar^2}{10m}k_f^2\right)\left(\frac{1}{27}K_{\text{n.m.}}-\left(1-\frac{6m^*}{5m}\right)\frac{\hbar^2}{9m^*}k_f^2\right)}{-B/A+\frac{1}{9}K_{\text{n.m.}}-\left(\frac{4m}{3m^*}-1\right)\frac{\hbar^2}{10m}k_f^2}\right. \\ &+ \left.\left(1-\frac{5m}{3m^*}\right)\frac{\hbar^2}{10m}k_f^2\right], \end{aligned} \tag{2.93}$$

$$t_1 = \frac{2}{3}\left[T_0+T_s\right], \tag{2.94}$$

$$t_2 = t_1 + \frac{8}{3}\left[\left(\frac{1}{4}t_0+\frac{1}{24}t_3\rho_{\text{n.m.}}^{\alpha}\right)\frac{2m^*}{\hbar^2}\frac{k_f}{\pi^2}+G_0'\right]\frac{\hbar^2}{m^*\rho_{\text{n.m.}}}, \tag{2.95}$$

$$t_3 = \frac{16}{\rho_{\text{n.m.}}^{\alpha+1}}\frac{\left(-B/A+\left(2m/m^*-3\right)\left(\hbar^2/10m\right)k_f^2\right)^2}{-B/A+\frac{1}{9}K_{\text{n.m.}}-\left(4m/3m^*-1\right)\left(\hbar^2/10m\right)k_f^2}, \tag{2.96}$$

$$x_0 = \frac{4}{t_0\rho_{\text{n.m.}}}\left[\frac{\hbar^2}{6m}k_f^2-\frac{1}{24}t_3(x_3+\frac{1}{2})\rho_{\text{n.m.}}^{\alpha+1}+\frac{1}{24}\left(t_2\left(4+5x_2\right)-3t_1x_1\right)\rho_{\text{n.m.}}k_f^2-J\right]-\frac{1}{2}, \tag{2.97}$$

$$x_1 = \frac{1}{t_1}\left[4\frac{\hbar^2\kappa}{m\rho_{\text{n.m.}}}-t_2(2+x_2)\right]-2, \tag{2.98}$$

$$x_2 = \frac{1}{4t_2}\left[8T_0 - 3t_1 - 5t_2\right], \tag{2.99}$$

$$x_3 = -\frac{8}{\alpha t_3 \rho_{\rm n.m.}^{\alpha+1}}\left[\frac{\hbar^2}{6m}k_f^2 - \frac{1}{12}\left((4+5x_2)t_2 - 3t_1x_1\right)\rho_{\rm n.m.}k_f^2 - 3J + L\right] - \frac{1}{2}, \tag{2.100}$$

$$\alpha = \frac{B/A - \frac{1}{9}K_{\rm n.m.} + (4m/3m^* - 1)\left(\hbar^2/10m\right)k_f^2}{-B/A + (2m/m^* - 3)\left(\hbar^2/10m\right)k_f^2}, \tag{2.101}$$

where,

$$T_0 = \frac{1}{8}\left(3t_1 + (5+4x_2)t_2\right) = \frac{\hbar^2}{m\rho_{\rm n.m.}}\left(\frac{m}{m^*} - 1\right), \tag{2.102}$$

$$T_s = \frac{1}{8}\left[9t_1 - (5+4x_2)t_2\right], \tag{2.103}$$

and

$$k_f = \left(\frac{3\pi^2}{2}\rho_{\rm n.m.}\right)^{1/3}. \tag{2.104}$$

In the above Eqs. (2.93)-(2.101), the various quantities characterizing the nuclear matter which are taken at the saturation density $\rho_{\rm n.m.}$ are the binding energy per nucleon $B/A$, isoscalar effective mass $m^*/m$, nuclear matter incompressibility coefficient $K_{\rm n.m.}$, symmetry energy coefficient $J$, the coefficient $L$ which is directly related to the slope of the symmetry energy coefficient ($L = 3\rho dJ/d\rho$), enhancement factor $\kappa$ and Landau parameter $G_0'$. It must be pointed out that the expression for the parameter $G_0'$ used in the above Eq. (2.95) includes the contributions from the spin-density term present in the Skyrme energy density functional [60].

When we know the value of $T_0$, then $T_s$ can be calculated for a given value of the surface energy $E_s$ as [35],

$$E_s = 8\pi r_0^2 \int_0^{\rho_{\rm n.m.}} d\rho \left[\frac{\hbar^2}{36m} - \frac{5}{36}T_0\rho + \frac{1}{8}T_s\rho - \frac{m^*}{\hbar^2}V_{\rm so}\rho^2\right]^{1/2}\left[\frac{B(\rho_{\rm n.m.}) - B(\rho)}{A}\right]^{1/2} \tag{2.105}$$

where, $\frac{B(\rho)}{A}$ is the binding energy per nucleon given by,

$$\frac{B(\rho)}{A} = -\left[\frac{3\hbar^2}{10m^*}k_f^2 + \frac{3}{8}t_0\rho + \frac{1}{16}t_3\rho^{\alpha+1}\right], \tag{2.106}$$

and,

$$r_0 = \left[\frac{3}{4\pi\rho_{\rm n.m.}}\right]^{1/3}, \tag{2.107}$$

$$V_{\rm so} = \frac{9}{16}{W_0}^2. \tag{2.108}$$

The way in which Eqs. (2.93) - (2.101) can be used to calculate the Skyrme parameters $t_i$, $x_i$ and $\alpha$ is the following. At first, the parameters $t_0$ and $\alpha$ can be calculated, in terms of $B/A$, $\rho_{\rm n.m.}$, $K_{\rm n.m.}$ and $m^*/m$, using Eqs. (2.93) and (2.101). Then, the parameter $t_3$ can be determined using Eq. (2.96). Next, $T_0$ and $T_s$ can be calculated using Eqs. (2.102) and (2.105), respectively. Once, the combinations $T_0$ and $T_s$ of the Skyrme parameters are known, one can calculate the remaining parameters in the following sequence, $t_1$, $t_2$, $x_2$, $x_1$, $x_3$ and $x_0$.

We have checked the values of $\kappa$, $L$ and $G_0'$ for many different parameters of the Skyrme interaction in Refs. [2, 31, 29, 8, 61, 62, 30]. We found that the values of $\kappa$, $L$ and $G_0'$ vary over a wide ranges $0 - 2$, $40 - 160$ MeV and $-0.15 - 1.0$, respectively. It shows that the experimental data used in the least-square procedure to fit the parameters of the Skyrme interaction can not constrain well the values of these quantities. We only have a very crude knowledge of these three quantities at the saturation density as discussed above. These quantities can be constrained by requiring a reasonable value for the critical density. Thus, we use the set of standard values for six quantities $\rho_{\rm n.m.} = 0.16$ fm$^{-3}$, $B/A = 16$ MeV, $K_{\rm n.m.} = 230$ MeV, $m^*/m = 0.7$, $E_s = 18$ MeV and $J = 32$ MeV as the standard values for the nuclear matter input. These values are precisely the same as those used in Ref. [35]

We study the dependence of $\rho_{\rm cr.}$ on the $\rho_{\rm n.m.}$, $B/A$, $m^*/m$, $K_{\rm n.m.}$, $E_s$ and $J$ by considering the variations of these quantities around their standard values as given above. For a given set of values for these quantities, we calculate the maximum value of $\rho_{\rm cr.}$, denoted as $\tilde{\rho}_{\rm cr.}$, by varying $\kappa$, $L$ and $G_0'$ at the saturation density $\rho_{\rm n.m.}$ within

acceptable limits. We note the difference between our calculation and that of Ref. [35] by the fact that we constrain the values of $\kappa$, $L$ and $G'_0$, whereas, in Ref. [35], the value of $\tilde{\rho}_{\rm cr.}$ was calculated by varying the combinations $t_i x_i$ ($i = 1, 2$, and 3) of Skyrme parameters with no restrictions. We now discuss some limits of the results in Ref. [35]. If the range of the combinations parameters $t_i x_i$ is not restricted, one can obtain unreasonable values of $\kappa$ and $L$. For example, with the standard values of nuclear matter input, $\tilde{\rho}_{cr.}$ is about $3.5\rho_0$ for $\kappa = 1.0$, $L = 36$ MeV and $G'_0 = 0.20$ (at $\rho_0$). The value of $G'_0$ is acceptable, but the value of $\kappa = 1.0$ is significantly large [31, 55]. And also for $\rho > \rho_0$ the value of $L$ decreases with increasing $\rho$ and it becomes negative for $\rho > 1.6\rho_0$, which makes the interaction not suitable to study neutron stars. We show in Fig. 1 the results for $\tilde{\rho}_{\rm cr.}$ obtained by varying the various quantities associated with the nuclear matter around their standard values. We set up the ranges following $0.25 \leq \kappa \leq 0.5$, $0 \leq L \leq 100$ MeV and $0 \leq G'_0 \leq 0.5$ at the saturation density $\rho_{\rm n.m.}$, we also require that $L > 0$ at $3\rho_0$. We can see from Fig. 1 that $\tilde{\rho}_{\rm cr.}$ depends strongly on $m^*/m$ and $E_s$; $\tilde{\rho}_{\rm cr.}$ depends weakly on $\rho_{\rm n.m.}$, $B/A$ and $K_{\rm n.m.}$ and it is almost independent of $J$. These results for $\tilde{\rho}_{\rm cr.}$ are qualitatively the same as the ones in Ref. [35]. But, with the restrictions on the values of $\kappa$, $L$ and $G'_0$, the values of $\tilde{\rho}_{\rm cr.}$ are smaller than the one obtained in Ref. [35] by up to 25%. With the effective mass $m^*/m = 0.6$ (0.7) and keeping all the other nuclear matter quantities equal to their standard values, we obtained $\tilde{\rho}_{\rm cr.} = 4.5\rho_0$ ($2.8\rho_0$) compared to $6\rho_0$ ($3.5\rho_0$) obtained in Ref. [35]. With a given set of values for the nuclear matter input, we should present the values of $\kappa$, $L$ and $G'_0$ required to obtained $\tilde{\rho}_{\rm cr.}$. We find that $\kappa$ lies in the range of $0.45-0.5$ for variations in the nuclear matter input by up to $\pm 15\%$ relative to their standard values. These features of $\kappa$ indicate that restricting $\kappa$ to take values in the range of $0.25 - 0.5$ delimits the $\tilde{\rho}_{\rm cr.}$ to a lower value. In Figs. 2 and 3 we show the values of $L$ and $G'_0$ (at saturation density $\rho_{\rm n.m.}$), respectively,

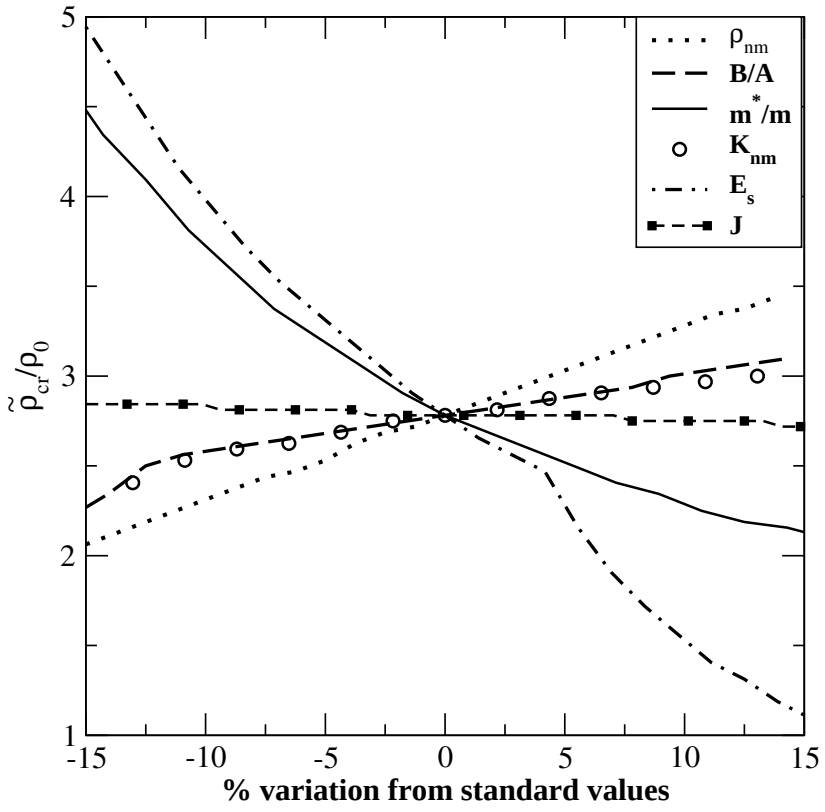


FIG. 1. The dependence of critical density $\tilde{\rho}_{\rm cr.}$ on the relative variation of $\rho_{\rm n.m.}$ (dotted line), $B/A$ (dashed line), $m^*/m$ (solid line), $K_{\rm n.m.}$ (open circles), $E_s$ (dashed-dot line), and $J$ (dashed-filled squares) around their standard values.

which are needed to yield the $\tilde{\rho}_{\rm cr.}$.

We see that for different values of the nuclear matter input, the value of $L$ varies from 20 to 60 MeV, and $L = 47$ MeV at $\rho = \rho_0$. This value is large compared to the values of $L = 35, 27$ and 16 MeV associated with the the Skz0, Skz1 and Skz2 interactions in [35], respectively, which were obtained for the same standard values of the nuclear matter input, but varying the combinations $t_1x_1$ and $t_2x_2$ with no restrictions and the value of $t_3x_3$ is fixed to some arbitrary values. From Fig. 3, except for $J$, the value of $G_0'$ (at saturation density $\rho_{\rm n.m.}$) depends strongly on the values of the various quantities associated with nuclear matter. The dependence of $G_0'$ on the surface energy coefficient $E_s$ is very prominent. We know that $E_s$ is mainly determined by the ground state properties of light nuclei. Therefore, the center of mass correction to the binding energy and charge radii which are very important for this case and may affect the values obtained for $E_s$ have to be taken into account appropriately. In Fig. 3, the value of $G_0'$ tends to vanish rapidly with increasing $E_s$.

From Fig. 1, we can see that the dependence of $\tilde{\rho}_{\rm cr.}$ on $\rho_{\rm n.m.}$, $J$, and $B/A$ is very weak. Therefore, it may be good enough to calculate $\tilde{\rho}_{\rm cr.}$ as a function of $m^*/m$, $E_s$ and $K_{\rm n.m.}$ only. In Fig. 4 we show the variation of $E_s$ as a function of effective mass $m^*/m$, in this case we fixed the values of $\tilde{\rho}_{\rm cr.}$ and the remaining nuclear matter quantities were kept equal to their standard values. We see from Fig. 4 that with a fixed value of $\tilde{\rho}_{\rm cr.}$, $E_s$ decreases while $m^*/m$ increases. It is very interesting to note that for $E_s = 18 \pm 1$ MeV (for most of the Skyrme interactions), $\tilde{\rho}_{\rm cr.} = 2\rho_0$ and $3\rho_0$ for $m^*/m = 0.72 - 0.85$ and $0.63 - 0.73$, respectively. To obtain $\tilde{\rho}_{\rm cr.} = 4\rho_0$ one must have $m^*/m \sim 0.65$ for not too low value of $E_s$. The value of the effective mass $m^*/m$ is also constrained by the centroid energy of the isoscalar giant quadrupole resonance [61] which has $m^*/m \geq 0.7$. So, for reasonable values of $E_s$ and $m^*/m$, one should obtain a Skyrme interaction with $\tilde{\rho}_{\rm cr.} = 2\rho_0$ to $3\rho_0$.

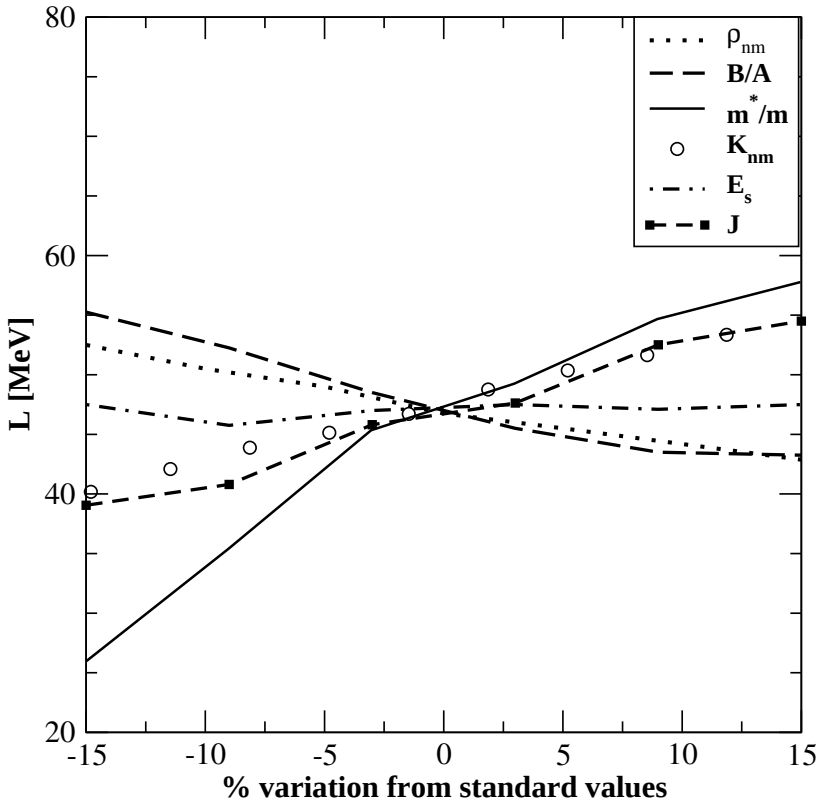


FIG. 2. The coefficient $L = 3\rho dJ/d\rho|_{\rho_{\rm n.m.}}$ as a function of the various quantities associated with the nuclear matter. The value of $L$ is determined by maximizing the critical density for a given set of values for the nuclear matter quantities.

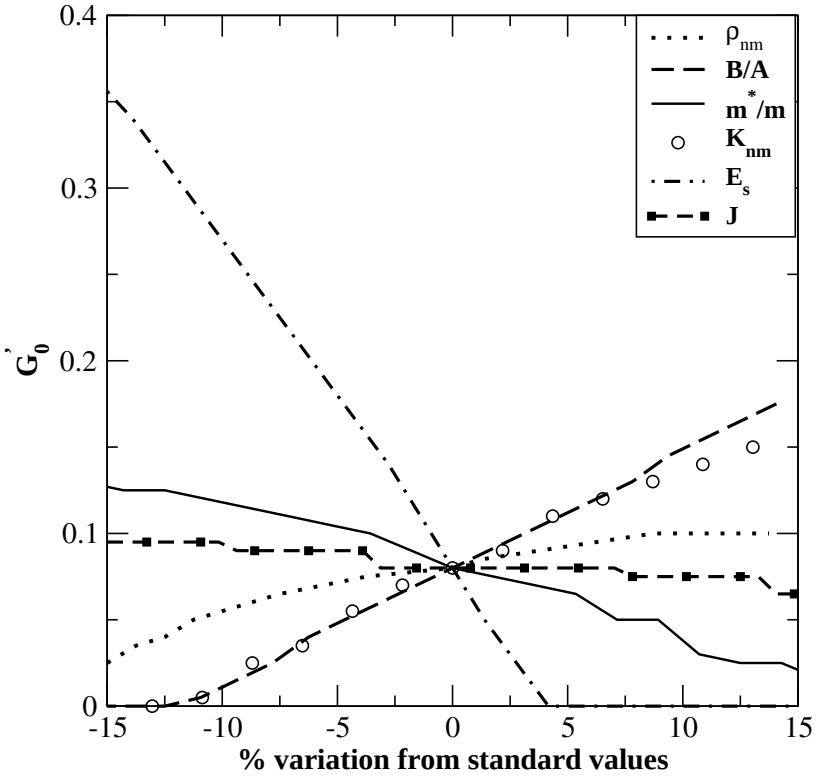


FIG. 3. The coefficient $G_0'$ as a function of the various quantities associated with the nuclear matter. The value of $G_0'$ is determined by maximizing the critical density for a given set of values for the nuclear matter quantities.

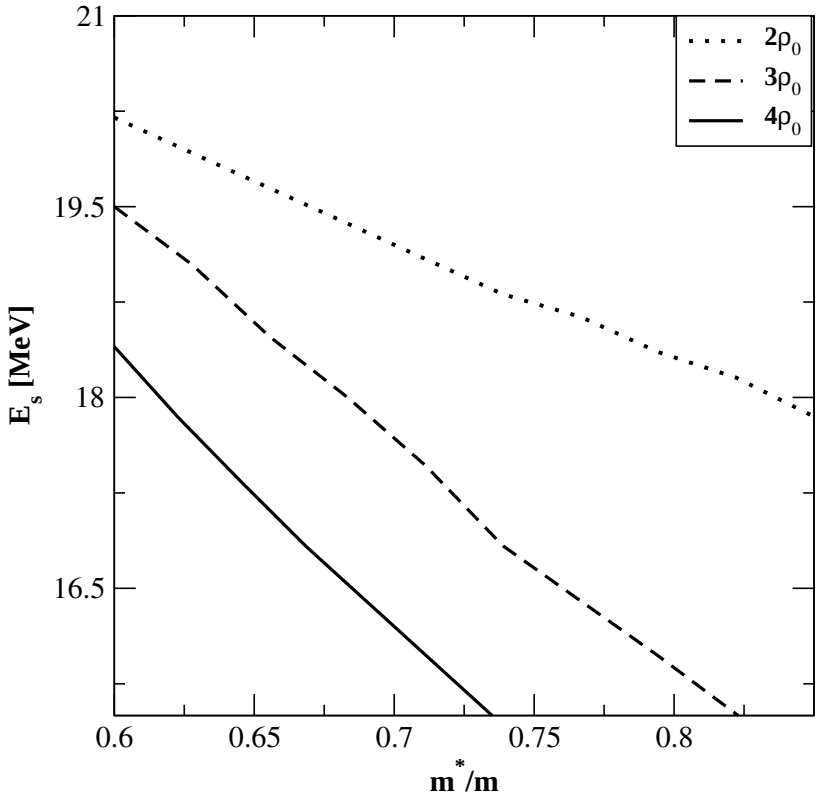


FIG. 4. Variations of the surface energy coefficient $E_s$ at $\rho_{\rm n.m.}$ as a function of the effective mass $m^*/m$ for fixed values of the critical density $\tilde{\rho}_{\rm cr.} = 2\rho_0, 3\rho_0$ and $4\rho_0$, as labeled. All the other nuclear matter quantities are kept equal to their standard values

### 4. Breathing mode

Beside the typical set of experimental data, we also include in our fit for the first time the experimental data on the breathing-mode energy for four nuclei, namely, $^{90}$Zr, $^{116}$Pb, $^{144}$Sm, and $^{208}$Pb [38]. We consider the fully self-consistent values for the breathing-mode constrained energy, given as

$$E_{\rm con} = \sqrt{\frac{m_1}{m_{-1}}}, \tag{2.109}$$

where $m_k$ are the energy moments

$$m_k = \int_0^\infty E^k S(E) dE, \tag{2.110}$$

of the response function

$$S(E) = \sum_n |\langle n \mid F \mid 0\rangle|^2 \, \delta(E - E_n). \tag{2.111}$$

The energy moments $m_k$ and the response function $S(E)$ will be discussed in Chapter IV. For the isoscalar giant monopole resonance, we have $F(r) = \sum_{i=1}^{A} f(r_i)$, with $f(r) = r^2$. The moments $m_k$ for $k = -1$ and 1 appearing in Eq. (2.109) can be obtained using the constrained HF (CHF) and the double-commutator sum rule, respectively [63, 64, 65]. The moment $m_1$ can be expressed in terms of the ground-state density $\rho$ as

$$m_1 = 2\frac{\hbar^2}{m}\langle r^2 \rangle, \tag{2.112}$$

where

$$\langle r^2 \rangle = \int r^2 \rho(r) d\mathbf{r}. \tag{2.113}$$

As described in detail in Ref. [63, 64, 65], $m_{-1}$ can be evaluated via the CHF approach and is given as,

$$m_{-1} = \frac{1}{2}\frac{d}{d\lambda}\langle r_\lambda^2\rangle\Big|_{\lambda=0}, \tag{2.114}$$

where $\langle r_\lambda^2\rangle = \langle \Phi_\lambda \left| r^2 \right| \Phi_\lambda\rangle$, where $\Phi_\lambda$ being the HF solution to the CHF Hamiltonian $H - \lambda f$.

# CHAPTER III

# SIMULATED ANNEALING METHOD FOR THE MINIMIZATION OF THE $\chi^2$ FUNCTION

## A. Statement of the problem

The simulated annealing method (SAM) is a generalization of a Monte Carlo technique, based on the Metropolis algorithm [37], initially developed for examining the equation of state (EOS) of a many-body system. The SAM is a popular technique for optimization problems of large scale, especially ones where a desired global extrema is hidden among many local extrema. The concept of SAM is an analogy with thermodynamics, in which liquids freeze or metals recrystallize in the process of annealing. In this process, at high temperature, a metal is disordered. The metal is gradually cooled down so that the system at any time is in thermodynamic equilibrium. The essence of the annealing process is slow cooling so that the metals have ample time to recrystallize. As cooling proceeds, the system becomes more ordered and approaches the state of minimum energy. This method has been used in many different areas of science [66, 67, 68] for minimization problems of large non-linear systems, and the SAM was used in Refs. [69, 70] to generate some initial trial parameter sets for the point coupling variant of the relativistic mean field model.

We use the SAM to determine the parameters of the new Skyrme type effective nucleon-nucleon interaction by searching for the global minimum in the hyper-surface of the $\chi^2$ function,

$$\chi^2 = \frac{1}{N_d - N_p} \sum_{i=1}^{N_d} \left( \frac{M_i^{\text{exp.}} - M_i^{\text{th.}}}{\sigma_i} \right)^2 , \tag{3.1}$$

with $N_d$ is the number of experimental data points, $N_p$ is the number of fitted parameters, $\sigma_i$ is the theoretical uncertainty and $M_i^{\text{exp.}}$ and $M_i^{\text{th.}}$ are the experimental

and the corresponding theoretical values, respectively, for a considered observable. The values of $\chi^2$ depends on the Skyrme parameters, since, the $M_i^{\text{th.}}$ in Eq. (3.1) is calculated by using the HF approach with a Skyrme type effective nucleon-nucleon interaction.

B. The procedure

We carry out the SAM to search for the global minimum of the $\chi^2$ function as given by Eq. (3.1). One of the main requirements in the SAM is to search the global minimum within the limits of parameters. In our case, we need to determine the lower and the upper limits for each of the Skyrme parameters. We know that the Skyrme parameters vary over a wide range [34, 59]. All the Skyrme parameters can be written in terms of the quantities related to the nuclear matter properties, as described in Sec. 3 of Chapter II. In the literature, the difference between the lower and the upper limits of these nuclear matter quantities vary within $10\% - 20\%$. To make the search process more efficient and convenient, we define a vector $\mathbf{v}$ with the components as nuclear matter quantities and other quantities

$$\mathbf{v} \equiv (B/A, K_{\text{n.m.}}, \rho_{\text{n.m.}}, m^*/m, E_s, J, L, \kappa, G_0', W_0). \tag{3.2}$$

Where $B/A$, $K_{\text{n.m.}}$, $\rho_{\text{n.m.}}$, $m^*/m$, $E_s$, $J$, $L$, $\kappa$, $G_0'$, and $W_0$ are the binding energy per nucleon, incompressibility coefficient, nuclear matter density, effective mass, surface energy, symmetry energy coefficient, the quantity which is related to the slope of the symmetry energy coefficient ($L = 3\rho dJ/d\rho$), the IVGDR EWSR enhancement factor, Landau parameter, and the Skyrme spin-orbit parameter, respectively. We search for the global minimum for the $\chi^2$ function within these limits of the component of vector $\mathbf{v}$. If we know the value of the vector $\mathbf{v}$, then we can calculate the values of all the

Skyrme parameters as discussed in Sec. 3 of Chapter II. We also define the vectors $\mathbf{v}_0$ as the lower limit, $\mathbf{v}_1$ as the upper limit, and $\mathbf{d}$ as the maximum displacement allowed in a single step for the components of the vector $\mathbf{v}$. Following the Metropolis algorithm, we implement the SAM algorithm using the following steps,

(1) Start with an initial value for the vector $\mathbf{v}$ and calculate $\chi^2$ (namely, $\chi^2_{\rm old}$) using Eq. (3.1) for a given set of the experimental data and the corresponding HF results, together with the theoretical errors.

(2) Generate randomly a new set of Skyrme parameters by first using a uniform random number to select a component $v_r$ of the vector $\mathbf{v}$, and then change the value of $v_r$ by a second random number $\eta$ by

$$v_r \rightarrow v_r + \eta d_r, \tag{3.3}$$

with $-1 < \eta < 1$. The second step is repeated until the new value of $v_r$ is found within its allowed limits of $\mathbf{v}$. We then use this modified $\mathbf{v}$ to generate a new set of Skyrme parameters. It may be noted that a change in the value of a component of the vector $\mathbf{v}$ may lead to changes in the values of several Skyrme parameters.

(3) The newly generated set of the Skyrme parameters is accepted by using the Metropolis algorithm as follows. We calculate the quantity

$$\mathcal{P}(\chi^2) = e^{(\chi^2_{\rm old} - \chi^2_{\rm new})/T}, \tag{3.4}$$

where $\chi^2_{\rm new}$ is obtained by using the newly generated set of the Skyrme parameters and $T$ is a control parameter (an effective temperature). The new set of

Skyrme parameters is accepted only if

$$\mathcal{P}(\chi^2) > \beta, \tag{3.5}$$

where $\beta$ is a uniform random number that lies between 0 and 1. If the new Skyrme parameters are accepted [i.e. Eq. (3.5) is satisfied], it is called a "successful reconfiguration".

We start with a reasonable value of the control parameter (the effective temperature) $T = T_i$ to search for the global minimum of the $\chi^2$ function. With initial value of $T_i$, we repeat steps (2) and (3) for, say, $100N_p$ reconfigurations, or for $10N_p$ successful reconfigurations, whichever comes first. Then, the effective temperature is reduced by following a suitable annealing schedule, we use the Cauchy annealing schedule [68] given by

$$T(k) = T_i/ck, \tag{3.6}$$

where $c$ is a constant, which is taken to be unity, and $k = 1, 2, 3, .....$ is the time index. One keep on reducing the value of $T$ by using Eq. (3.6) in the subsequent steps until the effort to reduce the value of $\chi^2$ further becomes sufficiently discouraging. The values of all the components of the vectors $\mathbf{v}$, $\mathbf{v}_0$, $\mathbf{v}_1$ and $\mathbf{d}$ used in the numerical computation are showed in Table II. We have varied the components of the vector $\mathbf{v}$ over a wide range. The values of the maximum displacement as defined by the components of $\mathbf{d}$ are so chosen that the corresponding component of the vector $\mathbf{v}$ can be varied over the entire range given by the vectors $\mathbf{v_0}$ and $\mathbf{v_1}$, within the adopted number of reconfigurations. We have carried out several sample runs and found that $T_i = 1.25$ along with the Cauchy annealing schedule yields reasonable values of the Skyrme parameters. We must mention here that the range for the quantities $L$, $\kappa$ and $G_0'$ as given in Table II are so chosen that they vary within acceptable limits [50].

TABLE II. Values of the components of the vectors $\mathbf{v}$, $\mathbf{v}_0$, $\mathbf{v}_1$ and $\mathbf{d}$ used for implementing the SAM based algorithm for searching the global minimum of $\chi^2$ . The vector $\mathbf{v}$ initializes the value of $\chi^2$, whereas, $\mathbf{v}_0$ and $\mathbf{v}_1$ limits the search space for the Skyrme parameters. The components of the vector $\mathbf{d}$ correspond to the maximum displacements allowed for the reconfiguration.

| | $\mathbf{v}$ | $\mathbf{v}_0$ | $\mathbf{v}_1$ | $\mathbf{d}$ |
|---|---|---|---|---|
| $B/A$(MeV) | 16.0 | 17.0 | 15.0 | 0.40 |
| $K_{nm}$(MeV) | 230.0 | 200.0 | 300.0 | 20.0 |
| $\rho_{nm}$(fm$^{-3}$) | 0.160 | 0.150 | 0.170 | 0.005 |
| $m^*/m$ | 0.70 | 0.60 | 0.90 | 0.04 |
| $E_s$(MeV) | 18.0 | 17.0 | 19.0 | 0.3 |
| $J$(MeV) | 32.0 | 25.0 | 40.0 | 4.0 |
| $L$(MeV) | 47.0 | 20.0 | 80.0 | 10.0 |
| $\kappa$ | 0.25 | 0.1 | 0.5 | 0.1 |
| $G'_0$ | 0.08 | 0.00 | 0.40 | 0.10 |
| $W_0$ (MeV.fm$^5$) | 120.0 | 100.0 | 150.0 | 5.0 |

## C. Set of experimental data and constraints

Beside the typically used experimental data on the binding energy, charge radii and spin-orbit splitting, our set of experimental data also include radii of valence neutron orbits and the breathing mode energies of several nuclei, as shown in Table III. These experimental data are taken from Refs. [1, 3, 4, 5, 6, 7, 38]. For the fitting procedure, we take the error of 1.0 MeV for the binding energy except for the $^{100}$Sn nuclei. The binding energy for the $^{100}$Sn nucleus is determined from systematics and is predicted to have large uncertainty. Therefore, we take a theoretical error of 2.0 MeV for this case. We assign the theoretical error of 0.02 fm for the charge rms radii except for the case of $^{56}$Ni nucleus. The charge rms radius for the $^{56}$Ni nucleus is calculated from systematics and we take the theoretical error of 0.04 fm. The experimental data on the spin-orbit splittings for the $2p$ neutrons and protons in the $^{56}$Ni nucleus are taken from Ref. [7],

$$\epsilon(2p_{1/2}) - \epsilon(2p_{3/2}) = \begin{cases} 1.88\text{MeV} & \text{Neutrons} \\ 1.83\text{MeV} & \text{Protons.} \end{cases} \tag{3.7}$$

Here $\epsilon$ is the "bare" single-particle energy determined by unfolding the experimental data for the energy levels in $^{57}$Ni and $^{57}$Cu nuclei by appropriately accounting for the coupling to excitations of the core. For the rms radii of the valence neutron orbits in $^{17}$O and $^{41}$Ca nuclei we use $r_v(\nu 1d_{5/2}) = 3.36$ fm and $r_v(\nu 1f_{7/2}) = 3.99$ fm [5, 6], respectively. The theoretical error taken for the spin-orbit splitting data is 0.2 MeV and for the rms radii for the valence neutron orbits we use the experimental error of 0.06 fm. The choice of the theoretical error on the rms radii for the valence neutron orbits is due to the large uncertainties associated with their extraction from the experimental measurements. We do not include the center of mass correction to these data, consistent with the method used in the experimental analysis.

TABLE III. Selected experimental data for the binding energy $B$, charge rms radius $r_{\text{ch.}}$, rms radii of valence neutron orbits $r_v$, spin-orbit splitting S-O, breathing mode constrained energy $E_0$ and critical density $\rho_{\text{cr.}}$ used in the fit to determine the parameters of the Skyrme interaction.

| Properties | Nuclei | Ref. |
|---|---|---|
| $B$ | $^{16,24}$O, $^{34}$Si, $^{40,48}$Ca, $^{48,56,68,78}$Ni, $^{88}$Sr, $^{90}$Zr, $^{100,132}$Sn, $^{208}$Pb | [1] |
| $r_{\text{ch.}}$ | $^{16}$O, $^{40,48}$Ca, $^{56}$Ni, $^{88}$Sr, $^{90}$Zr, $^{208}$Pb | [3, 4] |
| $r_v(\nu 1d_{5/2})$ | $^{17}$O | [5] |
| $r_v(\nu 1f_{7/2})$ | $^{41}$Ca | [6] |
| S-O | $2p$ orbits in $^{56}$Ni | [7] |
| $\rho_{\text{cr.}}$ | nuclear matter | see text |
| $E_0$ | $^{90}$Zr, $^{116}$Sn, $^{144}$Sm, $^{208}$Pb | [38] |

The experimental data for the breathing mode constrained energies $E_0$ included in our fit are 17.81, 15.90, 15.25 and 14.18 MeV for the $^{90}$Zr, $^{116}$Sn, $^{144}$Sm and $^{208}$Pb nuclei [38], respectively, with the theoretical error taken to be 0.5 MeV for the $^{90}$Zr nucleus and 0.3 MeV for the other nuclei. We also include the critical density $\rho_{\text{cr.}}$ in the fit assuming a value of $2.5\rho_0$ with an error of $0.5\rho_0$. Further, the values of the Skyrme parameters are constrained by requiring that (1) $P \geq 0$ for $\rho \leq 3\rho_0$ ($P \equiv L$ at $\rho = \rho_{\text{n.m.}}$), (2) $\kappa = 0.1 - 0.5$ and (3) $G_0' \geq 0$ at $\rho = \rho_0$.

### D. Results and discussion

We use the SAM to fit the values of the Skyrme parameters to the given set of the experimental data (see Table III). We carry out two different fits with the same set of experimental data along with some constraints as discussed in Sec. C. The results

for the Skyrme parameters are denoted by [9]

(1) KDE0, only the Coulomb direct term in the form of Eq. (2.61) is included,

(2) KDE, the direct and the Coulomb exchange terms in Eqs.(2.59)-(2.62) are included.

The CM corrections, not only to the total binding energy, Eqs. (2.67) and (2.68), but also to the charge rms radii, Eqs. (2.69) and (2.70), are analyzed with the some simple approximations described in Sec. 2 of Chapter II.

As we discuss the SAM earlier, there are two important points that control the calculation time and the quality of the fit: (1) initial value for the control parameter $T = T_i$ and (2) annealing schedule that determines the subsequent value for $T$. If we start with a smaller value of $T_i$, or use a faster annealing schedule, we can miss the global minimum of the objective function and also may get stuck in one of the local minima that we do not want. There are several annealing schedules such as linear, exponential, Boltzmann, and Cauchy. The Boltzmann schedule is the slowest one, and the exponential annealing schedule is the fastest one. We use the Cauchy annealing schedule which has a faster cooling rate than that of the Boltzmann schedule, but, a slower rate than the exponential annealing schedule. We find that with $T_i = 1.25$ and the Cauchy annealing schedule given in Eq. (3.6), reasonable values for the best-fit parameters are obtained. For checking the quality of the fit, we start with the final values of the Skyrme parameters obtained from the SAM and try to minimize further the value of $\chi^2$ using the Levenberg-Marquardt (LM) method [71] as conventionally used, but we find no further decrease in the value of the $\chi^2$. Fig. 5 shows the average value $\langle\chi^2\rangle_T$ as an inverse function of the effective temperature $T$ for the KDE0 interaction. The value of $\langle\chi^2\rangle_T$ is determined by averaging over all the successful reconfigurations for a given $T$. The curves labeled $v$ (solid line) and

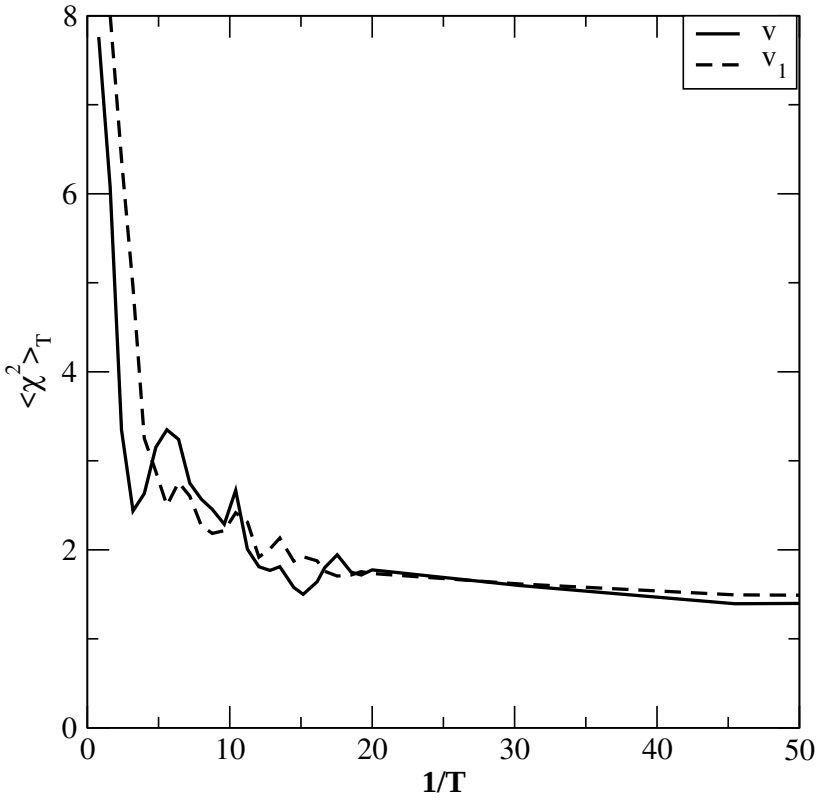


FIG. 5. Variation of the average value of chi-square, $\langle \chi^2 \rangle_T$, as a function of the inverse of the control parameter $T$ for the KDE0 interaction for the two different choices of the starting parameters.

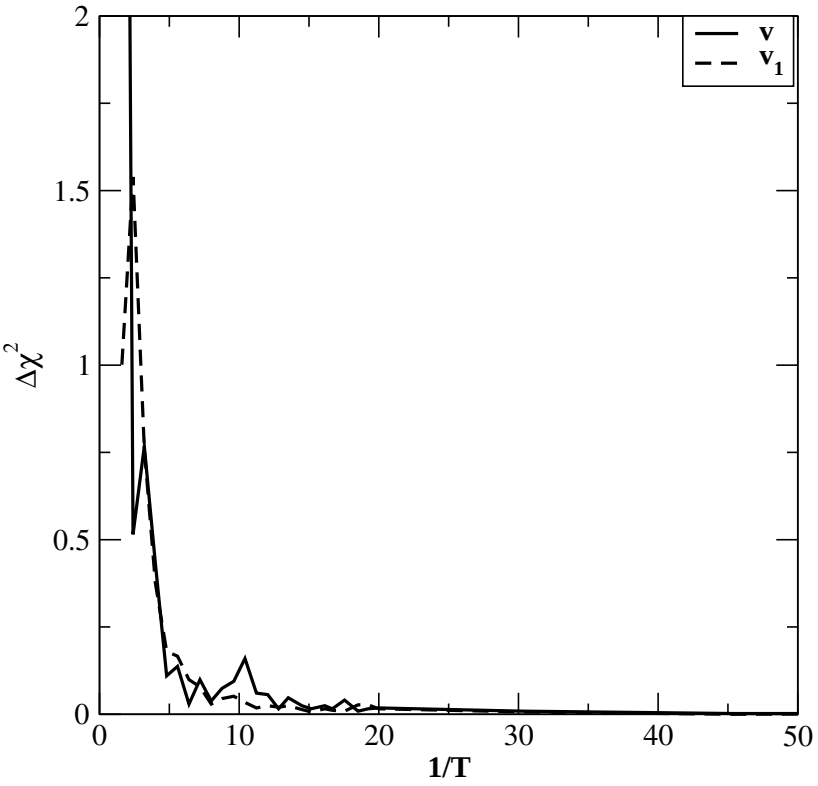


FIG. 6. Variation of the fluctuations $\Delta\chi^2_T$ in the value of $\chi^2$ as a function of $1/T$ for the KDE0 interaction for the two different choices of the starting parameters (see text for detail).

$v_1$ (dashed line) (their values are given in Table II) show the results obtained from two different choices of the starting values for the Skyrme parameters. We see from Fig. 5 that the value of $\langle\chi^2\rangle_T$ decreases rapidly at initial stages and then oscillates before saturating to a minimum value for $T \leq 0.05$. The value of $\chi^2$ at lower $T$ is almost independent of the starting values for the Skyrme parameters. The variation of $\Delta\chi^2_T = \langle(\chi^2 - \langle\chi^2\rangle)^2\rangle_T$ as an inverse function of $T$ is presented in Fig. 6. We can see that as $T$ decreases the fluctuations of $\chi^2$ also decrease rapidly. From this investigation, the initial value for the control parameter $T$ should not be too small,

because at smaller $T$ it is less likely to jump from a configuration with lower value of $\chi^2$ to one having a higher value. Therefore, it is possible to get trapped in a local minima. In Table IV, the values of the parameters for the KDE0 interaction at the minimum value of the $\chi^2$ are obtained from different choices for the starting values for the Skyrme parameters. We can see that the final value of the $\chi^2$ and the resulting Skyrme parameters are less sensitive to the choice of the initial parameters. The starting values to generate KDE0 and KDE are the components of $\mathbf{v}_0$ given in Table II.

The values of the Skyrme parameters obtained from the fits and the standard deviations are showed in Table V. The values of the standard deviations on the parameters for the KDE0 and KDE interactions are obtained from the LM method. The LM method requires the set of the experimental data and the starting values of the interaction parameters. The set of experimental data is the one used to generate the KDE0 and KDE interactions. The starting values of the interactions parameters used are the ones obtained using SAM for the KDE0 and KDE interactions. The values for the quantities characterizing the nuclear matter calculated at the minimum value of the $\chi^2$ for KDE0 and KDE interaction are showed in Table VI and compared to those obtained from SLy7 interaction. We note that the values of the $K_{\text{n.m.}}$ and $m^*/m$ come out automatically from the fitting, unlike the SLy type interactions where the values for these quantities were fixed. The values of the $K_{\text{n.m.}}$ and $m^*/m$ in our fitting are constrained by including the experimental data on breathing-mode energy and the value of critical density $\rho_{cr} = 2.5\rho_0 \pm 0.5\rho_0$ [35, 50].

The deviation $\Delta B = B^{\text{exp.}} - B^{\text{th.}}$ for the values of the binding energy and the charge rms radii $r_{\text{ch.}}$ determined from KDE0, KDE, Sly7 [2] interactions are showed in Table VII and Table VIII, respectively. From Table VII for the KDE0 interaction the error in the binding energy is quite less than 0.5%, and in case of KDE interaction,

the error in the values of the binding energy is about $(0.6 - 1.0\%)$ for the $^{16}$O, $^{48}$Ni and $^{100}$Sn nuclei. We know that, for the SKX interaction, the binding energy for the $^{56}$Ni nucleus was not considered in the fit and for the $^{100}$Sn nucleus was included in the fit with the theoretical error of 1.0 MeV. We find that if one attempt to do so, the binding energy for the $^{56}$Ni becomes off by more than 3 MeV. In Table VIII, except for the $^{16}$O and $^{48}$Ca nuclei, the error in the charge rms radii for the KDE0 interaction is less than 0.5%. We emphasize that the experimental value $r_{\rm ch.}$ for $^{132}$Sn was not included in our fit, but our results are in very good agreement with the very recent experimental data [72]. In Table IX, the value of $\rho_{\rm cr.}$ is greater than $2\rho_0$. Our values for the radii of valence neutron orbits and the spin-orbit splittings are in reasonable agreement with the corresponding experimental data. In Table X, we see that the breathing mode constrained energies obtained for KDE0 and KDE interactions are close to the experimental data.

We can see from Table VII that the binding energy difference $B(^{48}\mathrm{Ca}) - B(^{48}\mathrm{Ni})$ = 67.23 and 64.02 MeV for the KDE0 and KDE interactions, respectively. The experimental value is 68.85 MeV. The difference in the case of SKX interaction is 66.3 MeV, which is about 1.0 MeV lower than the results for KDE0 interaction. We note that most of the Skyrme interactions that include the contribution from the exchange Coulomb term yield $B(^{48}\mathrm{Ca}) - B(^{48}\mathrm{Ni}) \approx 63$ MeV, which is about 6 MeV lower than the corresponding experimental value. In Table XI, the values obtained for the neutron skin, $r_n - r_p$, which is the difference between the rms radii for the point neutrons and protons density distributions, are shown for the KDE0 and KDE interactions. The values of the single-particle energies for the $^{40}$Ca and $^{208}$Pb nuclei [73, 74] are shown in Tables XII and XIII together with the available experimental data. We can see that the single-particle energies for the occupied states near the Fermi-energy are quite close to the experimental ones. We note that the experimental

single-particle energies are not included in our fit. The values of the symmetry energy coefficient $S(\rho)$ and the resulting EOS for pure neutron matter at higher densities ($\rho > 2\rho_0$) are the key to understand the various properties of neutron star [75, 76]. The proton fraction at any density depends significantly on the value of $S(\rho)$ at that density, which affects the chemical compositions as well as the cooling mechanism of the neutron star [77]. In Fig. 7, we present the variation of the symmetry energy $S$ as a function of the nuclear matter density $\rho$. The value of $S$ increases with density for $\rho < 3\rho_0$ for the KDE0 and KDE interactions. These interactions are suitable for studying the neutron star with masses close to the canonical one [34], because they yield $S > 0$ for $\rho < 4\rho_0$. In Fig. 8, we show the EOS for the pure neutron matter resulting from the KDE0 and KDE interactions and compare them with the ones obtained for SLy7 interaction and the realistic UV14+UVII model [14]. We do not include in our fit the neutron matter EOS of the realistic UV14+UVII interaction.

TABLE IV. Comparison of the parameters for the KDE0 interaction at the minimum value of $\chi^2$ obtained from different choices for the starting values of the Skyrme parameters.

| Parameter | KDE0($\mathbf{v}$) | KDE0($\mathbf{v}_1$) |
|---|---|---|
| $t_0$(MeV·fm$^3$) | -2526.5110 | -2553.0843 |
| $t_1$(MeV·fm$^5$) | 430.9418 | 411.6963 |
| $t_2$(MeV·fm$^5$) | -398.3775 | -419.8712 |
| $t_3$ (MeV·fm$^{3(1+\alpha)}$) | 14235.5193 | 14603.6069 |
| $x_0$ | 0.7583 | 0.6483 |
| $x_1$ | -0.3087 | -0.3472 |
| $x_2$ | -0.9495 | -0.9268 |
| $x_3$ | 1.1445 | 0.9475 |
| $W_0$(MeV·fm$^5$) | 128.9649 | 124.4100 |
| $\alpha$ | 0.1676 | 0.1673 |

TABLE V. The values of the Skyrme parameters for KDE0 and KDE interactions obtained by minimizing the $\chi^2$. For the sake of comparison we have also listed the values of the parameters for the SLy7 interaction. The values in parenthesis are the standard deviations for the corresponding Skyrme parameters.

| Parameter | KDE0 | KDE | SLy7 |
|---|---|---|---|
| $t_0$(MeV·fm$^3$) | -2526.5110 (140.6256) | -2532.8842 (115.3165) | -2482.41 |
| $t_1$ (MeV·fm$^5$) | 430.9418 (16.6729) | 403.7285 (27.6336) | 457.97 |
| $t_2$ (MeV·fm$^5$) | -398.3775 (27.3099) | -394.5578 (14.2610) | -419.85 |
| $t_3$(MeV·fm$^{3(1+\alpha)}$) | 14235.5193 (680.7344) | 14575.0234 (641.9932) | 13677.0 |
| $x_0$ | 0.7583 (0.0655) | 0.7707 (0.0579) | 0.8460 |
| $x_1$ | -0.3087 (0.0165) | -0.5229 (0.0298) | -0.5110 |
| $x_2$ | -0.9495 (0.0179) | -0.8956 (0.0270) | -1.0000 |
| $x_3$ | 1.1445 (0.0862) | 1.1716 (0.0767) | 1.3910 |
| $W_0$ (MeV·fm$^5$) | 128.9649 (3.3258) | 128.0572 (4.3943) | 126.00 |
| $\alpha$ | 0.1676 (0.0163) | 0.1690 (0.0144) | 0.1667 |

TABLE VI. Nuclear matter properties for the KDE0 and KDE interactions at the $\chi^2 = \chi^2_{\text{min.}}$.

| Parameter | KDE0 | KDE | SLy7 |
|---|---|---|---|
| $B/A$ (MeV) | 16.11 | 15.99 | 15.92 |
| $K_{\text{n.m.}}$(MeV) | 228.82 | 223.89 | 229.7 |
| $\rho_{\text{n.m.}}$ | 0.161 | 0.164 | 0.158 |
| $m^*/m$ | 0.72 | 0.76 | 0.69 |
| $E_s$ (MeV) | 17.91 | 17.98 | 17.89 |
| $J$ (MeV) | 33.00 | 31.97 | 31.99 |
| $L$ (MeV) | 45.22 | 41.43 | 47.21 |
| $\kappa$ | 0.30 | 0.16 | 0.25 |
| $G'_0$ | 0.05 | 0.03 | 0.04 |
| $\chi^2_{\text{min.}}$ | 1.3 | 2.2 | |

TABLE VII. Results for the total binding energy $B$ (in MeV) for several nuclei. The experimental data $B^{\text{exp.}}$ used to fit the Skyrme parameters were taken from [1]. The theoretical error $\sigma$ was taken to be 2.0 MeV for the $^{100}$Sn nucleus and 1.0 MeV for the other nuclei. In the third and fourth columns we give the values for $\Delta B = B^{\text{exp.}} - B^{\text{th.}}$ obtained from our new fits. The last column contains the values for $\Delta B$ for the SLy7 Skyrme interaction taken from Ref. [2].

| | | $\Delta B = B^{\text{exp.}} - B^{\text{th.}}$ | | |
|---|---|---|---|---|
| Nuclei | $B^{\text{exp.}}$ | KDE0 | KDE | SLy7 |
| $^{16}$O | 127.620 | 0.394 | 1.011 | -0.93 |
| $^{24}$O | 168.384 | -0.581 | 0.370 | |
| $^{34}$Si | 283.427 | -0.656 | 0.060 | |
| $^{40}$Ca | 342.050 | 0.005 | 0.252 | -2.85 |
| $^{48}$Ca | 415.990 | 0.188 | 1.165 | 0.11 |
| $^{48}$Ni | 347.136 | -1.437 | -3.670 | |
| $^{56}$Ni | 483.991 | 1.091 | 1.016 | 1.71 |
| $^{68}$Ni | 590.408 | 0.169 | 0.539 | 1.06 |
| $^{78}$Ni | 641.940 | -0.252 | 0.763 | |
| $^{88}$Sr | 768.468 | 0.826 | 1.132 | |
| $^{90}$Zr | 783.892 | -0.127 | -0.200 | |
| $^{100}$Sn | 824.800 | -3.664 | -4.928 | -4.83 |
| $^{132}$Sn | 1102.850 | -0.422 | -0.314 | 0.08 |
| $^{208}$Pb | 1636.430 | 0.945 | -0.338 | -0.33 |

TABLE VIII. Results for the charge rms radii $r_{\text{ch.}}$ (in fm). The experimental data used in the fit to determine the values of the Skyrme parameters are taken from Refs. [3, 4]. The theoretical error $\sigma$ were taken to be 0.04 fm for the $^{56}$Ni nucleus and 0.02 fm for the other nuclei. The values for $r_{\text{ch.}}$ were obtained from our new fits and are compared to the values for $r_{\text{ch.}}$ for the SLy7 Skyrme interaction, taken from Ref. [2].

| Nuclei | $r_{\text{ch.}}^{\text{exp.}}$ | KDE0 | KDE | Sly7 |
|---|---|---|---|---|
| $^{16}$O | 2.730 | 2.771 | 2.761 | 2.747 |
| $^{24}$O | | 2.778 | 2.771 | |
| $^{34}$Si | | 3.220 | 3.208 | |
| $^{40}$Ca | 3.490 | 3.490 | 3.479 | 3.470 |
| $^{48}$Ca | 3.480 | 3.501 | 3.488 | 3.495 |
| $^{48}$Ni | | 3.795 | 3.777 | |
| $^{56}$Ni | 3.750 | 3.768 | 3.750 | 3.758 |
| $^{68}$Ni | | 3.910 | 3.893 | |
| $^{78}$Ni | | 3.969 | 3.950 | 3.967 |
| $^{88}$Sr | 4.219 | 4.211 | 4.200 | |
| $^{90}$Zr | 4.258 | 4.266 | 4.101 | |
| $^{100}$Sn | | 4.480 | 4.457 | |
| $^{132}$Sn | 4.709 | 4.710 | 4.685 | 4.713 |
| $^{208}$Pb | 5.500 | 5.489 | 5.459 | 5.498 |

TABLE IX. Critical density $\rho_{\rm cr.}$, rms radii of the valence neutron orbits $r_v$, and spin-orbit splitting (S-O). The experimental values ( and the theoretical error $\sigma$) used in the fit to determine the Skyrme parameters are taken as follows: For the $\rho_{\rm cr.}$ we assume a value of $2.5\rho_0$ ($\sigma = 0.5\rho_0$); the values of $r_v$ were taken from Ref. [5, 6] ($\sigma = 0.06$ fm); and the spin-orbit in $^{56}$Ni were taken from Ref. [7] ($\sigma = 0.2$ MeV). In columns $3-6$ we give the results obtained from our new fits.

| | Experimental | KDE0 | KDE |
|---|---|---|---|
| $\rho_{cr}/\rho_0$ | 2.5 | 2.5 | 2.1 |
| $r_v(\nu 1d_{5/2})$(fm) | 3.36 | 3.42 | 3.41 |
| $r_v(\nu 1f_{7/2})$(fm) | 3.99 | 4.05 | 4.03 |
| $\epsilon_n(2p_{1/2}) - \epsilon_n(2p_{3/2})$ (MeV) | 1.88 | 1.84 | 1.81 |
| $\epsilon_p(2p_{1/2}) - \epsilon_p(2p_{3/2})$ (MeV) | 1.83 | 1.64 | 1.63 |

TABLE X. Comparison of the breathing-mode constrained energies (in MeV) obtained for the KDE0 and KDE interactions with the experimental data.

| Nucleus | Experimental | KDE0 | KDE |
|---|---|---|---|
| $^{90}$Zr | 17.81 | 17.98 | 17.91 |
| $^{116}$Sn | 15.90 | 16.42 | 16.36 |
| $^{144}$Sm | 15.25 | 15.53 | 15.47 |
| $^{208}$Pb | 14.18 | 13.64 | 13.60 |

TABLE XI. Results for the neutron skin, $r_n - r_p$ (in fm), for all the nuclei considered to obtain the KDE0 and KDE interactions.

| | $r_n - r_p$ | |
|---|---|---|
| Nuclei | KDE0 | KDE |
| $^{16}$O | -0.031 | -0.025 |
| $^{24}$O | 0.510 | 0.510 |
| $^{34}$Si | 0.189 | 0.192 |
| $^{40}$Ca | -0.051 | -0.046 |
| $^{48}$Ca | 0.158 | 0.159 |
| $^{48}$Ni | -0.282 | -0.274 |
| $^{56}$Ni | -0.056 | -0.052 |
| $^{68}$Ni | 0.175 | 0.174 |
| $^{78}$Ni | 0.287 | 0.285 |
| $^{88}$Sr | 0.095 | 0.096 |
| $^{90}$Zr | 0.064 | 0.065 |
| $^{100}$Sn | -0.081 | -0.078 |
| $^{132}$Sn | 0.220 | 0.217 |
| $^{208}$Pb | 0.160 | 0.155 |

TABLE XII. Single-particle energies (in MeV) for $^{40}$Ca nucleus.

| Orbits | Experimental | KDE0 | KDE |
|---|---|---|---|
| | Protons | | |
| $1s_{1/2}$ | $-50\pm11$ | -39.40 | -38.21 |
| $1p_{3/2}$ | – | -26.95 | -26.42 |
| $1p_{1/2}$ | $-34\pm6$ | -22.93 | -22.34 |
| $1d_{5/2}$ | — | -14.49 | -14.51 |
| $2s_{1/2}$ | $-10.9$ | -9.48 | -9.66 |
| $1d_{3/2}$ | $-8.3$ | -7.59 | -7.53 |
| $1f_{7/2}$ | $-1.4$ | -2.38 | -2.76 |
| | Neutrons | | |
| $1s_{1/2}$ | – | -47.77 | -46.13 |
| $1p_{3/2}$ | – | -34.90 | -33.92 |
| $1p_{1/2}$ | – | -30.78 | -29.73 |
| $1d_{5/2}$ | – | -22.08 | -21.66 |
| $2s_{1/2}$ | $-18.1$ | -17.00 | -16.78 |
| $1d_{3/2}$ | $-15.6$ | -14.97 | -14.48 |
| $1f_{7/2}$ | $-8.32$ | -9.60 | -9.58 |
| $2p_{3/2}$ | $-6.2$ | -4.98 | -5.15 |

TABLE XIII. Single-particle energies (in MeV) for $^{208}$Pb.

| Orbits | Experimental | KDE0 | KDE |
|---|---|---|---|
| | Protons | | |
| $1g_{9/2}$ | −15.43 | -17.85 | -17.34 |
| $1g_{7/2}$ | −11.43 | -13.77 | -13.39 |
| $2d_{5/2}$ | −9.70 | -11.37 | -11.23 |
| $1h_{11/2}$ | −9.37 | -9.87 | -9.68 |
| $2d_{3/2}$ | −8.38 | -9.43 | -9.30 |
| $3s_{1/2}$ | −8.03 | -8.67 | -8.62 |
| $1h_{9/2}$ | −3.77 | -4.00 | -3.99 |
| $2f_{7/2}$ | −2.87 | -2.78 | -3.00 |
| $1i_{13/2}$ | −2.16 | -1.62 | -1.72 |
| $3p_{3/2}$ | −0.95 | 0.60 | 0.26 |
| $2f_{5/2}$ | −0.47 | -0.19 | -0.42 |
| | Neutrons | | |
| $1h_{9/2}$ | −10.85 | -12.39 | -12.24 |
| $2f_{7/2}$ | −9.72 | -11.60 | -11.64 |
| $1i_{13/2}$ | −9.01 | -9.33 | -9.20 |
| $3p_{3/2}$ | −8.27 | -8.67 | -8.77 |
| $2f_{5/2}$ | −7.95 | -8.59 | -8.64 |
| $3p_{1/2}$ | −7.38 | -7.54 | -7.65 |
| $2g_{9/2}$ | −3.94 | -2.86 | -3.06 |
| $1i_{11/2}$ | −3.15 | -1.65 | -1.69 |
| $1j_{15/2}$ | −2.53 | -0.41 | -0.43 |
| $3d_{5/2}$ | −2.36 | -0.43 | -0.64 |
| $4s_{1/2}$ | −1.91 | 0.08 | -0.08 |
| $2g_{7/2}$ | −1.45 | 0.38 | 0.20 |
| $3d_{3/2}$ | −1.42 | 0.56 | 0.40 |

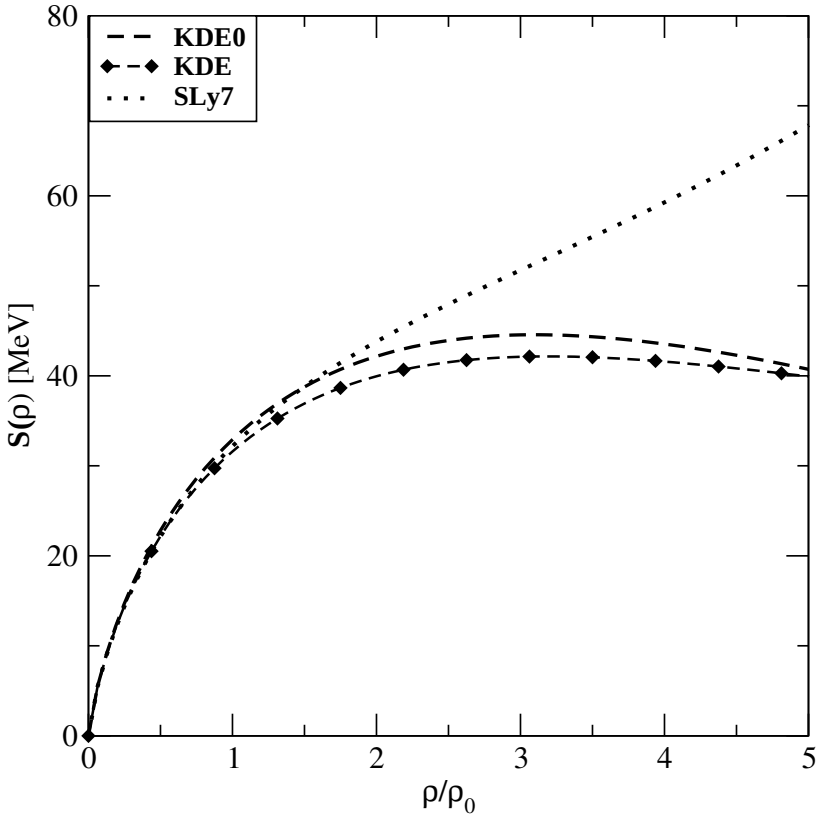


FIG. 7. Variation of the symmetry energy coefficient $S(\rho)$ as a function of the nuclear matter density $\rho$.

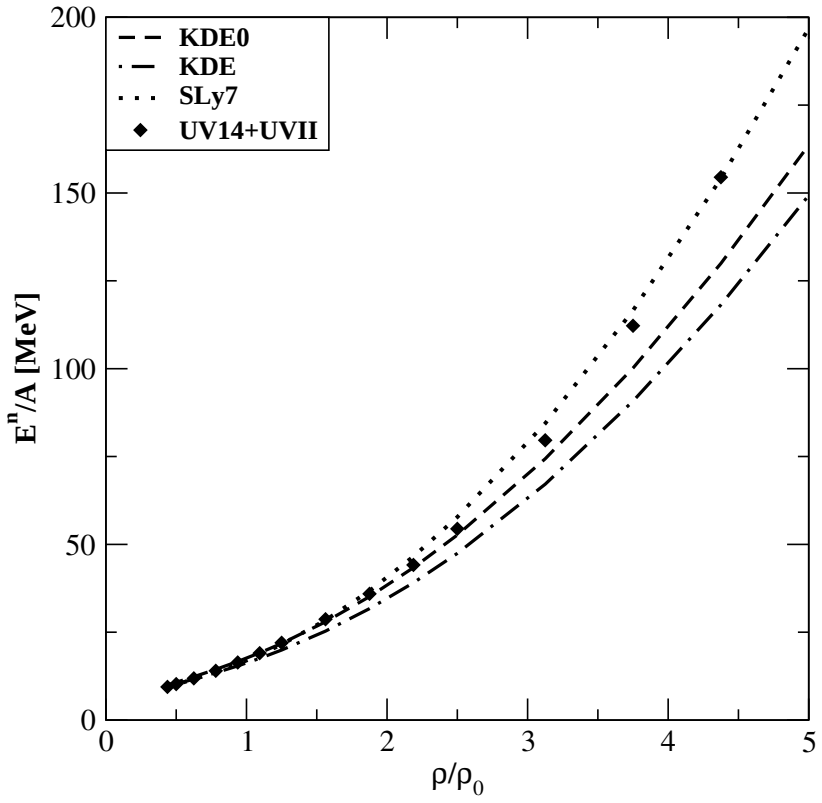


FIG. 8. Energy per particle for pure neutron matter $E^{(n)}/A$ as a function of density. Results for the two newly generated Skyrme interactions KDE0 and KDE are compared with those obtained for the SLy7 Skyrme force and the realistic UV14+UVII model of Wiringa et al. [14].

# CHAPTER IV

## HARTREE-FOCK BASED RANDOM PHASE APPROXIMATION DESCRIPTION OF NUCLEAR EXCITATIONS

### A. Nuclear response in the coordinate space

We have learned from Chapter II that for the nuleus many-body system, the Hartree-Fock (HF) method describes well the properties of ground state of nuclei and the characteristics of the single-particle excitations, i.e., the HF is a good model for describing the ground-state properties of the nucleus. But in order to describe the collective phenomena, one should take into account the residual nucleon-nucleon interaction. In this section, we summarize briefly one of the methods used successfully to describe the nuclear excitation due to a weak external field. The Random Phase Approximation (RPA) has been very successful in describing properties of both low excitation energy collective states and giant resonances in nuclei. In the RPA theory, the excited state of the nucleus are considered as a superposition of one particle-one hole (ph) excitations over the RPA correlated ground state. There are many formalisms of the RPA theory [78, 79, 80, 81, 82, 83], such as the matrix formulation, Green's function approach, collective coordinate RPA and the small amplitude time dependent Hartree-Fock (TDHF) approach. Also, different numerical methods for RPA calculations and the treatment of the single-particle continuum were developed and used [25, 84, 85, 86, 87, 88, 89, 90, 91, 92].

The continuum Green's function RPA method which was first introduced in Ref. [88] is a very fast numerical method for continuum RPA calculations. The RPA Green's function is given by

$$G^{\mathrm{RPA}} = G^0 \left[1 + V_{\mathrm{ph}} G^0\right]^{-1}, \tag{4.1}$$

where $V_{\rm ph}$ is the particle-hole interaction and $G^0$ is the free the p-h Green's function. In the case of a nucleon-nucleon Skyrme type interaction, the zero range particle-hole interaction can be obtained by functional differentiation of the energy density, $\mathcal{H}_{\rm I}(\mathbf{r})$, which is the sum of the Skyrme interaction and the kinetic energy density.

$$\begin{aligned} V_{\rm ph}(\mathbf{r}_1,\mathbf{r}_2) &= \delta(\mathbf{r}_1,\mathbf{r}_2)\sum_{s't't}\frac{1}{16}\left[1+(-1)^{s-s'}\vec{\sigma}_1\cdot\vec{\sigma}_2\right] \\ &\quad\times\left[1+(-1)^{t-t'}\vec{\tau}_1\cdot\vec{\tau}_2\right]\frac{\delta^2\mathcal{H}_{\rm I}}{\delta\rho_{st}\delta\rho_{s't'}}. \end{aligned} \tag{4.2}$$

The free p-h Green's function $G^0$ is given in terms of the HF Hamiltonian $H_0$, its occupied eigenstates $\phi_h$, and the eigenenergies $\varepsilon_h$, as

$$G^0(\mathbf{r}_1,\mathbf{r}_2,\omega) = -\sum_h \phi_h^*(\mathbf{r}_1)\left(\frac{1}{H_0-\varepsilon_h-\omega}+\frac{1}{H_0-\varepsilon_h+\omega}\right)\phi_h(\mathbf{r}_2). \tag{4.3}$$

The sum in Eq. (4.3) is over the occupied states. Note that the Eqs. (4.1) and (4.3) are operator equations in coordinate space. If $H_0$ has only a discrete spectrum, then the single-particle Green's function is evaluated in coordinate space as

$$\left(\frac{1}{H_0-E}\right)_{\mathbf{r}_1\mathbf{r}_2} = \sum_p \phi_p^*(\mathbf{r}_1)\frac{1}{\varepsilon_p-E}\phi_p(\mathbf{r}_2). \tag{4.4}$$

Substituting Eq. (4.4) into Eq. (4.3), we obtain a double sum, where the sum over $p$ is limited to unoccupied states, since the two terms in Eq. (4.3) will cancel contributions from occupied orbits. The single-particle Green's function with the famous representation [93, 94] for exact treatment of continuum is given as

$$g_{lj}(r_1,r_2,E) = \frac{1}{H_0-E} = -\frac{2m}{\hbar^2}u_{lj}(r_<)v_{lj}(r_>)/W, \tag{4.5}$$

where $u_{lj}$ is the regular solution of the HF Hamiltonian for the $lj$ partial wave and $v_{lj}$ is the irregular solution, and $r_<$ and $r_>$ are the lesser and the greater of $r_1$ and $r_2$, respectively.

The irregular solution is determined by the boundary condition at $r \rightarrow \infty$. For negative energies, this is

$$v(r) \simeq exp[-\sqrt{2mE/\hbar^2}r], \qquad r \rightarrow \infty. \tag{4.6}$$

For positive energies, $v(r)$ describes an outgoing wave asymptotically,

$$v(r) \simeq exp[i\sqrt{2mE/\hbar^2}r], \qquad r \rightarrow \infty. \tag{4.7}$$

The normalization of the Green's function is determined by the Wronskian, $W$,

$$W = u\frac{dv}{dr} - v\frac{du}{dr}. \tag{4.8}$$

The response function $S(E)$ and transition density $\hat{\rho}_t$ corresponding to a transition operator $\hat{F}$ are the quantities characterizing giant resonances. In general the transition operator has the form

$$\hat{F} = \sum \hat{f}(i), \tag{4.9}$$

with

$$\hat{f} = f(r)\left[Y_L \times S^\sigma\right]^J T^q. \tag{4.10}$$

where $J(= 1, 2, ...)$, $L = (0, 1, 2, ...)$, $\sigma = (0, 1)$ and $q = (0, 1)$ are the total angular momentum, orbital angular momentum, spin and isospin , respectively, transfered by the excitations. Note that $T^\tau = 1$ (isoscalar) or $\vec{\tau}$ (isovector) and $S^\sigma = 1$ (electric) or $\vec{\sigma}$ (magnetic).

The response function $S(E)$ is defined by

$$S(E) = \sum_n \left|\langle 0 \mid \hat{F} \mid n\rangle\right|^2 \delta(E_n - E_0 - E), \tag{4.11}$$

where the sum is over the complete set of eigenstates $\mid n\rangle$ with eigenenergies $E_n$ of the Hamiltonian $H$ of the many-body system. The energy moments $m_k$, which are

also sum rules, are given by

$$\begin{aligned} m_k &= \int E^k S(E) dE = \sum_n (E_n - E_0)^k \left| \langle 0 \mid \hat{F} \mid n \rangle \right|^2 \\ &= \langle 0 \mid \hat{F} (\mathcal{H} - E_0)^k \hat{F} \mid 0 \rangle. \end{aligned} \tag{4.12}$$

The energy weighted sum rule (EWSR) $m_1$ is written as

$$\sum_n (E_n - E_0) \left| \langle 0 \mid \hat{F} \mid n \rangle \right|^2 = \frac{1}{2} \langle 0 \mid [\hat{F}, [\mathcal{H}, \hat{F}]] \mid 0 \rangle. \tag{4.13}$$

A giant resonance is a state associated with a large fraction of the EWSR. The response function $S(E)$ is characterized by certain energies obtained from ratio of the energy moments $m_k$. The centroid energy, $E_{\rm c}$, constrained energy, $E_{\rm con}$ and scaling energy, $E_{\rm scal}$ are defined as

$$E_{\rm c} = \frac{m_1}{m_0}, \quad E_{\rm con} = \sqrt{\frac{m_1}{m_{-1}}}, \quad E_{\rm scal} = \sqrt{\frac{m_3}{m_1}}. \tag{4.14}$$

We can calculate the values of $m_1$, $m_{-1}$ and $m_3$ within the HF theory, see Chapter II. If the nucleon-nucleon interaction does not include momentum dependent parts then for an isoscalar single-particle operator $\hat{F} = \sum \hat{f}(\vec{r}_i)$ only the kinetic energy term contributes to the commutator $[\mathcal{H}, \hat{F}]$ and the EWSR becomes

$$m_1 = \frac{1}{2} \langle 0 \mid [\hat{F}, [\mathcal{H}, \hat{F}]] \mid 0 \rangle = \frac{\hbar^2}{2m} A \langle 0 \mid (\vec{\nabla} f)^2 \mid 0 \rangle. \tag{4.15}$$

Within the Greens' function RPA approach the strength function $S(E)$ is obtained from

$$S(E) = \sum_n \left| \langle 0 \mid \hat{F} \mid n \rangle \right|^2 \delta(E - E_n) = \frac{1}{\pi} Im \left[ Tr(\hat{f} G \hat{f}) \right], \tag{4.16}$$

and the transition density $\hat{\rho}_t = \rho_t(r) \left[ Y_L \times S^\sigma \right]^J T^q$ is obtained from

$$\hat{\rho}_t(E) = \frac{\Delta E}{\sqrt{S(E) \Delta E}} \frac{1}{\pi} Im[\hat{f} G]. \tag{4.17}$$

For the case of isoscalar electric resonance the scattering operator $\hat{f}$ has the form

$$\hat{f} = f(r)Y_L \tag{4.18}$$

The EWSR associated with isoscalar electric resonance is given as [82]

$$\begin{aligned} EWSR(\hat{f}) &= \int ES(E)dE = \frac{\hbar^2}{2m}\frac{A}{4\pi}(2L+1) \\ &\times \left[\langle 0 \mid \left(\frac{df}{dr}\right)^2 + L(L+1)\left(\frac{f}{r}\right)^2 \mid 0\rangle\right]. \end{aligned} \tag{4.19}$$

If there is only one collective state [82] with energy $E_{\rm coll}$, exhausting 100% of the EWSR associated with the scattering operator $\hat{f}_L = f(r)Y_L$, then the corresponding transition density, derived using the continuity equations, is given by

$$\begin{aligned} \rho^L_{\rm coll}(r) &= -\frac{\hbar^2}{2m}(2L+1)\sqrt{\frac{1}{EWSR(\hat{f})E_{\rm coll}}} \\ &\left[\left(\frac{1}{r}\frac{d^2}{dr^2}(rf) - \frac{L(L+1)}{r^2}f\right)\rho_0 + \frac{df}{dr}\frac{d\rho_0}{dr}\right]. \end{aligned} \tag{4.20}$$

For the ISGMR, we use the scattering operator

$$\hat{f}_0 = r^2 Y_{00}. \tag{4.21}$$

From Eqs. (4.19) and (4.20) we find that

$$EWSR(\hat{f}_0) = \frac{\hbar^2}{2m}\frac{A}{4\pi}\langle r^2\rangle, \tag{4.22}$$

with

$$\langle r^k\rangle = \frac{\int r^2\rho_0(r)r^k dr}{\int r^2\rho_0 dr}. \tag{4.23}$$

and the collective transition density associated with 100% of the EWSR is

$$\rho^0_{\rm coll}(r) = \left[2\pi\frac{\hbar^2}{mA\langle r^2\rangle E_{\rm coll}}\right]^{1/2}\left(3\rho_0 + r\frac{d\rho_0}{dr}\right). \tag{4.24}$$

For the ISGDR, the scattering operator

$$\hat{f}_1 = rY_{10} \tag{4.25}$$

leads to a coherent spurious state associated with the center of mass motion. We have

$$EWSR(\hat{f}_1) = \frac{\hbar^2}{2m}\frac{9A}{4\pi}, \tag{4.26}$$

and the corresponding spurious state transition density, $\rho_{\rm ss}$, has the form

$$\rho_{\rm ss} = \left[\frac{\hbar^2}{2m}\frac{4\pi}{AE_{\rm ss}}\right]^{1/2}\frac{d\rho_0}{dr}. \tag{4.27}$$

For a fully self-consistent HF-RPA calculation the spurious state appears at zero energy and no spurious state mixing (SSM) with the ISGDR takes place. However, in some numerical implementation of the HF-RPA theory, self-consistency is violated, leading to SSM in the ISGDR. It was shown in Refs. [95, 96] that in order to correct for the effects of SSM on $S(E)$ and $\rho_t$, the scattering operator $\hat{f}$ is replaced by

$$\hat{f}_\eta = \hat{f} - \eta\hat{f}_1, \tag{4.28}$$

where

$$\eta = \frac{\langle\hat{f}\rho_{\rm ss}\rangle}{\langle\hat{f}_1\rho_{\rm ss}\rangle}. \tag{4.29}$$

The revised ISGDR response function is written as

$$S_\eta(E) = \frac{1}{\pi}Im\langle\hat{f}_\eta G\hat{f}_\eta\rangle = S_3(E) - 2\eta S_{13}(E) + \eta^2 S_1(E), \tag{4.30}$$

where $S_3$ and $S_1$ are the response functions associated with $\hat{f}_3$ and $\hat{f}_1$, respectively, and

$$S_{13} = \frac{1}{\pi}Im\langle\hat{f}_1 G\hat{f}_3\rangle. \tag{4.31}$$

The revised transition density is obtained from

$$\rho_t(r) = \rho_\eta - a\rho_{ss}, \tag{4.32}$$

where $\rho_\eta$ is determined from Eq. (4.17) using $\hat{f}_\eta$ and

$$a = \frac{\langle \hat{f}_1 \rho_\eta \rangle}{\langle \hat{f}_1 \rho_{ss} \rangle}. \tag{4.33}$$

In theoretical investigations of the ISGDR, we adopt the scattering operator $\hat{f} = r^3 Y_1$. We have

$$\hat{f}_\eta = (r^3 - \eta r) Y_1 \tag{4.34}$$

where

$$\eta = \frac{5}{3}\langle r^2 \rangle. \tag{4.35}$$

Using Eqs. (4.19) and (4.20), we have the corresponding EWSR and $\rho_{\rm coll}$

$$EWSR(\hat{f}_\eta) = \frac{\hbar^2}{2m}\frac{3A}{4\pi}\left[11\langle r^4\rangle - \frac{25}{3}\langle r^2\rangle^2\right] \tag{4.36}$$

and

$$\rho^1_{\rm coll}(r) = \left[3\frac{\hbar^2 2\pi}{E_{\rm coll} mA\left[11\langle r^4\rangle - \frac{25}{3}\langle r^2\rangle^2\right]}\right]^{1/2}\left(10r\rho_0 + (3r^2 - \frac{5}{3}\langle r^2\rangle)\frac{d\rho_0}{dr}\right), \tag{4.37}$$

For isoscalar resonances of higher multi-polarities, $L \geq 2$, the scattering operator is given by

$$\hat{f}_L = r^L Y_L. \tag{4.38}$$

The EWSR, and $\rho_t$ obtained from Eqs. (4.19) and (4.20) are

$$EWSR(\hat{f}_L) = \frac{\hbar^2}{2m}\frac{A}{4\pi}L(2L+1)^2\langle r^{2L-2}\rangle, \tag{4.39}$$

$$\rho^{L\geq 2}_{\rm coll}(r) = \left[\frac{\hbar^2 2\pi}{mAE_{\rm coll}\langle r^{2L-2}\rangle}\right]^{1/2} r^{L-1}\frac{d\rho_0}{dr}. \tag{4.40}$$

## B. Description of the ISGMR in $^{90}$Zr, $^{116}$Sn, $^{144}$Sm, and $^{208}$Pb

In the fully self-consistent HF-RPA calculations, one starts with a specific effective nucleon-nucleon interaction $V_{ij}$ and solves the HF equations. Then one solves the RPA equations using the particle-hole (p-h) interaction $V_{ph}$ which is consistent with $V_{ij}$. Some available HF-RPA calculations are not fully self-consistent due to the following approximations: (i) Numerical accuracy and smearing parameter ($\Gamma/2$), (ii) Limiting the p-h space in a discretized calculations and (iii) $V_{ph}$ is not consistent with $V_{ij}$ by neglecting parts of the p-h interaction $V_{ph}$ such as the spin-orbit and Coulomb interactions. The consequences of these violations of self-consistency on the strength function $S(E)$ and the transition density $\rho_t(E)$ are often ignored. The error in the centroid energy (especially for ISGMR) can give large error in the extracted value of the incompressibility coefficient $K_{\text{n.m.}}$, due to the relation $\Delta K_{\text{n.m.}}/K_{\text{n.m.}} = 2\Delta E_{\text{cen.}}/E_{\text{cen.}}$. For example, the error $\Delta E_{\text{cen.}} \sim 1$ MeV on the centroid energy of the ISGMR for $^{208}$Pb can lead an error $\Delta K_{\text{n.m.}} \sim 30 - 40$ MeV for $K_{\text{n.m.}} = 200 - 300$ MeV. Note that the current experimental error in $E_{\text{cen.}}$ is about $0.2 - 0.3$ MeV. In this section we give the results of fully self-consistent HF-RPA calculations for the breathing mode for four nuclei, namely, $^{90}$Zr, $^{116}$Sn, $^{144}$Sm and $^{208}$Pb. In the Fig. 9 we show the strength functions and the centroid energies are given in Table XIV. We use the SGII and KDE0 Skyrme interactions. Note that these interactions are successful in reproducing not only the ground state properties but also the energies of the isoscalar giant monopole resonance excitation for nuclei. Our results for the centroid energy $E_0$ are very close to the experimental values. Note that for our KDE0 interaction the value of the symmetry energy coefficient $J$ and the incompressibility coefficient $K_{\text{n.m.}}$ are higher than the ones for SGII.

TABLE XIV. Fully self-consistent HF-RPA results for the ISGMR centroid energy $E_0 = m_1/m_0$ (in MeV) obtained using the interactions SGII [8], KDE0 [9] and compared with relativistic RPA results obtained with the NL3 interaction [10] (the energy range $\omega_1 - \omega_2$ (MeV) and the experimental data is taken from Refs. [11, 12]). The incompressibility ($K_{\text{n.m.}}$) and symmetry energy ($J$) coefficients are given in units of MeV.

| Nucleus | $\omega_1 - \omega_2$ | Expt. | NL3 | SGII | KDE0 |
|---|---|---|---|---|---|
| $^{90}$Zr | $0-60$ | | 18.7 | 17.9 | 18.1 |
| | $10-35$ | 17.81±0.30 | | 17.9 | 18.0 |
| $^{116}$Sn | $0-60$ | | 17.1 | 16.2 | 16.6 |
| | $10-35$ | 15.85±0.20 | | 16.2 | 16.6 |
| $^{144}$Sm | $0-60$ | | 16.1 | 15.3 | 15.5 |
| | $10-35$ | 15.40±0.40 | | 15.3 | 15.4 |
| $^{208}$Pb | $0-60$ | | 14.2 | 13.6 | 13.8 |
| | $10-35$ | 13.96±0.20 | | 13.6 | 13.8 |
| $K_{\text{n.m.}}$ | | | 272 | 215 | 229 |
| $J$ | | | 37 | 29 | 33 |

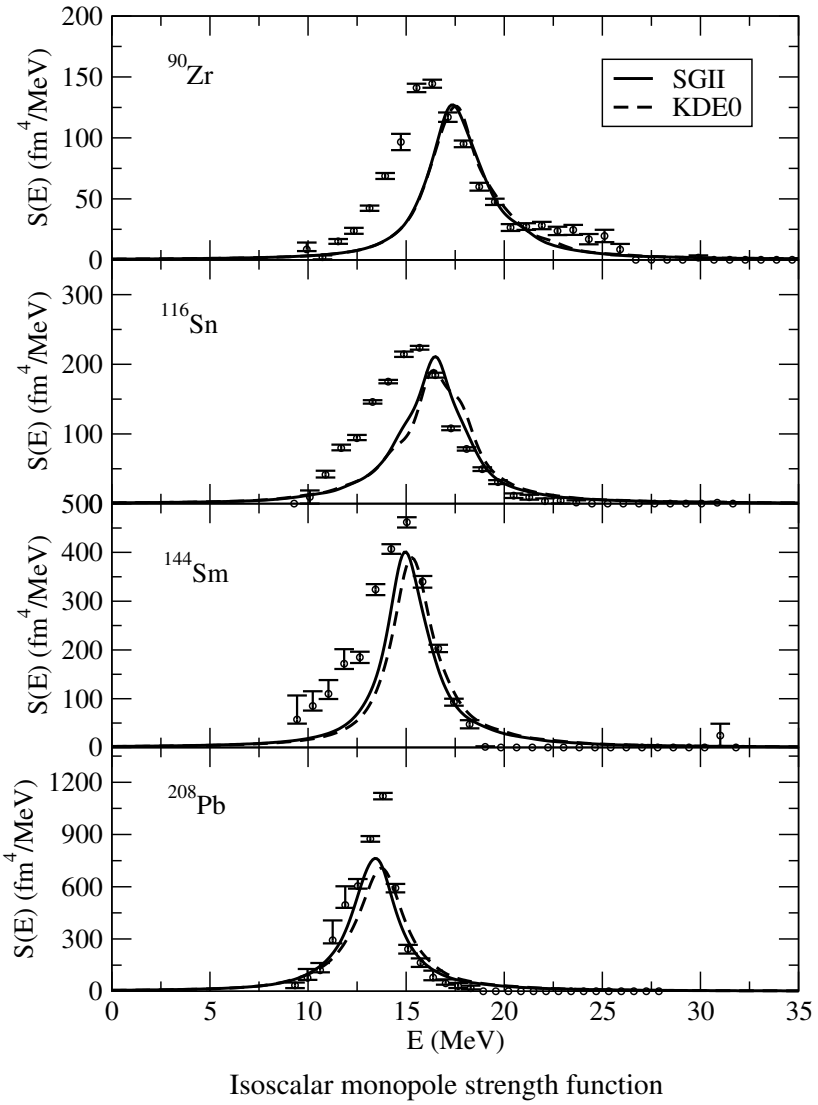


FIG. 9. Fully self-consistent HF-RPA results for the ISMGR strength functions of $^{90}$Zr, $^{116}$Sn, $^{144}$Sm, and $^{208}$Pb obtained using the interactions SGII and KDE0 and compared with the experimental data (circles with error bars) [11, 12].

## C. Nuclear matter incompressibility coefficient

An accurate nuclear matter equation of state (EOS), $E = E(\rho)$ is very important in the study of nuclear properties, heavy-ion collisions, neutron stars, and supernovas. From electron and particle scattering experiments and the extrapolation of an empirical mass formula, we know accurately only the saturation point $(\rho_0, E(\rho_0))$, where the density of nuclear matter is $\rho_0 = 0.16$ fm$^{-3}$, and the binding energy per nucleon is $E(\rho_0) = -16$ MeV. It is common to use the expansion,

$$E(\rho) = E(\rho_0) + \left(\frac{dE}{d\rho}\right)_{\rho_0} (\rho - \rho_0) + \frac{1}{18} K \left(\frac{\rho - \rho_0}{\rho_0}\right)^2 + .... \tag{4.41}$$

At ground state the second term vanishes and the symmetric nuclear matter incompressibility coefficient is defined as

$$K_{\text{n.m.}} = 9\rho_0^2 \left(\frac{d^2(E/A)}{d\rho^2}\right)_{\rho_0}. \tag{4.42}$$

Since $K_{\text{n.m.}}$ is directly related to the curvature of the EOS, an accurate value of $K_{\text{n.m.}}$ will extend our knowledge of the EOS around the saturation point. There have been many attempts to determine an accurate value of $K_{\text{n.m.}}$ over the years using properties of nuclei which are sensitive to a certain extent to $K_{\text{n.m.}}$ [97]. In a macroscopic approach which relies on the liquid drop model of expansion for the breathing mode restoring force, the value of $K$ was determined by a direct fit to the data. The value deduced for $K_{\text{n.m.}}$ is in the range of 100 to 400 MeV [98, 99]. We can see that for this approach, the constrain on the value $K$ is below 50%. In the microscopic approach, starting with many various effective two-body interactions which have different values of $K_{\text{n.m.}}$, but can reproduce the data of the other physical quantities, such as binding energies, radii; one then determines the effective interaction which can fit well the data for a physical quantity that is sensitive to $K_{\text{n.m.}}$.

The first two experimental observations of the isovector giant dipole resonance (IVGDR) by photon excitation [100] and the isoscalar giant quadrupole resonance (ISGQR) by using inelastic scattering of electrons and hardrons [101, 102] brought an extensive experimental and theoretical research on collective motion in nuclei. The measurements of the centroid energy of the isoscalar giant monopole resonance (ISGMR) provides a very sensitive method [82, 103] to determine the value of $K_{\text{n.m.}}$. Many attempts have been made to measure very accurately the value of the centroid energy $E_0$ of the ISGMR. The recent experimental data [38] for the $E_0$ in heavy nuclei are accurate enough (within $02 - 0.3$ MeV) to provide accurate information on the value of $K_{\text{n.m.}}$ (within 10 MeV).

During the 1970s, HF calculations using the Skyrme interaction for heavy nuclei became available. The parameters of the Skyrme type interaction improved over time to better reproduce the experimental data of a wide range of nuclei, such as nuclear mass, charge radii. Then the Skyrme parameters were additionally constrained by taking into account the experimental data on the nuclear giant resonances. The Hartree-Fock based random phase approximation (HF-RPA) calculations [19, 23] using the early introduced Skyrme interactions, which reproduced quite well the properties of the ground state nuclei, also reproduced quite well the available experimental data on isovector giant dipole resonance (IVGMR) and isoscalar giant quadrupole resonance (ISGQR). These interactions are associated with the value of about 370 MeV for $K_{\text{n.m.}}$. Using these interactions the ISGMR in $^{208}$Pb was predicted to be located at an excitation energy $E_0$ of about 18 MeV. The experimental observation for $E_0$ in $^{208}$Pb, at an excitation energy of 13.7 MeV [104], led to a revision of the existing effective Skyrme interaction. At present, the HF-RPA calculations with Skyrme [41, 42] and Gogny [105] interactions predict a value of $K_{\text{n.m.}}$ in the range of 210-220 MeV.

The experimental observation on the isoscalar giant dipole resonance (ISGDR) in $^{208}$Pb gives an excitation energy $E_1$ of about 21 MeV [106, 107, 108]. On the other hand, the value of $E_1$ obtained from HF-RPA calculation in [109], using the interaction which reproduced the experimental values of $E_0$, is higher than $E_1$ by more than 3 MeV. Therefore, the value of $K_{\text{n.m.}}$ deduced from ISGMR is quite larger than the one deduced from ISGDR. We note that this long-standing problem of the conflicting results deduced for $K_{\text{n.m.}}$ from data on the ISGDR and the ISGMR was explained by Shlomo and Sanzhur [95] as being due to a missing strength in the experimental data for the high energy region of the ISGDR.

The relativistic mean-field based RPA (RRPA) calculations, with the neglect of contribution from negative-energy sea, yielded for $K_{\text{n.m.}}$ a value in the range of 280-350 MeV [110]. With the inclusion of negative-energy states in the calculation of the response function, RRPA calculations [39, 40] yield a value of $K_{\text{n.m.}} = 250 - 270$ MeV. In a semi-classical approach $E_0 \propto \sqrt{K_{\text{n.m.}}}$, so the discrepancy of about 20% in $K$ obtained from relativistic and nonrelativistic models led to the uncertainty of 10% in value of $E_0$. This discrepancy is significant in view of the accuracy of about 2% in the experimental data on the ISGMR centroids energies. It was shown in Ref. [13] that the calculated value of $E_0$ can deviate by about 5% if the particle-hole space is quite limited and/or self-consistency is not properly maintained. In the literature, the values of the centroid energy $E_0$ for $^{208}$Pb, obtained for the same interaction, differs by up to 0.3 MeV [111, 112, 113]. It was claimed [111, 114] that this significant difference is due to the model dependence of $K_{\text{n.m.}}$. There have been some works to resolve this problem. It was pointed out in Ref. [115] that the differences in the values of $K_{\text{n.m.}}$ can come from the differences in the density dependence of the symmetry energy in relativistic and non-relativistic models. But the analysis in Ref. [115] was limited to the nucleus $^{208}$Pb and also the interaction parameters for the several families of the

effective Lagrangian considered were fitted only to the empirical values of saturation density, binding energy per nucleon in symmetric nuclear matter and the charge radius of $^{208}$Pb. In Ref. [116] a reasonable value of the centroid energy $E_0$ for $^{208}$Pb was obtained by using an effective interaction with $K_{\rm n.m.} = 400$ MeV, but in case of the $^{90}$Zr nucleus this effective interaction overestimated the value of $E_0$. Therefore, to explain the discrepancy between the relativistic and the non-relativistic calculations, one must compare the results obtained from these models for many nuclei.

We investigate systematically the discrepancy in the value of $K_{\rm n.m.}$, which is deduced from the ISGMR centroid energy, as obtained from relativistic and non-relativistic models. We generate different parameter sets for the Skyrme interaction and calculate the ISGMR strength function for several nuclei using the HF-RPA approach. In order for the comparison to be clear, our calculations using different parameter sets of Skyrme interaction are performed with the same procedure and numerical accuracy. The Skyrme parameters are obtained by a least square fit to the same experimental data for the nuclear binding energies, charge radii, and neutron radii as used in Ref. [10] for generating the NL3 parameter set for the effective Lagrangian used in the RMF model.

In a non-relativistic self-consistent HF-RPA calculation [84], one starts with a specific effective nucleon-nucleon interaction $V_{12}$ in Eq. (2.14). The parameters of the Skyrme interaction are obtained by fitting the HF results to a set of experimental data. Once the HF equations are solved using an appropriate parameter set for the Skyrme interaction, then one obtains the RPA Green's function Eq. (4.1) [84] For the single-particle operator

$$F = \sum_{i=1}^{A} f(\mathbf{r}_i), \tag{4.43}$$

the strength function is given by Eq. (4.16). The effective nucleon-nucleon interac-

tion in case of relativistic mean field models are generated through the exchange of many mesons. The effective Lagrangian representing a system of interacting nucleons, adopted for the NL3 interaction, has the form [10]

$$\begin{aligned}\mathcal{L} &= \bar{\psi}\left[\gamma\left(i\partial - g_\omega\omega - g_\rho\overrightarrow{\rho}\overrightarrow{\tau} - eA\right) - m - g_\sigma\sigma\right]\psi + \frac{1}{2}\left(\partial\sigma\right)^2 \\ &\quad -U(\sigma) - \frac{1}{4}\Omega_{\mu\nu}\Omega^{\mu\nu} + \frac{1}{2}m_\omega^2\omega^2 - \frac{1}{4}\overrightarrow{R}_{\mu\nu}\overrightarrow{R}^{\mu\nu} \\ &\quad +\frac{1}{2}m_\rho^2\overrightarrow{\rho}^2 - \frac{1}{4}F_{\mu\nu}F^{\mu\nu},\end{aligned} \tag{4.44}$$

with nucleons $\psi$ with mass $m$; $\sigma$, $\omega$, $\rho$ mesons; the electromagnetic fields; and non-linear self-interactions of the $\sigma$ field,

$$U(\sigma) = \frac{1}{2}m_\sigma^2\sigma^2 + \frac{1}{3}g_2\sigma^3 + \frac{1}{4}g_3\sigma^4. \tag{4.45}$$

The Lagrangian parameters are obtained in the same way as in the case of non-relativistic mean field calculations, by a fitting procedure to some bulk properties of a set of spherical nuclei [18]. The values of various coupling constants and the meson masses appearing in Eqs. (4.44) and (4.45) for the most widely used parameter set NL3 are $m_\sigma = 508.194$ MeV, $m_\omega = 782.501$ MeV, $m_\rho = 763.000$ MeV, $g_\sigma = 10.217$, $g_\omega = 12.868$, $g_\rho = 4.474$, $g_2 = -10.431$ fm$^{-1}$, and $g_3 = -28.885$.

Beside the same set of experimental data used in Ref. [10] for a least square fit, we consider the center of mass correction to the total binding energy, finite size effects of the proton, and the Coulomb energy in a similar way to that employed in determining the NL3 parameter set in Ref. [10]. However, pairing is not included in our HF calculations since we study seven closed shell nuclei instead of the ten nuclei in Ref. [10]. The open shell nuclei $^{58}$Ni, $^{124}$Sn, and $^{214}$Pb are excluded from our least square fit. We also neglect the proton and the neutron pairing gaps in $^{90}$Zr and $^{116}$Sn nuclei, respectively. We found that if we increase the error bars for the experimental

data on these two nuclei in order to compensate for the missing pairing interaction, the values of the Skyrme interaction parameters remain practically the same.

We generate a Skyrme interaction having $K_{\text{n.m.}} = 271.76$ and $J = 37.4$ MeV similar to those associated with the NL3 interaction. Also this set of parameters reproduce with high accuracy the root mean square charge radius of $^{208}$Pb. We denote this set of parameters as SK272. We also generate another set SK255 having characteristics very close to SK272 set, but with $K_{\text{n.m.}} = 255$ MeV. The value of the parameters of SK272 and SK255 are displayed in Table XV together with the parameters of SGII. In Table XVI we show the nuclear matter properties such as the saturation density $\rho_0$, effective nucleon mass $m^*/m$, the slope of the symmetry energy coefficient ($L = 3\rho_0\, dJ/d\rho_0$) obtained with the SK272 and SK255 interactions and compare them with those obtained with the NL3 and SGII interactions. In Table XVII we show the experimental data for the total binding energy $E$, charge radii $r_c$, and neutron radii $r_n$ used in Ref. [10] and in our least square fit, with error bars in percent. For comparison we show the corresponding values obtained from the SK272, SK255, NL3 and SGII interaction. From this table we can see that our results are in good agreement with those obtained with the NL3 and SGII interactions. The value of the difference between rms radii for neutrons and protons $\Delta r = r_n - r_p$, which is calculated by using $r_p = \sqrt{r_c^2 - 0.64}$, is neglected in the least square fit. We can see that the values of $\Delta r$ for the SK272, SK255, and NL3 interactions are closer, but are larger compared with the corresponding values for the SGII interaction. This is explained by noting that the values of the slope of the symmetry energy $L$ associated with the SK272, SK255, and NL3 interactions are quite larger than that associated with the SGII interaction (see Table XVI). As is shown in Ref. [57], the value of $\Delta r$ is very sensitive to the density dependent form adopted for the symmetry interaction.

It was demonstrated in Ref. [13] that the strength functions for giant resonances

are quite sensitive to the numerical approximations such as the size of the box used for the discretization of the continuum, limiting the maximum energy for the particle-hole excitations ($E_{ph}^{max}$) and the value of the smearing parameter ($\Gamma/2$) used to smear the strength function. In order to reproduce the results obtained in the continuum RPA calculation the size of the box must be consistent with the value used for the smearing width. For example, for $\Gamma/2 = 1$ MeV one must use a large box of size 72 fm. Our box size is 90 fm and $\Gamma/2 = 1$ MeV. We note [13] that to obtain an accurate value for the ISGMR centroid energy $E_0$, with an accuracy within 0.1 MeV, one must have $E_{ph}^{max} > 400$ MeV. The centroid energy is determined by $E_0 = m_1/m_0$, where $m_0$ and $m_1$ are the non-energy-weighted and energy-weighted sums of $S(E)$ of Eq. (4.16), respectively. Our lowest value of $E_{ph}^{max}$ is higher than 500 MeV. On the other hand, the centroid energy depends strongly on the range of the excitation energy interval of the giant resonance adopted to evaluate $E_0$. We note that in the published literature the excitation energy interval is sometime not given.

For example, in the case of the $^{208}$Pb nucleus using SGII interaction, we find that $E_0 = 13.7$, 13.9, 14.4 MeV with the excitation energy ranges 0-40, 0-60, and 10-40 MeV, respectively. These differences are very significant, since as we discussed earlier, a variation of 5% in $E_0$ corresponds to a change in $K_{\rm n.m.}$ by 10%. For the consistency of comparison, we used the energy range 0-60 MeV for $E_0$, since the RMF results in Ref. [111] for the NL3 parameter set were obtained using the same energy range and the strength function was smeared using $\Gamma/2 = 1$ MeV [117].

We show in Table XVIII the fully self-consistent HF-RPA results for the ISGMR centroid energy obtained by using the SK255 interaction and compare them with those obtained with the SGII Skyrme interaction and with the RRPA results of Ref. [111] for the NL3 interaction. The differences between the values of $E_0$ obtained from SK255 and NL3 interaction are within the uncertainty associated with the experimental data

for $E_0$. The values of $E_0$ for $^{208}$Pb nucleus for SK255 and SGII interaction are quite close within 0.3 MeV, however the difference in the values of $K_{\text{n.m.}}$ for these interaction is about 40 MeV. Therefore, with a fixed value of $E_0$ if we increase the value of $J$ by 10%, $K_{\text{n.m.}}$ will increase by about 5%. Therefore, from our investigation, we see that the discrepancy in the values of $K_{\text{n.m.}}$ obtained in the relativistic and non-relativistic models is mainly due to the differences in the values of the symmetry energy coefficient $J$ and its slope $L$ associated with these models. We also calculate the values of $E_0$ over the same energy range as used in experimental determination of the centroid energy [38]. As can be seen in Table XVIII, our results for $E_0$ with the SK255 interaction, calculated over the experimental excitation energy range, are a little bit higher than the experimental data, which is consistent with $K_{\text{n.m.}}$ being some what less than 255 MeV.

TABLE XV. Skyrme parameters for different interactions used in the present calculations. Value of the parameters for the SGII interaction are taken from Ref. [8].

| Parameter | SK272 | SK255 | SGII |
|---|---|---|---|
| $t_0$(MeV fm$^3$) | -1496.84 | -1689.35 | -2645 |
| $t_1$(MeV fm$^5$) | 397.66 | 389.30 | 340 |
| $t_2$(MeV fm$^5$) | -112.82 | -126.07 | -41.9 |
| $t_3$(MeV fm$^{3(1+\alpha)}$) | 10191.64 | 10989.60 | 15595 |
| $x_0$ | 0.0008 | -0.1461 | 0.09 |
| $x_1$ | 0.0102 | 0.1160 | -0.0588 |
| $x_2$ | 0.0020 | 0.0012 | 1.425 |
| $x_3$ | -0.5519 | -0.7449 | 0.06044 |
| $\alpha$ | 0.4492 | 0.3563 | 1/6 |
| $W_0$(MeV fm$^5$) | 106.58 | 95.39 | 105 |

TABLE XVI. Nuclear matter properties calculated from the RMF theory with the NL3 parameter set and the non-relativistic HF calculations with different Skyrme parameter sets. The "experimental data" are the ones used in Ref. [10] in the least square fit together with the bulk properties for finite nuclei in obtaining the NL3 parameter set. The values in parentheses represent the error bars (in percent) used in the fit.

| | Expt. | NL3 | SK272 | SK255 | SGII |
|---|---|---|---|---|---|
| $E/A$(MeV) | -16.0(5) | -16.299 | -16.280 | -16.334 | -15.67 |
| $K_{\rm n.m.}$ (MeV) | 250.0(10) | 271.76 | 271.55 | 254.96 | 214.57 |
| $\rho_0$ (fm$^{-3}$) | 0.153(10) | 0.148 | 0.155 | 0.157 | 0.159 |
| $m^*/m$ | | 0.60 | 0.77 | 0.80 | 0.79 |
| $J$ (MeV) | 33.0(10) | 37.4 | 37.4 | 37.4 | 26.8 |
| $L$ (MeV) | | 118.5 | 91.7 | 95.0 | 37.6 |

TABLE XVII. Experimental data for $E$, $r_c$, $r_n$, and the error bars (in percent) are used in the fit. $\Delta r = r_n - r_p$ is not included in the fit. For comparison, the results obtained from the SK272, SK255, NL3, SGII interactions are presented.

| Nucleus | Property | Expt. | NL3 | SK272 | SK255 | SGII |
|---|---|---|---|---|---|---|
| $^{16}$O | $E$ | -127.62(0.1) | -128.83 | -127.76 | -128.05 | -131.93 |
| | $r_c$ | 2.730(0.2) | 2.730 | 2.800 | 2.813 | 2.793 |
| | $r_n$ | | 2.580 | 2.662 | 2.674 | 2.650 |
| $^{40}$Ca | $E$ | -342.06(0.1) | -342.02 | -341.35 | -342.50 | -342.42 |
| | $r_c$ | 3.450(0.2) | 3.469 | 3.496 | 3.504 | 3.490 |
| | $r_n$ | 3.370(2.0) | 3.328 | 3.363 | 3.369 | 3.348 |
| | $\Delta r$ | 0.014 | -0.047 | -0.041 | -0.043 | -0.049 |
| $^{48}$Ca | $E$ | -416.00(0.1) | -415.15 | -414.17 | -413.89 | -418.22 |
| | $r_c$ | 3.451(0.2) | 3.470 | 3.524 | 3.531 | 3.526 |
| | $r_n$ | 3.625(2.0) | 3.603 | 3.635 | 3.649 | 3.582 |
| | $\Delta r$ | 0.268 | 0.227 | 0.203 | 0.210 | 0.147 |
| $^{90}$Zr | $E$ | -783.90(0.1) | -782.63 | -782.73 | -783.28 | -775.49 |
| | $r_c$ | 4.258(0.2) | 4.287 | 4.282 | 4.286 | 4.286 |
| | $r_n$ | 4.289(2.0) | 4.306 | 4.310 | 4.317 | 4.266 |
| | $\Delta r$ | 0.107 | 0.094 | 0.103 | 0.106 | 0.056 |
| $^{116}$Sn | $E$ | -988.69(0.1) | -987.67 | -982.37 | -984.48 | -971.66 |
| | $r_c$ | 4.627(0.2) | 4.611 | 4.617 | 4.619 | 4.630 |
| | $r_n$ | 4.692(2.0) | 4.735 | 4.696 | 4.701 | 4.639 |
| | $\Delta r$ | 0.135 | 0.194 | 0.149 | 0.152 | 0.079 |
| $^{208}$Pb | $E$ | -1636.47(0.1) | -1639.54 | -1631.78 | -1637.48 | -1622.21 |
| | $r_c$ | 5.503(0.2) | 5.520 | 5.503 | 5.503 | 5.519 |
| | $r_n$ | 5.593(2.0) | 5.741 | 5.687 | 5.694 | 5.597 |
| | $\Delta r$ | 0.148 | 0.279 | 0.243 | 0.250 | 0.136 |

TABLE XVIII. Fully self-consistent HF-RPA results for the ISGMR centroid energy (in MeV) obtained using the interactions SK255 [13] and SGII [8] and compared with the RRPA results obtained with the NL3 interaction [10] (the range of integration $\omega_1 - \omega_2$ is given in the second column and the experimental data are from Refs. [11, 12]).

| Nucleus | $\omega_1 - \omega_2$ | Experiment | NL3 | SK255 | SGII |
|---|---|---|---|---|---|
| $^{90}$Zr | 0-60 | | 18.7 | 18.90 | 17.89 |
| | 10-35 | 17.81± 0.30 | | 18.85 | 17.87 |
| $^{116}$Sn | 0-60 | | 17.1 | 17.31 | 16.36 |
| | 10-35 | 15.85± 0.20 | | 17.33 | 16.38 |
| $^{144}$Sm | 0-60 | | 16.1 | 16.21 | 15.26 |
| | 10-35 | 15.40± 0.40 | | 16.19 | 15.22 |
| $^{208}$Pb | 0-60 | | 14.2 | 14.34 | 13.57 |
| | 10-35 | 13.96± 0.20 | | 14.38 | 13.58 |

# CHAPTER V

## SUMMARY

The main purpose of this dissertation is to determine a new set of parameters of the Skyrme effective nucleon-nucleon interaction. Since the work of Vautherin and Brink [19], the effective Skyrme nucleon-nucleon interaction has been used in the mean-field models for many decades and proved successful to describe the ground state properties of nuclei. Many different parameterizations of the Skyrme interaction have been realized to better reproduce nuclear masses, radii, and various data. Most of the parameters of Skyrme interactions available in the literature are obtained by fitting Hartree-Fock result to experimental data on the bulk properties, such as charge radii, binding energies, and other nuclear experimental, for a few closed shell nuclei. Some of parameterizations of the Skyrme effective interactions have been constructed depending on the selected set of nuclear properties to be reproduced. Today there are more available experimental data for nuclei at and far from $\beta$-line. Therefore, we have generated a new set of Skyrme type interaction, named KDE0, which includes all the merits of many sets of existing Skyrme parameters.

We summarize here the details of the Hartree-Fock calculations using the KDE0 Skyrme interaction. In our mean-field results we carry out the center of mass correction not only to the binding energy but also for the charge radii. For the correction to the binding energy, we use the center of mass energy given in Eq. (2.67) and the oscillator frequency $\hbar\omega$ given in Eq. (2.68). With this simple approximation, our results agree quite well in the values of binding energy with the case of taking into account both the one and two body terms in Eqs. (2.66) [2]. For the correction to the charge radii, we use Eq. (2.70). There are many approaches for the Coulomb energy, used to account for the effects of long range correlation (LRC) and charge

symmetry breaking (CBS) in the strong nucleon-nucleon interaction. In our work we adopt the approach of including only the direct term of the Coulomb interaction. We use the stability conditions of the Landau parameters for symmetric nuclear matter and pure neutron matter to calculate the critical density $\rho_{\rm cr.}$ for the Skyrme parameters. We find that the critical density $\rho_{\rm cr.}$ can be maximized by adjusting the values of the IVGDR enhancement factor $\kappa$, the quantity $L$ associated with slope of the symmetry coefficient $J$, and the Landau parameter $G_0'$, as these quantities are not well determined by the Skyrme parameters, conventionally obtained by fitting the experimental data for the ground state properties of finite nuclei. We have applied restrictions on these quantities as follows: the range of the value of $\kappa$ is $0.25 - 0.5$, needed to describe the TRK sum rule for the isovector giant dipole resonance [31, 55]; $L > 0$ for $0 \leq \rho \leq 3\rho_0$, a condition necessary for a Skyrme interaction to be suitable for studying the properties of neutron star [34]; and $G_0' > 0$ to reproduce the energies of the isovector $M1$ and Gamow-Teller states [55, 58]. Our maximum value of the critical density $\rho_{\rm cr.}$ obtained is lower by up to 25% compared to the ones obtained without any such restrictions [35]. We show that the critical density obtained for realistic values of the surface energy coefficient ($E_s = 18 \pm 1$ MeV) and isoscalar effective mass ($m^*/m = 0.7 \pm 0.1$) is in the range of $2\rho_0 - 3\rho_0$. However, we do not include the effect of pairing correlations.

For the first time we use the simulated annealing method to determine the the parameters of the Skyrme effective nucleon-nucleon interaction of Eq. (2.14) by searching for the global minimum in the hyper surface of the $\chi^2$ function, Eq. (3.1). We obtain the Skyrme parameters by fitting the Hartree-Fock mean-field results to an extensive set of experimental data together with the additional constraints mentioned above. Our set of experimental data consists of the binding energies for 15 nuclei ranging from the normal to exotic (proton or neutron rich) ones, charge rms radii for

7 nuclei, spin-orbit splittings for the $2p$ proton and neutron orbits of the $^{56}$Ni nucleus and rms radii for $1d_{5/2}$ and $1f_{7/2}$ valence neutron orbits in the $^{17}$O and $^{41}$Ca nuclei, respectively, and the breathing mode energy for four nuclei. We also include in the fit the critical density $\rho_{cr}$ determined from the stability conditions for the Landau parameters. The purpose of selection of experimental data and additional constraints is to generate Skyrme parameters that describe well not only the ground-state properties of nuclei at and far from the stability line, but also the properties of neutron stars. We obtain two sets of Skyrme parameters, KDE0, only the Coulomb direct term is included; and KDE, the direct and Coulomb exchange terms are included. Our parameter sets for the Skyrme interaction include the merits of the recent parameters sets Sly [2, 31] and SKX [32]. We note here that the quality of the parameters can be improved by several ways. The set of experimental data can include the giant dipole and quadrupole resonances. The effects on the binding energy and radii due to the correlations beyond mean-field [118, 119, 120] can be included in the fit. These effects are, in particular, important for the light nuclei. One may also include in the spin-orbit splitting the contributions due to the electromagnetic spin-orbit interaction [7] and modify the spin-orbit interaction by using the form proposed by Sagawa in Ref. [121]. In the implementation of SAM, by randomly selecting a component of the vector $\mathbf{v}$ as defined by Eq. (3.2), we change from one configuration to another, we can perform random selection of a component of $\mathbf{v}$ by assigning a more plausible weight factors to these components. We can try different annealing schedules to determine the rate of cooling. In Chapter IV, we describe fully self-consistent HF-RPA calculations for the strength functions, and the centroid energies of the isoscalar giant monopole resonance for four nuclei using our set of Skyrme interaction KDE0 and compare to the ones obtained by using the SG2 interaction and the available experiment data. We also analyze in detail the recent claim that the nuclear matter

incompressibility coefficient $K_{\text{n.m.}}$ extracted from the ISGMR centroid energy calculated using the relativistic and non-relativistic based RPA models differ by about 20%. We have determined Skyrme parameter sets by a least square fitting procedure using the same experimental data for the bulk properties of nuclei considered in Ref. [10] for determining the NL3 parametrization of an effective Lagrangian used in the relativistic mean field models. In addition, the values of $K_{\text{n.m.}}$, $J$, and the charge radius of the $^{208}$Pb nucleus are fixed to be close to those obtained with the NL3 interaction. The values of $E_0$ for the deduced SK272 interaction are higher by about 5% compared to the corresponding NL3 results. This means that the discrepancy between the values of $K_{\text{n.m.}}$ obtained in the relativistic and the non-relativistic microscopic models would be only about 10% instead of 20%. The SK255 interaction with $K_{\text{n.m.}} = 255$ MeV gives values of the ISGMR centroid energies $E_0$ which are quite close to the NL3 results but a little bit higher than experimental data. From our investigation, we see that the discrepancy in the values of $K_{\text{n.m.}}$ obtained in the relativistic and non-relativistic models is mainly due to the differences in the values of the symmetry energy coefficient $J$ and its slope $L$ associated with these models.

# REFERENCES


[1] G. Audi, A. H. Wapstra, and C. Thibault, Nucl. Phys. **A729**, 337 (2003).

[2] E. Chabanat, P. Bonche, P. Haensel, J. Meyer, and R. Schaeffer, Nucl. Phys. **A635**, 231 (1998).

[3] E. W. Otten, *Treatise on Heavy-Ion Science,* Vol. 8*,* edited by D. A. Bromley (Plenum, New York, 1989).

[4] H. D. Vries, C. W. D. Jager, and C. D. Vries, At. Data Nucl. Data Tables **36**, 495 (1987).

[5] N. Kalantar-Nayestanaki, H. Baghaei, W. Bertozzi, S. Dixit, J. M. Finn, C. E. Hyde-Wright, S. Kowalski, R. W. Lourie, C. P. Sargent, P. E. Ulmer, L. Weinstein, M. V. Hynes, B. L. Berman, and J. J. Kelly, Phys. Rev. Lett. **60**, 1707 (1988).

[6] S. Platchkov, A. Amroun, P. Bricault, J. M. Cavedon, P. K. A. de Witt Huberts, P. Dreux, B. Frois, C. D. Goodman, D. Goutte, J. Martino, V. Meot, G. A. Peterson, X. H. Phan, S. Raman, and I. Sick, Phys. Rev. Lett. **61**, 1465 (1988).

[7] L. Trache, A. Kolomiets, S. Shlomo, K. Heyde, C. A. Gagliardi, R. E. Tribble, X. G. Zhou, V. E. Iacob, and A. M. Oros, Phys. Rev. C **54**, 2361 (1996).

[8] N. V. Giai and H. Sagawa, Phys. Lett. **B106**, 379 (1981).

[9] B. K. Agrawal, S. Shlomo, and V. K. Au, Phys. Rev. C **72**, 014310 (2005).

[10] G. A. Lalazissis, J. Konig, and P. Ring, Phys. Rev. C **55**, 540 (1997).

[11] D. H. Youngblood, Y.-W. Lui, H. L. Clark, B. John, Y. Tokimoto, and X. Chen, Phys. Rev. C **69**, 034315 (2004).

[12] D. H. Youngblood, Y.-W. Lui, B. John, Y. Tokimoto, H. L. Clark, and X. Chen, Phys. Rev. C **69**, 054312 (2004).

[13] B. K. Agrawal, S. Shlomo, and V. K. Au, Phys. Rev. C **68**, 031304(R) (2003).

[14] R. B. Wiringa, V. Fiks, and A. Fabrocini, Phys. Rev. C **38**, 1010 (1988).

[15] T. Hamada and I. D. Johnston, Nucl. Phys. **34**, 382 (1962).

[16] G. Breit, Rev. Mod. Phys. **34**, 766 (1962).

[17] R. V. Reid, Ann. Phys. **50**, 411 (1968).

[18] P. G. Reinhard, Rep. Prog. Phys. **52**, 439 (1989).

[19] D. Vautherin and D. M. Brink, Phys. Rev. C **5**, 626 (1972).

[20] T. H. R. Skyrme, Phil. Mag. **1**, 1043 (1956).

[21] J. S. Bell and T. H. R. Skyrme, Phil. Mag. **1**, 1055 (1956).

[22] T. H. R. Skyrme, Nucl. Phys. **9**, 615 (1959).

[23] M. Beiner, H. Flocard, N. V. Giai, and P. Quentin, Nucl. Phys. **A238**, 29 (1975).

[24] D. H. Youngblood, C. M. Rozsa, J. M. Moss, D. R. Brown, and J. D. Bronson, Phys. Rev. Lett. **39**, 1188 (1977).

[25] J. P. Blaizot, Phys. Rep. **64**, 171 (1980).

[26] H. Krivine, J. Treiner, and O. Bohigas, Nucl. Phys. **A336**, 155 (1980).

[27] J. Bartel, P. Q. Brack, C. Guet, and H. B. Hkansson, Nucl. Phys. **A386**, 79 (1982).

[28] S. Bjornholm and J. E. Lynn, Rev. Mod. Phys. **52**, 725 (1980).

[29] J. Friedrich and P.-G. Reinhard, Phys. Rev. C **33**, 335 (1986).

[30] P. G. Reinhard and H. Flocard, Nucl. Phys. **A584**, 467 (1995).

[31] E. Chabanat, P. Bonche, P. Haensel, J. Meyer, and R. Schaeffer, Nucl. Phys. **A627**, 710 (1997).

[32] B. A. Brown, Phy. Rev. C **58**, 220 (1998).

[33] P. G. Reinhard, D. J. Dean, W. Nazarewicz, J. Dobaczewski, J. A. Maruhn, and M. R. Strayer, Phys. Rev. C **60**, 014316 (1999).

[34] J. R. Stone, J. C. Miller, R. Koncewicz, P. D. Stevenson, and M. R. Strayer, Phys. Rev. C **68**, 034324 (2003).

[35] J. Margueron, J. Navarro, and N. V. Giai, Phys. Rev. C **66**, 014303 (2002).

[36] S. Krewald, V. Klemt, J. Speth, and A. Faessler, Nucl. Phys. **A281**, 166 (1977).

[37] N. Metropolis, A. W. Rosenbluth, M. N. Rosenbluth, A. H. Teller, and E. Teller, J. Chem. Phys. **21**, 1087 (1953).

[38] D. H. Youngblood, H. L. Clark, and Y. W. Lui, Phys. Rev. Lett. **82**, 691 (1999).

[39] Z. Ma, N. V. Giai, A. Wandelt, and D.Vretenar, Nucl. Phys. **A686**, 173 (2001).

[40] D. Vretenar, T. Niksic, and P. Ring, Phys. Rev. C **68**, 024310 (2003).

[41] G. Colo, P. F. Bortignon, N. V. Giai, and A. Bracco, Phys. Lett. **B276**, 279 (1992).

[42] I. Hamamoto, H. Sagawa, and H. Z. Zhang, Phys. Rev. C **56**, 3121 (1997).

[43] M. J. Giannoni and P. Quentin, Phys. Rev. C **21**, 2076 (1980).

[44] S. Shlomo, Rep. Prog. Phys. **41**, 957 (1978).

[45] S. Shlomo and W. G. Love, Phys. Scr. **26**, 280 (1982).

[46] J. A. Nolen and J. P. Schiffer, Annu. Rev. Nucl. Sci. **19**, 471 (1969).

[47] B. K. Agrawal, T. Sil, S. K. Samaddar, J. N. De, and S. Shlomo, Phys. Rev. C **64**, 024305 (2001).

[48] B. A. Brown, W. A. Richter, and R. Lindsay, Phys. Lett. **B483**, 49 (2000).

[49] M. Bender, K. Rutz, P. G. Reinhard, and J. A. Maruhn, Eur. Phys. J. A **7**, 467 (2000).

[50] B. K. Agrawal, S. Shlomo, and V. K. Au, Phys. Rev. C **70**, 057302 (2004).

[51] P. Ring, Y. K. Gambhir, and G. A. Lalazissis, Comput. Phys. Commun. **105**, 77 (1997).

[52] W. Bertozzi, J. Friar, J. Heisenberg, and J. W. Negele, Phys. Lett. **B4**, 408 (1972).

[53] I. Sick, Phys. Lett. **B576**, 62 (2003).

[54] A. B. Migdal, *Theory of Finite Fermi Systems, and Application to Atomic Nuclei* (Interscience Pub., New York, 1967).

[55] K. F. Liu, H. Luo, Z. Ma, Q. Shen, and S. A. Mozkowski, Nucl. Phys. **A534**, 25 (1991).

[56] R. J. Furnstahl, Nucl. Phys. **A706**, 85 (2002).

[57] E. Friedman and S. Shlomo, Z. Phys. A **283**, 67 (1977).

[58] K. F. Liu, H. Luo, Z. Ma, and Q. Shen, Nucl. Phys. **A534**, 1 (1991).

[59] J. M. G. Gomez, C. Prieto, and J. Navarro, Nucl. Phys. **A549**, 125 (1992).

[60] M. Bender, J. Dobaczewski, J. Engel, and W. Nazarewicz, Phys. Rev. C **65**, 054322 (2002).

[61] P. G. Reinhard, Phys. Rev. C **60**, 014316 (1999).

[62] F. Tondeur, M. Brack, M. Farine, and J. M. Pearson, Nucl. Phys. **A420**, 297 (1984).

[63] O. Bohigas, A. M. Lane, and J. Martorell, Phys. Rep. **51**, 267 (1979).

[64] G. Colo and N. V. Giai, Nucl. Phys. **A731**, 15c (2004).

[65] B. K. Agrawal and S. Shlomo, Phys. Rev. C **70**, 014308 (2004).

[66] S. Kirkpatrik, J. Stat. Phys. **34**, 975 (1984).

[67] L. Ingber, Math. Comput. Modelling **12**, 967 (1989).

[68] B. Cohen, Master's thesis, Tel-Aviv University, 1994.

[69] T. Burvenich, D. G. Madland, J. A. Maruhn, and P.-G. Reinhard, Phys. Rev. C **65**, 044308 (2002).

[70] T. Burvenich, D. G. Madland, and P.-G. Reinhard, Nucl. Phys. **A744**, 92 (2004).

[71] W. H. Press, S. A. Teukolsky, W. T. Vetterling, and B. P. Flannery, *Numerical Recipes in Fortran* (Cambridge University Press, New York, 1992).

[72] F. L. Blanc, L. Cabaret, E. Cottereau, J. E. Crawford, S. Essabaa, J. Genevey, R. Horn, G. Huber, J. Lassen, J. K. P. Lee, G. L. Scornet, J. Lettry, J. Obert, J. Oms, A. Ouchrif, J. Pinard, H. Ravn, B. Roussire, J. Sauvage, and D. Verney, Phys. Rev. C **72**, 034305 (2005).

[73] A. Bohr and B. R. Mottelson, *Nuclear Structure,* Vol. I (Benjamin, New York, 1969).

[74] A. N. James, P. T. Andrews, P. Kirkby, and B. G. Lowe, Nucl. Phys. **A138**, 145 (1969).

[75] M. Kutschera, Phys. Lett. **B340**, 1 (1994).

[76] M. Kutschera and J. Niemiec, Phys. Rev. C **62**, 025802 (2000).

[77] J. M. Lattimer, C. J. Pethick, M.Prakash, and P. Haensel, Phys. Rev. Lett. **66**, 2701 (1991).

[78] D. J. Rowe, *Nuclear Collective Motion Models and Theory* (Methuen and Co. Ltd., London, 1970).

[79] J. M. Eisenberg and W. Greiner, *Nuclear Theory* (North-Holland, Amsterdam, 1970).

[80] G. E. Brown, *Many Body Problems* (North-Holland, Amsterdam, 1972).

[81] A. deShalit and H. Feshbach, *Theoretical Nuclear Physics,* Vol. I: *Nuclear Physics Structure* (John Wiley & Sons, Inc., New York, 1974).

[82] A. Bohr and B. R. Mottelson, *Nuclear Structure,* Vol. II (Benjamin, New York, 1975).

[83] P. Ring and P. Schuck, *The Nuclear Many Body Problems* (Springer, New York-Heidelberg-Berlin, 1980).

[84] G. F. Bertsch and S. F. Tsai, Phys. Lett. **18**, 125 (1975).

[85] H. Imagawa and Y. Hashimoto, Phys. Rev. C **67**, 037302 (2003).

[86] P. G. Reinhard and Y. K. Gambhir, Ann. Phys. (Leipzig) **1**, 598 (1992).

[87] A. M. Saruis, Phys. Rep. **235**, 57 (1993).

[88] S. Shlomo and G. F. Bertsch, Nucl. Phys. **A243**, 507 (1975).

[89] J. Ryckebusch, M. Waroquier, K. Heyde, J. Moreau, and D. Ryckbosh, Nucl. Phys. **476**, 237 (1988).

[90] B. Buck and A. D. Hill, Nucl. Phys. **A95**, 271 (1967).

[91] T. Udagawa and B. T. Kim, Phys. Rev. C **40**, 2271 (1989).

[92] K. Kawahigashi and M. Ichimura, Prog. Theo. Phys. **85**, 829 (1991).

[93] H. Sagan, *Boundary and Eigenvalue Problems in Mathematical Physics* (Wiley, New York, 1961).

[94] C. Mahaux and H. A. Weidenmuller, *Shell Model Approach to Nuclear Reactions* (North-Holland, Amsterdam, 1969).

[95] S. Shlomo and A. I. Sanzhur, Phys. Rev. C **65**, 044310 (2002).

[96] S. Shlomo, Pramana **57**, 557 (2001).

[97] N. K. Glendenning, Phys. Rev. C **57**, 3020 (1988).

[98] J. M. Pearson, Phys. Lett. **B271**, 12 (1991).

[99] S. Shlomo and D. H. Youngblood, Phys. Rev. C **47**, 529 (1993).

[100] G. C. Baldwin and G. S. Klaiber, Phys. Rev. **71**, 3 (1947).

[101] A. Pitthan and T. Walcher, Phys. Lett. B **36**, 563 (1971).

[102] M. B. Lewis and F. E. Bartrand, Nucl. Phys. **A196**, 337 (1972).

[103] S. Stringari, Phys. Lett. B **108**, 232 (1982).

[104] N. Marty, M. Morlet, A. Willis, V. Comparat, and R. Frascaria, Nucl. Phys. **A238**, 93 (1975).

[105] J. P. Blaizot, J. F. Berger, J. Decharge, and N. Girod, Nucl. Phys. **A591**, 435 (1995).

[106] H. P. Morsch, M. Rogge, P. Turek, and C. Mayer-Broicke, Phys. Rev. Lett. **45**, 337 (1980).

[107] C. Djalali, N. Marty, M. Morlet, and A. Willis, Nucl. Phys. **A380**, 42 (1982).

[108] H. L. Clark, Y.-W. Lui, and D. H. Youngblood, Phys. Rev. C **63**, 03130 (2001).

[109] T. S. Dumitrescu and F. E. Serr, Phys. Rev. C **27**, 811 (1983).

[110] Z. Ma, N. V. Giai, and H. Toki, Phys. Rev. C **55**, 2385 (1997).

[111] N. V. Giai, B. F. Bortignon, G. Colo, Z. Ma, and M. Quaglia, Nucl. Phys. **A687**, 44c (2001).

[112] G. Colo, N. V. Giai, P. F. Bortignon, and M. R. Quaglia, RIKEN Review No. **23**, (1999).

[113] G. Colo, N. V. Giai, P. F. Bortignon, and M. R. Quaglia, Phys. At. Nucl. **64**, 1044 (2001).

[114] T. Niksic, D. Vretenar, and P. Ring, Phys. Rev. C **66**, 064302 (2002).

[115] J. Piekarewicz, Phys. Rev. C **66**, 034305 (2002).

[116] F. E. Serr, in Proceedings of the Nuclear Physics Workshop, Trieste, (Italy), 1981 (North-Holland, Amsterdam, 1982).

[117] Z. Ma, (China Institute of Atomic Energy, Beijing, China, 2003).

[118] H. Esbensen and G. F. Bertsch, Phys. Rev. C **28**, 355 (1983).

[119] S. Shlomo, Phys. Lett. **B209**, 23 (1988).

[120] M. Bender, G. F. Bertsch, and P.-H. Heenen, Phys. Rev. C **69**, 034340 (2004).

[121] H. Sagawa and S. Yoshida, Nucl. Phys. **A688**, 755 (2001).

# APPENDIX A

## THE SKYRME ENERGY DENSITY

In this appendix, we give details of the calculation of the energy density $H(\mathbf{r})$. First we want to derive some useful formulas. We assume that the subspace of the occupied state is invariant under time reversal. This means that if a single-particle state $|i\rangle$ is occupied then the time-reversed state $|\bar{i}\rangle = K|i\rangle$ is also occupied. For our case of spin $\frac{1}{2}$ particles, the time-reversal operator can be written as, $K = -i\sigma_y K_o$, where $K_o$ is the complex-conjugation operator. The single-particle wave function of the time-reversed state is given by

$$\phi_{\bar{i}}(\mathbf{r}, \sigma, q) = -i \sum_{\sigma'} \langle \sigma | \sigma_y | \sigma' \rangle \phi_i^*(\mathbf{r}, \sigma', q) \tag{A.1}$$

Where $\mathbf{r}$ is the spatial coordinate, $\sigma$ is the spin, and $q$ is the isospin of the nucleon. Note that

$$\sigma_y = \begin{pmatrix} 0 & -i \\ i & 0 \end{pmatrix}, \quad \sigma_{+\frac{1}{2}} = \begin{pmatrix} 1 \\ 0 \end{pmatrix}, \quad \sigma_{-\frac{1}{2}} = \begin{pmatrix} 0 \\ 1 \end{pmatrix} \tag{A.2}$$

and also

$$\langle \sigma | \sigma_y | \sigma' \rangle = -2i\sigma\delta_{-\sigma,\sigma'}. \tag{A.3}$$

We get

$$\phi_{\bar{i}}(\mathbf{r}, \sigma, q) = -2\sigma\phi_i^*(\mathbf{r}, -\sigma, q) \tag{A.4}$$

With the assumption that the states are invariant under time reversal, we have

$$\begin{aligned} &\sum_i \phi_i^*(\mathbf{r}, \sigma_1, q)\phi_i(\mathbf{r}, \sigma_2, q) = \qquad (A.5) \\ &\quad = \frac{1}{2} \sum_i \left[ \phi_i^*(\mathbf{r}, \sigma_1, q)\phi_i(\mathbf{r}, \sigma_2, q) + \phi_{\bar{i}}^*(\mathbf{r}, \sigma_1, q)\phi_{\bar{i}}(\mathbf{r}, \sigma_2, q) \right] \\ &\quad = \frac{1}{2} \sum_i \left[ \phi_i^*(\mathbf{r}, \sigma_1, q)\phi_i(\mathbf{r}, \sigma_2, q) + 4\sigma_1\sigma_2\phi_i^*(\mathbf{r}, -\sigma_1, q)\phi_i(\mathbf{r}, -\sigma_2, q) \right]. \end{aligned}$$

From here we can see that, if $\sigma_1 = \sigma_2$, we have

$$\begin{aligned}\sum_i \phi_i^*(\mathbf{r},\sigma_1,q)\phi_i(\mathbf{r},\sigma_1,q) = & \qquad (A.6)\\ = \frac{1}{2}\sum_i [\phi_i^*(\mathbf{r},\sigma_1,q)\phi_i(\mathbf{r},\sigma_1,q) + \phi_i^*(\mathbf{r},-\sigma_1,q)\phi_i(\mathbf{r},-\sigma_1,q)] \\ = \frac{1}{2}\sum_{i\sigma} \phi_i^*(\mathbf{r},\sigma_1,q)\phi_i(\mathbf{r},\sigma_1,q) = \frac{1}{2}\rho_q(\mathbf{r}).\end{aligned}$$

In the case of $\sigma_1 = -\sigma_2$

$$\sum_i \phi_i^*(\mathbf{r},\sigma_1,q)\phi_i(\mathbf{r},-\sigma_1,q) = 0, \qquad (A.7)$$

so we can write

$$\sum_i \phi_i^*(\mathbf{r},\sigma_1,q)\phi_i(\mathbf{r},-\sigma_2,q) = \frac{1}{2}\delta_{\sigma_1\sigma_2}\rho_q(\mathbf{r}). \qquad (A.8)$$

Since the trace of the Pauli spin matrices is zero and the identities below,

$$\langle\sigma|\sigma_x|\sigma'\rangle = \delta_{\sigma,-\sigma'}, \qquad (A.9)$$

$$\langle\sigma|\sigma_y|\sigma'\rangle = -2i\sigma\delta_{\sigma,\sigma'}, \qquad (A.10)$$

$$\langle\sigma|\sigma_z|\sigma'\rangle = 2\sigma\delta_{\sigma,\sigma'}, \qquad (A.11)$$

the equation A.8 implies that

$$\sum_{i\sigma_1\sigma_2} \phi_i^*(\mathbf{r},\sigma_1,q)\langle\sigma_1|\vec{\sigma}|\sigma_2\rangle\phi_i(\mathbf{r},\sigma_2,q) = 0. \qquad (A.12)$$

for the two-body interaction

$$|ij\rangle_{sys} = \frac{1}{\sqrt{2}}\left(|ij\rangle - |ji\rangle\right) = \frac{1}{\sqrt{2}}\left(1-P\right)|ij\rangle \qquad (A.13)$$

where $P$ is the exchange operator, and because $V_{ij}^{NN} = V_{ji}^{NN}$, in other word $\left[P, V_{ij}^{NN}\right] = 0$. We calculate the matrix elements for the Slater determinant wave function $\Phi$, for

the two-body interaction $\frac{1}{2}\sum_{ij} V_{ij}^{NN}$ is

$$\frac{1}{2}\langle\Phi|\sum_{ij} V_{ij}^{NN}|\Phi\rangle = \frac{1}{4}\sum_{ij}\langle ij|V_{12}^{NN}\left(1-P\right)^2|ij\rangle = \frac{1}{2}\sum_{ij}\langle ij|V_{12}^{NN}\left(1-P\right)|ij\rangle, \quad \text{(A.14)}$$

where

$$P = P_{12}^r P_{12}^\sigma P_{12}^\tau, \quad \text{(A.15)}$$

$P_{12}^r$, $P_{12}^\sigma$, and $P_{12}^q$ are the exchange operator for space, spin, and isospin, respectively. For the S-wave $P_{12}^r = 1$, $P_{12}^\sigma = \frac{1}{2}\left(1+\vec{\sigma_1}\vec{\sigma_2}\right)$, and with the assumption that there is no charge mixing in the Hartree-Fock single-particle states, so $P_{12}^q = \delta_{q_1,q_2}$.

Now we calculate the contribution to the energy density from each term of the Skyrme potential. For the $t_0$ term

$$t_0\left(1+x_0P_{ij}^\sigma\right)\delta(\mathbf{r}_i-\mathbf{r}_j), \quad \text{(A.16)}$$

$$\int\mathcal{H}_0(r)d\mathbf{r} = \frac{1}{2}\sum_{ij}\langle ij|t_0\left(1+x_0P_{12}^\sigma\right)\delta(\mathbf{r}_i-\mathbf{r}_j)\left(1-P_{12}^rP_{12}^\sigma P_{12}^q\right)|ij\rangle. \quad \text{(A.17)}$$

We have

$$\begin{aligned}\left(1+x_0P_{12}^\sigma\right)\left(1-P_{12}^rP_{12}^\sigma P_{12}^q\right) &= \left(1+x_0P_{12}^\sigma\right)\left(1-P_{12}^\sigma\delta_{q_1,q_2}\right)\\ &= 1+\frac{1}{2}\left(x_0-\delta_{q_1,q_2}\right)\left(1+\vec{\sigma_1}\vec{\sigma_2}\right)-x_0\delta_{q_1,q_2}, \quad \text{(A.18)}\end{aligned}$$

$$\begin{aligned}&\int\mathcal{H}_0(r)d\mathbf{r} = \quad \text{(A.19)}\\ &\quad=\frac{1}{2}\sum_{ij}\langle ij|t_0\delta(\mathbf{r}_i-\mathbf{r}_j)\left(1+\frac{1}{2}\left(x_0-\delta_{q_1,q_2}\right)\left(1+\vec{\sigma_1}\vec{\sigma_2}\right)-x_0\delta_{q_1,q_2}\right)|ij\rangle.\end{aligned}$$

We also have

$$\begin{aligned}&\sum_{ij}\langle ij|\delta(\mathbf{r}_1-\mathbf{r}_2)|ij\rangle =\\ &\quad=\sum_{ij}\int d\mathbf{r_1}d\mathbf{r_2}\delta(\mathbf{r}_1-\mathbf{r}_2)\phi_i^*\left(\mathbf{r}_1\right)\phi_i\left(\mathbf{r}_1\right)\phi_j^*\left(\mathbf{r}_2\right)\phi_j\left(\mathbf{r}_2\right)\end{aligned}$$

$$= \sum_{ij} \int d\mathbf{r_1} \phi_i^* (\mathbf{r}_1) \phi_i (\mathbf{r}_1) \phi_j^* (\mathbf{r}_1) \phi_j (\mathbf{r}_1) = \int \rho^2 d\mathbf{r}, \tag{A.20}$$

$$\sum_{ij} \langle ij|\delta(\mathbf{r}_1 - \mathbf{r}_2)\delta_{q_1,q_2}|ij\rangle = \int \left(\rho_n^2 + \rho_p^2\right) d\mathbf{r}, \tag{A.21}$$

and

$$\sum_{ij} \langle ij|\delta(\mathbf{r}_1 - \mathbf{r}_2)\vec{\sigma_i}\vec{\sigma_j}|ij\rangle = \sum_{ij} \langle ij|\delta(\mathbf{r}_1 - \mathbf{r}_2)\vec{\sigma_i}\vec{\sigma_j}\delta_{q_i,q_j}|ij\rangle = 0. \tag{A.22}$$

We get

$$\begin{aligned} \int \mathcal{H}_0(r) d\mathbf{r} &= \frac{1}{2} \sum_{ij} \langle ij|t_0 \delta(\mathbf{r}_1 - \mathbf{r}_2)|ij\rangle \\ &\quad -\frac{1}{2} \sum_{ij} \langle ij|x_0 t_0 \delta_{q_1,q_2} \delta(\mathbf{r}_1 - \mathbf{r}_2)|ij\rangle \\ &\quad +\frac{1}{4} \sum_{ij} \langle ij| \left(x_0 - \delta_{q_1,q_2}\right) \left(1 + \vec{\sigma_1}\vec{\sigma_2}\right) t_0 \delta(\mathbf{r}_1 - \mathbf{r}_2)|ij\rangle, \end{aligned} \tag{A.23}$$

$$\begin{aligned} \int \mathcal{H}_0(r) d\mathbf{r} &= \int \left(\frac{1}{2} t_0 \rho^2 - \frac{1}{2} t_0 x_0 \left(\rho_n^2 + \rho_p^2\right) + \frac{1}{4} x_0 t_0 \rho^2 - \frac{1}{4} t_0 \left(\rho_n^2 + \rho_p^2\right)\right) d\mathbf{r} \\ &= \int \frac{1}{4} t_0 \left[\left(2 + x_0\right) \rho^2 - \left(\rho_n^2 + \rho_p^2\right) \left(2x_0 + 1\right)\right] d\mathbf{r}. \end{aligned} \tag{A.24}$$

So

$$\mathcal{H}_0(r) = \frac{1}{4} t_0 \left[\left(2 + x_0\right) \rho^2 - \left(\rho_n^2 + \rho_p^2\right) \left(2x_0 + 1\right)\right] \tag{A.25}$$

Now we calculate the $t_1$ term.

$$\frac{1}{2} t_1 \left(1 + x_1 P_{ij}^{\sigma}\right) \left[\overleftarrow{k}_{ij}^2 + \overrightarrow{k}_{ij}^2\right] \delta(\mathbf{r}_i - \mathbf{r}_j). \tag{A.26}$$

First, we have

$$\overrightarrow{k}_{12}^2 + \overleftarrow{k}_{12}^2 = -\frac{1}{4} \left[\overrightarrow{\nabla}_1^2 + \overrightarrow{\nabla}_2^2 + \overleftarrow{\nabla}_1^2 + \overleftarrow{\nabla}_2^2 - 2\overrightarrow{\nabla}_1 \overrightarrow{\nabla}_2 - 2\overleftarrow{\nabla}_1 \overleftarrow{\nabla}_2\right], \tag{A.27}$$

and

$$\begin{aligned}\overrightarrow{\nabla}^2\rho &= \sum_i \overrightarrow{\nabla}\left[\overrightarrow{\nabla}\phi_i^*(\mathbf{r})\phi_i(\mathbf{r}) + \phi_i^*(\mathbf{r})\overrightarrow{\nabla}\phi_i(\mathbf{r})\right] \\ &= \sum_i \left[\overrightarrow{\nabla}^2\phi_i^*(\mathbf{r})\phi_i(\mathbf{r}) + 2\overrightarrow{\nabla}\phi_i^*(\mathbf{r})\overrightarrow{\nabla}\phi_i(\mathbf{r}) + \phi_i^*(\mathbf{r})\overrightarrow{\nabla}^2\phi_i(\mathbf{r})\right] \\ &= 2\tau + 2\sum_i \overrightarrow{\nabla}^2\phi_i^*(\mathbf{r})\phi_i(\mathbf{r}). \end{aligned} \tag{A.28}$$

Then

$$\sum_i \overrightarrow{\nabla}^2\phi_i^*(\mathbf{r})\phi_i(\mathbf{r}) = \sum_i \phi_i^*(\mathbf{r})\overrightarrow{\nabla}^2\phi_i(\mathbf{r}) = -\tau + \frac{1}{2}\overrightarrow{\nabla}^2\rho, \tag{A.29}$$

hence

$$\begin{aligned}\sum_{ij}\langle ij|\delta\left(\mathbf{r}_1-\mathbf{r}_2\right)\overrightarrow{\nabla}_1^2|ij\rangle &= \sum_{ij}\langle ij|\delta\left(\mathbf{r}_1-\mathbf{r}_2\right)\overrightarrow{\nabla}_2^2|ij\rangle \\ &= \sum_{ij}\langle ij|\delta\left(\mathbf{r}_1-\mathbf{r}_2\right)\overleftarrow{\nabla}_1^2|ij\rangle \\ &= \sum_{ij}\langle ij|\delta\left(\mathbf{r}_1-\mathbf{r}_2\right)\overleftarrow{\nabla}_2^2|ij\rangle \\ &= \int\left(-\tau\rho + \frac{1}{2}\rho\overrightarrow{\nabla}^2\rho\right)d\mathbf{r}. \end{aligned} \tag{A.30}$$

Also

$$\begin{aligned}&\sum_{ij}\langle ij|\delta\left(\mathbf{r}_1-\mathbf{r}_2\right)\overrightarrow{\nabla}_1^2\delta_{q_1,q_2}|ij\rangle = \\ &\quad= \sum_{ij}\langle ij|\delta\left(\mathbf{r}_1-\mathbf{r}_2\right)\overrightarrow{\nabla}_2^2\delta_{q_1,q_2}|ij\rangle \\ &\quad= \sum_{ij}\langle ij|\delta\left(\mathbf{r}_1-\mathbf{r}_2\right)\overleftarrow{\nabla}_1^2\delta_{q_1,q_2}|ij\rangle \\ &\quad= \sum_{ij}\langle ij|\delta\left(\mathbf{r}_1-\mathbf{r}_2\right)\overleftarrow{\nabla}_2^2\delta_{q_1,q_2}|ij\rangle \\ &\quad= \int\left[-\tau_p\rho_p - \tau_n\rho_n + \frac{1}{2}\rho_p\overrightarrow{\nabla}^2\rho_p + \frac{1}{2}\rho_n\overrightarrow{\nabla}^2\rho_n\right]d\mathbf{r}, \end{aligned} \tag{A.31}$$

and

$$\begin{aligned}\sum_{ij}\langle ij|\delta\left(\mathbf{r}_1-\mathbf{r}_2\right)\overrightarrow{\nabla}_1\overrightarrow{\nabla}_2|ij\rangle &= \sum_{ij}\langle ij|\delta\left(\mathbf{r}_1-\mathbf{r}_2\right)\overleftarrow{\nabla}_1\overleftarrow{\nabla}_2|ij\rangle \\ &= \sum_{ij}\int d\mathbf{r}_1 d\mathbf{r}_2\phi_i^*(\mathbf{r}_1)\overrightarrow{\nabla}\phi_i(\mathbf{r}_1)\phi_j^*(\mathbf{r}_2)\overrightarrow{\nabla}\phi_j(\mathbf{r}_2)\delta\left(\mathbf{r}_1-\mathbf{r}_2\right) \\ &= \sum_{ij}\int d\mathbf{r}_1\phi_i^*(\mathbf{r}_1)\overrightarrow{\nabla}\phi_i(\mathbf{r}_1)\int d\mathbf{r}_2\phi_j^*(\mathbf{r}_2)\overrightarrow{\nabla}\phi_j(\mathbf{r}_2)\delta\left(\mathbf{r}_1-\mathbf{r}_2\right) \\ &= \sum_{ij}\Big(-\int d\mathbf{r}_1\overrightarrow{\nabla}\phi_i^*(\mathbf{r}_1)\phi_i(\mathbf{r}_1)\Big)\Big(-\int d\mathbf{r}_1\overrightarrow{\nabla}\phi_j^*(\mathbf{r}_1)\phi_j(\mathbf{r}_1)\Big) \\ &\quad \delta\left(\mathbf{r}_1-\mathbf{r}_2\right) \\ &= \int\frac{1}{4}\big(\overrightarrow{\nabla}\rho\big)^2 d\mathbf{r}, \end{aligned} \tag{A.32}$$

and

$$\begin{aligned}\sum_{ij}\langle ij|\delta\left(\mathbf{r}_1-\mathbf{r}_2\right)\overrightarrow{\nabla}_1\overrightarrow{\nabla}_2\delta_{q_1,q_2}|ij\rangle &= \sum_{ij}\langle ij|\delta\left(\mathbf{r}_1-\mathbf{r}_2\right)\overleftarrow{\nabla}_1\overleftarrow{\nabla}_2\delta_{q_1,q_2}|ij\rangle \\ &= \int\frac{1}{4}\left[\big(\overrightarrow{\nabla}\rho_p\big)^2+\big(\overrightarrow{\nabla}\rho_n\big)^2\right]d^3r. \end{aligned} \tag{A.33}$$

We have the identity

$$\begin{aligned}&\left(\overrightarrow{\nabla}_1\overrightarrow{\nabla}_2\right)\left(\vec{\sigma}_1\vec{\sigma}_2\right)= \\ &\quad\frac{1}{3}\left(\overrightarrow{\nabla}_1\vec{\sigma}_1\right)\left(\overrightarrow{\nabla}_2\vec{\sigma}_2\right)+\frac{1}{2}\left(\overrightarrow{\nabla}_1\times\vec{\sigma}_1\right)\left(\overrightarrow{\nabla}_2\times\vec{\sigma}_2\right)+\left(\overrightarrow{\nabla}_1\times\vec{\sigma}_1\right)^{(2)}\left(\overrightarrow{\nabla}_2\times\vec{\sigma}_2\right)^{(2)}.\end{aligned} \tag{A.34}$$

With assuming axial symmetry in addition to time-reversal invariance, we have

$$\sum_i\phi_i^*(\mathbf{r})\left(\overrightarrow{\nabla}\vec{\sigma}\right)\phi_i(\mathbf{r})=\sum_i\phi_i^*(\mathbf{r})\left(\overrightarrow{\nabla}\times\vec{\sigma}\right)^{(2)}\phi_i(\mathbf{r})=0. \tag{A.35}$$

So

$$\begin{aligned}&\sum_{ij}\langle ij|\delta\left(\mathbf{r}_1-\mathbf{r}_2\right)\left(\overrightarrow{\nabla}_1\overrightarrow{\nabla}_2\right)\left(\vec{\sigma}_1\vec{\sigma}_2\right)|ij\rangle= \\ &\quad=\frac{1}{2}\sum_{ij}\int d\mathbf{r}_1 d\mathbf{r}_2\delta\left(\mathbf{r}_1-\mathbf{r}_2\right)\phi_i^*(\mathbf{r}_1)\left(\overrightarrow{\nabla}_1\times\vec{\sigma}_1\right)\phi_i(\mathbf{r}_1)\phi_j^*(\mathbf{r}_2)\left(\overrightarrow{\nabla}_2\times\vec{\sigma}_2\right)\phi_j(\mathbf{r}_2)\end{aligned} \tag{A.36}$$

$$= \int -\frac{1}{2}\mathbf{J}^2 d\mathbf{r},$$

where

$$\mathbf{J}(\mathbf{r}) = -i \sum_i \phi_i^*(\mathbf{r}) \left( \overrightarrow{\nabla}_i \times \vec{\sigma}_i \right) \phi_i(\mathbf{r}), \tag{A.37}$$

or

$$\sum_{ij} \langle ij | \delta \left( \mathbf{r}_1 - \mathbf{r}_2 \right) \left( \overleftarrow{\nabla}_1 \overleftarrow{\nabla}_2 \right) \left( \vec{\sigma}_1 \vec{\sigma}_2 \right) | ij \rangle = \int -\frac{1}{2}\mathbf{J}^2 d\mathbf{r}, \tag{A.38}$$

and

$$\begin{aligned} \sum_{ij} \langle ij | \delta \left( \mathbf{r}_1 - \mathbf{r}_2 \right) \left( \overrightarrow{\nabla}_1 \overrightarrow{\nabla}_2 \right) \left( \vec{\sigma}_1 \vec{\sigma}_2 \right) \delta_{q_i,q_j} | ij \rangle = & \\ = \sum_{ij} \langle ij | \delta \left( \mathbf{r}_1 - \mathbf{r}_2 \right) \left( \overleftarrow{\nabla}_1 \overleftarrow{\nabla}_2 \right) \left( \vec{\sigma}_1 \vec{\sigma}_2 \right) \delta_{q_i,q_j} | ij \rangle & \\ = \int -\frac{1}{2} \left( \mathbf{J}_p^2 + \mathbf{J}_n^2 \right) d\mathbf{r}. & \end{aligned} \tag{A.39}$$

We have

$$\begin{aligned} \left( 1 + x_1 P_{12}^\sigma \right) \left( 1 - P \right) &= \left( 1 + x_1 P_{12}^\sigma \right) \left( 1 - P_{12}^\sigma \delta_{q_1,q_2} \right) \\ &= 1 + \frac{1}{2} \left( x_1 - \delta_{q_1,q_2} \right) \left( 1 + \vec{\sigma_1} \vec{\sigma_2} \right) - x_1 \delta_{q_1,q_2}. \end{aligned} \tag{A.40}$$

Thus we get

$$\begin{aligned} \int \mathcal{H}_1(r) d\mathbf{r} &= \frac{1}{2} \sum_{ij} \langle ij | \frac{1}{2} t_1 \left( 1 + x_1 P_{12}^\sigma \right) \delta(\mathbf{r}_1 - \mathbf{r}_2) \left( \overrightarrow{k}_{12}^2 + \overleftarrow{k}_{12}^2 \right) \left( 1 - P \right) | ij \rangle \\ &= \sum_{ij} \langle ij | - \frac{1}{16} t_1 \delta(\mathbf{r}_1 - \mathbf{r}_2) \left( \overrightarrow{k}_{12}^2 + \overleftarrow{k}_{12}^2 \right) | ij \rangle \\ &\quad + \sum_{ij} \langle ij | - \frac{1}{32} t_1 \delta(\mathbf{r}_1 - \mathbf{r}_2) \left( x_1 - \delta_{q_1,q_2} \right) \left( \overrightarrow{k}_{12}^2 + \overleftarrow{k}_{12}^2 \right) \left( 1 + \vec{\sigma_1} \vec{\sigma_2} \right) | ij \rangle \\ &\quad + \sum_{ij} \langle ij | \frac{1}{16} t_1 \delta(\mathbf{r}_1 - \mathbf{r}_2) x_1 \delta_{q_1,q_2} \left( \overrightarrow{k}_{12}^2 + \overleftarrow{k}_{12}^2 \right) | ij \rangle. \end{aligned} \tag{A.41}$$

We have

$$\int \mathcal{H}_1(r) d\mathbf{r} = \frac{1}{16} t_1 \int \left( 4\tau\rho - 2\rho \overrightarrow{\nabla}^2 \rho + \left( \overrightarrow{\nabla} \rho \right)^2 \right) d\mathbf{r}$$

$$
\begin{aligned}
& -\frac{1}{16}t_1x_1\int\left(-2\tau\rho+\rho\overrightarrow{\nabla}^2\rho-\frac{1}{2}\left(\overrightarrow{\nabla}\rho\right)^2\right)d\mathbf{r}-\frac{1}{16}t_1x_1\int\mathbf{J}^2d\mathbf{r}\\
& -\frac{1}{16}t_1x_1\int\left(-2\tau_p\rho_p-2\tau_n\rho_n+\rho_p\overrightarrow{\nabla}^2\rho_p+\rho_n\overrightarrow{\nabla}^2\rho_n\right)d\mathbf{r}\\
& -\frac{1}{32}t_1\int\left[\left(\overrightarrow{\nabla}\rho_p\right)^2+\left(\overrightarrow{\nabla}\rho_n\right)^2\right]d\mathbf{r}+\frac{1}{16}t_1\int\left(\mathbf{J}_p^2+\mathbf{J}_n^2\right)d\mathbf{r}\\
& -\frac{1}{16}t_1x_1\int\left(-4\tau_p\rho_p-4\tau_n\rho_n+2\rho_p\overrightarrow{\nabla}^2\rho_p+2\rho_n\overrightarrow{\nabla}^2\rho_n\right)d\mathbf{r}\\
& -\frac{1}{16}t_1x_1\int\left[\left(\overrightarrow{\nabla}\rho_p\right)^2+\left(\overrightarrow{\nabla}\rho_n\right)^2\right]d\mathbf{r}\\
= \;& \frac{1}{16}t_1\left(1+\frac{1}{2}x_1\right)\left[4\tau\rho-2\rho\overrightarrow{\nabla}^2\rho+\left(\overrightarrow{\nabla}\rho\right)^2\right]\\
& -\frac{1}{16}t_1\left(\frac{1}{2}+x_1\right)\left[4\tau_p\rho_p+4\tau_n\rho_n-2\rho_p\overrightarrow{\nabla}^2\rho_p-2\rho_n\overrightarrow{\nabla}^2\rho_n+\left(\overrightarrow{\nabla}\rho_p\right)^2+\left(\overrightarrow{\nabla}\rho_n\right)^2\right]\\
& +\frac{1}{16}t_1\left(-x_1\mathbf{J}^2+\mathbf{J}_p^2+\mathbf{J}_n^2\right), \qquad \text{(A.42)}
\end{aligned}
$$

$$
\begin{aligned}
\mathcal{H}_1(r) \;=\; & \frac{1}{16}t_1\left(1+\frac{1}{2}x_1\right)\left[4\tau\rho-3\rho\overrightarrow{\nabla}^2\rho\right]\\
& -\frac{1}{16}t_1\left(\frac{1}{2}+x_1\right)\left[4\tau_p\rho_p+4\tau_n\rho_n-3\rho_p\overrightarrow{\nabla}^2\rho_p-3\rho_n\overrightarrow{\nabla}^2\rho_n\right]\\
& +\frac{1}{16}t_1\left(-x_1\mathbf{J}^2+\mathbf{J}_p^2+\mathbf{J}_n^2\right). \qquad \text{(A.43)}
\end{aligned}
$$

For the $t_2$ term

$$
t_2\left(1+x_2P_{ij}^{\sigma}\right)\overleftarrow{k}_{ij}\delta(\mathbf{r}_i-\mathbf{r}_j)\overrightarrow{k}_{ij}, \qquad \text{(A.44)}
$$

we have to calculate

$$
\int\mathcal{H}_2(r)d\mathbf{r}=\frac{1}{2}\sum_{ij}\langle ij|t_2\left(1+x_2P_{12}^{\sigma}\right)\overleftarrow{k}_{ij}\delta(\mathbf{r}_i-\mathbf{r}_j)\overrightarrow{k}_{ij}\left(1-P\right)|ij\rangle. \qquad \text{(A.45)}
$$

In this case the exchange operator $P$ is given by

$$
P=P_{12}^rP_{12}^{\sigma}P_{12}^q=-\frac{1}{2}\left(1+\vec{\sigma_1}\vec{\sigma_2}\right)\delta_{q_1,q_2}, \qquad \text{(A.46)}
$$

and

$$
\left(1+x_2P_{12}^{\sigma}\right)\left(1-P\right)=1+\frac{1}{2}x_2+\frac{1}{2}\left(x_2+\delta_{q_1,q_2}\right)\vec{\sigma_1}\vec{\sigma_2}+\left(\frac{1}{2}+x_2\right)\delta_{q_1,q_2}. \qquad \text{(A.47)}
$$

We have

$$\overleftarrow{k}_{ij}\overrightarrow{k}_{ij} = \frac{1}{4}\left[\overleftarrow{\nabla}_i\overrightarrow{\nabla}_i + \overleftarrow{\nabla}_j\overrightarrow{\nabla}_j - \overleftarrow{\nabla}_j\overrightarrow{\nabla}_i - \overleftarrow{\nabla}_i\overrightarrow{\nabla}_j\right]. \tag{A.48}$$

We use the following equations

$$\begin{aligned}\sum_{ij}\langle ij|\delta(\mathbf{r}_1-\mathbf{r}_2)\overleftarrow{\nabla}_1\overrightarrow{\nabla}_1|ij\rangle &= \sum_{ij}\int d\mathbf{r}_1 d\mathbf{r}_2\delta(\mathbf{r}_1-\mathbf{r}_2)\phi_i^*(\mathbf{r}_1)\phi_j^*(\mathbf{r}_2)\overleftarrow{\nabla}_1\overrightarrow{\nabla}_1\phi_i(\mathbf{r}_1)\phi_j(\mathbf{r}_2)\\ &= \sum_{ij}\int d\mathbf{r}_1 d\mathbf{r}_2|\overrightarrow{\nabla}\phi_i(\mathbf{r}_1)|^2|\phi_j(\mathbf{r}_2)|^2\delta(\mathbf{r}_1-\mathbf{r}_2)\\ &= \int \tau\rho d\mathbf{r}, \end{aligned}\tag{A.49}$$

$$\sum_{ij}\langle ij|\delta(\mathbf{r}_1-\mathbf{r}_2)\overleftarrow{\nabla}_1\overrightarrow{\nabla}_1\delta_{q_1,q_2}|ij\rangle = \int\left(\tau_p\rho_p+\tau_n\rho_n\right)d\mathbf{r}, \tag{A.50}$$

$$\sum_{ij}\langle ij|\delta(\mathbf{r}_1-\mathbf{r}_2)\overleftarrow{\nabla}_1\overrightarrow{\nabla}_2\vec{\sigma_1}\vec{\sigma_2}|ij\rangle = \int -\frac{1}{2}\mathbf{J}^2 d\mathbf{r}, \tag{A.51}$$

$$\sum_{ij}\langle ij|\delta(\mathbf{r}_1-\mathbf{r}_2)\overleftarrow{\nabla}_1\overrightarrow{\nabla}_2\vec{\sigma_1}\vec{\sigma_2}\delta_{q_1,q_2}|ij\rangle = \int -\frac{1}{2}\left(\mathbf{J}_p^2+\mathbf{J}_n^2\right)d\mathbf{r}, \tag{A.52}$$

$$\sum_{ij}\langle ij|\delta(\mathbf{r}_1-\mathbf{r}_2)\overleftarrow{\nabla}_1\overrightarrow{\nabla}_1\vec{\sigma_1}\vec{\sigma_2}|ij\rangle = \sum_{ij}\langle ij|\delta(\mathbf{r}_1-\mathbf{r}_2)\overleftarrow{\nabla}_1\overrightarrow{\nabla}_1\vec{\sigma_1}\vec{\sigma_2}\delta_{q_1,q_2}|ij\rangle = 0, \tag{A.53}$$

$$\begin{aligned}\sum_{ij}\langle ij|\delta(\mathbf{r}_1-\mathbf{r}_2)\overleftarrow{\nabla}_1\overrightarrow{\nabla}_2|ij\rangle &= \sum_{ij}\int d\mathbf{r}_1 d\mathbf{r}_2\delta(\mathbf{r}_1-\mathbf{r}_2)\phi_i^*(\mathbf{r}_1)\phi_j^*(\mathbf{r}_2)\overleftarrow{\nabla}_1\overrightarrow{\nabla}_2\phi_i(\mathbf{r}_1)\phi_j(\mathbf{r}_2)\\ &= \sum_{ij}\int d\mathbf{r}_1 d\mathbf{r}_2\delta(\mathbf{r}_1-\mathbf{r}_2)\overrightarrow{\nabla}_1\phi_i^*(\mathbf{r}_1)\phi_i(\mathbf{r}_1)\phi_j^*(\mathbf{r}_2)\overrightarrow{\nabla}_2\phi_j(\mathbf{r}_2)\\ &= \sum_{ij}\int d\mathbf{r}\overrightarrow{\nabla}\phi_i^*(\mathbf{r})\phi_i(\mathbf{r})\left(\overrightarrow{\nabla}\phi_j^*(\mathbf{r})\phi_j(\mathbf{r})\right)^*\\ &= \frac{1}{4}\int\left(\overrightarrow{\nabla}\rho\right)^2 d\mathbf{r}, \end{aligned}\tag{A.54}$$

$$\sum_{ij}\langle ij|\delta(\mathbf{r}_1-\mathbf{r}_2)\overleftarrow{\nabla}_1\overrightarrow{\nabla}_2\delta_{q_1,q_2}|ij\rangle = \frac{1}{4}\int\left[\left(\overrightarrow{\nabla}\rho_p+\right)^2+\left(\overrightarrow{\nabla}\rho_n\right)^2\right]d\mathbf{r}. \tag{A.55}$$

Hence

$$\begin{aligned}\int\mathcal{H}_2(r)d\mathbf{r} &= \frac{1}{2}t_2\sum_{ij}\langle ij|t_2\left(1+x_2P_{12}^\sigma\right)\overleftarrow{k}_{ij}\delta(\mathbf{r}_i-\mathbf{r}_j)\overrightarrow{k}_{ij}\left(1-P\right)|ij\rangle\\ &= \frac{1}{2}t_2\left(1+\frac{1}{2}x_2\right)\sum_{ij}\langle ij|\left(\overleftarrow{k}_{ij}\overrightarrow{k}_{ij}\right)\delta(\mathbf{r}_i-\mathbf{r}_j)|ij\rangle\end{aligned}$$

$$
\begin{aligned}
&+\frac{1}{2}t_2\left(\frac{1}{2}+x_2\right)\sum_{ij}\langle ij|\left(\overleftarrow{k}_{ij}\overrightarrow{k}_{ij}\right)\delta(\mathbf{r}_i-\mathbf{r}_j)\delta_{q_1,q_2}|ij\rangle\\
&+\frac{1}{4}t_2x_2\sum_{ij}\langle ij|\left(\overleftarrow{k}_{ij}\overrightarrow{k}_{ij}\right)\delta(\mathbf{r}_i-\mathbf{r}_j)\vec{\sigma_1}\vec{\sigma_2}|ij\rangle\\
&+\frac{1}{4}t_2\sum_{ij}\langle ij|\left(\overleftarrow{k}_{ij}\overrightarrow{k}_{ij}\right)\delta(\mathbf{r}_i-\mathbf{r}_j)\vec{\sigma_1}\vec{\sigma_2}\delta_{q_1,q_2}|ij\rangle\\
=\;&\frac{1}{8}t_2\left(1+\frac{1}{2}x_2\right)\int\left(2\tau\rho-\frac{1}{2}\left(\overrightarrow{\nabla}\rho\right)^2\right)d\mathbf{r}\\
&+\frac{1}{8}t_2\left(\frac{1}{2}+x_2\right)\int\left(2\tau_p\rho_p+2\tau_n\rho_n-\frac{1}{2}\left(\overrightarrow{\nabla}\rho_p\right)^2-\frac{1}{2}\left(\overrightarrow{\nabla}\rho_n\right)^2\right)d\mathbf{r}\\
&-\frac{1}{16}t_2\int\left(x_2\mathbf{J}^2+\mathbf{J}_p^2+\mathbf{J}_n^2\right)d\mathbf{r}. \qquad \text{(A.56)}
\end{aligned}
$$

With

$$
\begin{aligned}
\mathcal{H}_2(r)\;=\;&\frac{1}{16}t_2\left(2+x_2\right)\left(2\tau\rho+\frac{1}{2}\rho\overrightarrow{\nabla}^2\rho\right)\\
&+\frac{1}{16}t_2\left(1+2x_2\right)\left(2\tau_p\rho_p+2\tau_n\rho_n+\frac{1}{2}\rho_p\overrightarrow{\nabla}^2\rho_p+\frac{1}{2}\rho_n\overrightarrow{\nabla}^2\rho_n\right)\\
&-\frac{1}{16}t_2\left(x_2\mathbf{J}^2+\mathbf{J}_p^2+\mathbf{J}_n^2\right). \qquad \text{(A.57)}
\end{aligned}
$$

For the $t_3$ term

$$
\frac{1}{6}t_3\left(1+x_3P_{ij}^{\sigma}\right)\rho^{\alpha}\left(\frac{\mathbf{r}_i-\mathbf{r}_j}{2}\right)\delta(\mathbf{r}_i-\mathbf{r}_j). \qquad \text{(A.58)}
$$

Again we have

$$
\left(1+x_3P_{12}^{\sigma}\right)\left(1-P\right)=1+\frac{1}{2}x_3-\frac{1}{2}\delta_{q_1,q_2}+\frac{1}{2}x_3\vec{\sigma_1}\vec{\sigma_2}-\frac{1}{2}\delta_{q_1,q_2}\vec{\sigma_1}\vec{\sigma_2}-x_3\delta_{q_1,q_2}. \qquad \text{(A.59)}
$$

We obtain

$$
\begin{aligned}
\int\mathcal{H}_3(r)d\mathbf{r}\;=\;&\frac{1}{2}\sum_{ij}\langle ij|\frac{1}{6}t_3\left(1+x_3P_{ij}^{\sigma}\right)\rho^{\alpha}\left(\frac{\mathbf{r}_i-\mathbf{r}_j}{2}\right)\delta(\mathbf{r}_i-\mathbf{r}_j)\left(1-P\right)|ij\rangle\\
=\;&\frac{1}{12}t_3\left(1+\frac{1}{2}x_3\right)\sum_{ij}\langle ij|\rho^{\alpha}\left(\frac{\mathbf{r}_i-\mathbf{r}_j}{2}\right)\delta(\mathbf{r}_i-\mathbf{r}_j)|ij\rangle\\
&-\frac{1}{24}t_3\sum_{ij}\langle ij|\rho^{\alpha}\left(\frac{\mathbf{r}_i-\mathbf{r}_j}{2}\right)\delta(\mathbf{r}_i-\mathbf{r}_j)\delta_{q_1,q_2}|ij\rangle
\end{aligned}
$$

$$
\begin{aligned}
&+\frac{1}{24}t_3x_3\sum_{ij}\langle ij|\rho^\alpha\left(\frac{\mathbf{r}_i-\mathbf{r}_j}{2}\right)\delta(\mathbf{r}_i-\mathbf{r}_j)\vec{\sigma_1}\vec{\sigma_2}|ij\rangle\\
&-\frac{1}{24}t_3\sum_{ij}\langle ij|\rho^\alpha\left(\frac{\mathbf{r}_i-\mathbf{r}_j}{2}\right)\delta(\mathbf{r}_i-\mathbf{r}_j)\vec{\sigma_1}\vec{\sigma_2}\delta_{q_1,q_2}|ij\rangle\\
&-\frac{1}{12}t_3x_3\sum_{ij}\langle ij|\rho^\alpha\left(\frac{\mathbf{r}_i-\mathbf{r}_j}{2}\right)\delta(\mathbf{r}_i-\mathbf{r}_j)\delta_{q_1,q_2}|ij\rangle\\
=\;&\frac{1}{12}t_3\left(1+\frac{1}{2}x_3\right)\int\rho^{\alpha+2}d\mathbf{r}-\frac{1}{24}t_3\int\rho^\alpha\left(\rho_p^2+\rho_n^2\right)d\mathbf{r}\\
&-\frac{1}{12}t_3x_3\int\rho^\alpha\left(\rho_p^2+\rho_n^2\right)d\mathbf{r},
\end{aligned}
\tag{A.60}
$$

or

$$
\mathcal{H}_3(r)=\frac{1}{12}t_3\rho^\alpha\left[\left(1+\frac{1}{2}x_3\right)\rho^2-\left(\frac{1}{2}+x_3\right)\left(\rho_p^2+\rho_n^2\right)\right]. \tag{A.61}
$$

For the spin-orbit term

$$
iW_o\overleftarrow{k}_{ij}\delta(\mathbf{r}_i-\mathbf{r}_j)\left(\vec{\sigma_i}+\vec{\sigma_j}\right)\times\overrightarrow{k}_{ij}. \tag{A.62}
$$

This term contributes only in triplet $P$ states therefore $P_{12}^r=-1$, $P_{12}^\sigma=1$. We calculate

$$
\int\mathcal{H}_{sp}(r)d\mathbf{r}=\frac{1}{2}\sum_{ij}\langle ij|iW_o\overleftarrow{k}_{ij}\delta(\mathbf{r}_i-\mathbf{r}_j)\left(\vec{\sigma_i}+\vec{\sigma_j}\right)\times\overrightarrow{k}_{ij}\left(1-P\right)|ij\rangle. \tag{A.63}
$$

Note that

$$
\overleftarrow{k}_{ij}\times\overrightarrow{k}_{ij}=\frac{1}{4}\left(\overleftarrow{\nabla}_i\times\overrightarrow{\nabla}_i+\overleftarrow{\nabla}_j\times\overrightarrow{\nabla}_j-\overleftarrow{\nabla}_j\times\overrightarrow{\nabla}_i-\overleftarrow{\nabla}_i\times\overrightarrow{\nabla}_j\right), \tag{A.64}
$$

$$
\begin{aligned}
4\left(\vec{\sigma_i}+\vec{\sigma_j}\right)\overleftarrow{k}_{ij}\times\overrightarrow{k}_{ij}\;=\;&\vec{\sigma_i}\left(\overleftarrow{\nabla}_i\times\overrightarrow{\nabla}_i\right)+\vec{\sigma_i}\left(\overleftarrow{\nabla}_j\times\overrightarrow{\nabla}_j\right)-\vec{\sigma_i}\left(\overleftarrow{\nabla}_j\times\overrightarrow{\nabla}_i\right)\\
&-\vec{\sigma_i}\left(\overleftarrow{\nabla}_i\times\overrightarrow{\nabla}_j\right)+\vec{\sigma_j}\left(\overleftarrow{\nabla}_i\times\overrightarrow{\nabla}_i\right)+\vec{\sigma_j}\left(\overleftarrow{\nabla}_j\times\overrightarrow{\nabla}_j\right)\\
&-\vec{\sigma_j}\left(\overleftarrow{\nabla}_j\times\overrightarrow{\nabla}_i\right)-\vec{\sigma_j}\left(\overleftarrow{\nabla}_i\times\overrightarrow{\nabla}_j\right)\\
=\;&2\vec{\sigma_i}\left(\overleftarrow{\nabla}_i\times\overrightarrow{\nabla}_i\right)+2\vec{\sigma_i}\left(\overleftarrow{\nabla}_j\times\overrightarrow{\nabla}_j\right)\\
&-2\vec{\sigma_i}\left(\overleftarrow{\nabla}_j\times\overrightarrow{\nabla}_i+\overleftarrow{\nabla}_i\times\overrightarrow{\nabla}_j\right).
\end{aligned}
\tag{A.65}
$$

Therefore,

$$\begin{aligned}\int \mathcal{H}_{sp}(r)d\mathbf{r} &= \frac{iW_o}{4}\sum_{ij}\langle ij|\delta(\mathbf{r}_i-\mathbf{r}_j)\vec{\sigma_i}\left(\overleftarrow{\nabla}_i\times\overrightarrow{\nabla}_i\right)\left(1+\delta_{q_i,q_j}\right)|ij\rangle \\ &+ \frac{iW_o}{4}\sum_{ij}\langle ij|\delta(\mathbf{r}_i-\mathbf{r}_j)\vec{\sigma_i}\left(\overleftarrow{\nabla}_j\times\overrightarrow{\nabla}_j\right)\left(1+\delta_{q_i,q_j}\right)|ij\rangle \\ &- \frac{iW_o}{4}\sum_{ij}\langle ij|\delta(\mathbf{r}_i-\mathbf{r}_j)\vec{\sigma_i}\left(\overleftarrow{\nabla}_i\times\overrightarrow{\nabla}_j\right)\left(1+\delta_{q_i,q_j}\right)|ij\rangle \\ &- \frac{iW_o}{4}\sum_{ij}\langle ij|\delta(\mathbf{r}_i-\mathbf{r}_j)\vec{\sigma_i}\left(\overleftarrow{\nabla}_j\times\overrightarrow{\nabla}_i\right)\left(1+\delta_{q_i,q_j}\right)|ij\rangle. \quad \text{(A.66)}\end{aligned}$$

The second term will not contribute to the energy density. The integration by parts of the third term is given by

$$\begin{aligned}-\vec{\sigma_i}\left(\overleftarrow{\nabla}_i\times\overrightarrow{\nabla}_j\right) &= \vec{\sigma_i}\left(\overleftarrow{\nabla}_j\times\overrightarrow{\nabla}_j\right)+\vec{\sigma_i}\left(\overrightarrow{\nabla}_i\times\overrightarrow{\nabla}_j\right)+\vec{\sigma_i}\left(\overrightarrow{\nabla}_j\times\overrightarrow{\nabla}_j\right) \\ &= \vec{\sigma_i}\left(\overrightarrow{\nabla}_i\times\overrightarrow{\nabla}_j\right) \\ &= -\overrightarrow{\nabla}_j\left(\overrightarrow{\nabla}_i\times\vec{\sigma_i}\right), \quad \text{(A.67)}\end{aligned}$$

and because of time-reversal, the fourth term reduces to

$$\vec{\sigma_i}\left(\overleftarrow{\nabla}_j\times\overrightarrow{\nabla}_i\right)=\overleftarrow{\nabla}_j\left(\overrightarrow{\nabla}_i\times\vec{\sigma_i}\right)=\overrightarrow{\nabla}_j\left(\overrightarrow{\nabla}_i\times\vec{\sigma_i}\right). \quad \text{(A.68)}$$

The first term is calculated below

$$\begin{aligned}\vec{\sigma_i}\left(\overleftarrow{\nabla}_i\times\overrightarrow{\nabla}_i\right) &= -\vec{\sigma_i}\left(\overleftarrow{\nabla}_j\times\overrightarrow{\nabla}_i\right)-\vec{\sigma_i}\left(\overrightarrow{\nabla}_i\times\overrightarrow{\nabla}_i\right)-\vec{\sigma_i}\left(\overrightarrow{\nabla}_j\times\overrightarrow{\nabla}_i\right) \\ &= -\overleftarrow{\nabla}_j\left(\overrightarrow{\nabla}_i\times\vec{\sigma_i}\right)-\overrightarrow{\nabla}_j\left(\overrightarrow{\nabla}_i\times\vec{\sigma_i}\right) \\ &= -2\overleftarrow{\nabla}_j\left(\overrightarrow{\nabla}_i\times\vec{\sigma_i}\right)=-2\overrightarrow{\nabla}_j\left(\overrightarrow{\nabla}_i\times\vec{\sigma_i}\right). \quad \text{(A.69)}\end{aligned}$$

So

$$\begin{aligned}\int \mathcal{H}_{sp}(r)d\mathbf{r} &= -iW_o\sum_{ij}\langle ij|\delta(\mathbf{r}_i-\mathbf{r}_j)\left(1+\delta_{q_i,q_j}\right)\overrightarrow{\nabla}_j\left(\overrightarrow{\nabla}_i\times\vec{\sigma_i}\right)|ij\rangle \\ &= -iW_o\sum_{ij}\int\delta(\mathbf{r}_i-\mathbf{r}_j)\left(1+\delta_{q_i,q_j}\right)\phi_j^*\overrightarrow{\nabla}\phi_j\phi_i^*\left(\overrightarrow{\nabla}_i\times\vec{\sigma_i}\right)\phi_i d\mathbf{r}_i d\mathbf{r}_j\end{aligned}$$

$$
\begin{aligned}
&= \frac{W_o}{2}\int \left(\overrightarrow{\nabla}\rho\mathbf{J} + \overrightarrow{\nabla}\rho_p\mathbf{J}_p + \overrightarrow{\nabla}\rho_n\mathbf{J}_n\right) d\mathbf{r} \\
&= -\frac{W_o}{2}\int \left(\rho\overrightarrow{\nabla}\mathbf{J} + \rho_p\overrightarrow{\nabla}\mathbf{J}_p + \rho_n\overrightarrow{\nabla}\mathbf{J}_n\right) d\mathbf{r}. \qquad \text{(A.70)}
\end{aligned}
$$

Or

$$
\mathcal{H}_{sp} = -\frac{W_o}{2}\left(\rho\overrightarrow{\nabla}\mathbf{J} + \rho_p\overrightarrow{\nabla}\mathbf{J}_p + \rho_n\overrightarrow{\nabla}\mathbf{J}_n\right). \qquad \text{(A.71)}
$$

In summary, the Skyrme energy density is given by:

$$
\begin{aligned}
\mathcal{H}_{\text{Skyrme}}(r) &= \frac{1}{4}t_0\left[\left(2+x_0\right)\rho^2 - \left(\rho_n^2+\rho_p^2\right)\left(2x_0+1\right)\right] \\
&\quad + \frac{1}{16}t_1\left(1+\frac{1}{2}x_1\right)\left[4\tau\rho - 3\rho\overrightarrow{\nabla}^2\rho\right] \\
&\quad - \frac{1}{16}t_1\left(\frac{1}{2}+x_1\right)\left[4\tau_p\rho_p + 4\tau_n\rho_n - 3\rho_p\overrightarrow{\nabla}^2\rho_p - 3\rho_n\overrightarrow{\nabla}^2\rho_n\right] \\
&\quad + \frac{1}{16}t_1\left(-x_1\mathbf{J}^2 + \mathbf{J}_p^2 + \mathbf{J}_n^2\right) \\
&\quad + \frac{1}{16}t_2\left(2+x_2\right)\left(2\tau\rho + \frac{1}{2}\rho\overrightarrow{\nabla}^2\rho\right) \\
&\quad + \frac{1}{16}t_2\left(1+2x_2\right)\left(2\tau_p\rho_p + 2\tau_n\rho_n + \frac{1}{2}\rho_p\overrightarrow{\nabla}^2\rho_p + \frac{1}{2}\rho_n\overrightarrow{\nabla}^2\rho_n\right) \\
&\quad - \frac{1}{16}t_2\left(x_2\mathbf{J}^2 + \mathbf{J}_p^2 + \mathbf{J}_n^2\right) \\
&\quad + \frac{1}{2}t_3\left[\left(1+\frac{1}{2}x_3\right)\rho^{\alpha+2} - \left(\frac{1}{2}+x_3\right)\rho^{\alpha}\left(\rho_p^2+\rho_n^2\right)\right] \\
&\quad - \frac{W_o}{2}\left(\rho\overrightarrow{\nabla}\mathbf{J} + \rho_p\overrightarrow{\nabla}\mathbf{J}_p + \rho_n\overrightarrow{\nabla}\mathbf{J}_n\right) \\
&= \frac{1}{4}t_0\left[\left(2+x_0\right)\rho^2 - \left(\rho_n^2+\rho_p^2\right)\left(2x_0+1\right)\right] + \frac{1}{16}t_1\left(1+\frac{1}{2}x_1\right)\left[4\tau\rho - 3\rho\overrightarrow{\nabla}^2\rho\right] \\
&\quad - \frac{1}{16}t_1\left(\frac{1}{2}+x_1\right)\left[4\tau_p\rho_p + 4\tau_n\rho_n - 3\rho_p\overrightarrow{\nabla}^2\rho_p - 3\rho_n\overrightarrow{\nabla}^2\rho_n\right] \\
&\quad + \frac{1}{16}t_1\left(-x_1\mathbf{J}^2 + \mathbf{J}_p^2 + \mathbf{J}_n^2\right) + \frac{1}{16}t_2\left(2+x_2\right)\left(2\tau\rho + \frac{1}{2}\rho\overrightarrow{\nabla}^2\rho\right) \\
&\quad + \frac{1}{16}t_2\left(1+2x_2\right)\left(2\tau_p\rho_p + 2\tau_n\rho_n + \frac{1}{2}\rho_p\overrightarrow{\nabla}^2\rho_p + \frac{1}{2}\rho_n\overrightarrow{\nabla}^2\rho_n\right) \\
&\quad - \frac{1}{16}t_2\left(x_2\mathbf{J}^2 + \mathbf{J}_p^2 + \mathbf{J}_n^2\right) + \frac{1}{12}t_3\rho^{\alpha}\left[\left(1+\frac{1}{2}x_3\right)\rho^2 - \left(\frac{1}{2}+x_3\right)\left(\rho_p^2+\rho_n^2\right)\right] \\
&\quad - \frac{W_o}{2}\left(\rho\overrightarrow{\nabla}\mathbf{J} + \rho_p\overrightarrow{\nabla}\mathbf{J}_p + \rho_n\overrightarrow{\nabla}\mathbf{J}_n\right), \qquad \text{(A.72)}
\end{aligned}
$$

or we can wite

$$\begin{aligned}
\mathcal{H}_{\text{Skyrme}}(r) &= \frac{1}{4}t_0\left[(2+x_0)\,\rho^2-\left(\rho_n^2+\rho_p^2\right)(2x_0+1)\right] \\
&+\frac{1}{16}t_1\left(1+\frac{1}{2}x_1\right)\left[4\tau\rho-3\rho\overrightarrow{\nabla}^2\rho\right] \\
&-\frac{1}{16}t_1\left(\frac{1}{2}+x_1\right)\left[4\tau_p\rho_p+4\tau_n\rho_n-3\rho_p\overrightarrow{\nabla}^2\rho_p-3\rho_n\overrightarrow{\nabla}^2\rho_n\right] \\
&+\frac{1}{16}t_1\left(-x_1\mathbf{J}^2+\mathbf{J}_p^2+\mathbf{J}_n^2\right)+\frac{1}{16}t_2\,(2+x_2)\left(2\tau\rho+\frac{1}{2}\rho\overrightarrow{\nabla}^2\rho\right) \\
&+\frac{1}{16}t_2\,(1+2x_2)\left(2\tau_p\rho_p+2\tau_n\rho_n+\frac{1}{2}\rho_p\overrightarrow{\nabla}^2\rho_p+\frac{1}{2}\rho_n\overrightarrow{\nabla}^2\rho_n\right) \\
&-\frac{1}{16}t_2\left(x_2\mathbf{J}^2+\mathbf{J}_p^2+\mathbf{J}_n^2\right)+\frac{1}{12}t_3\rho^\alpha\left[\left(1+\frac{1}{2}x_3\right)\rho^2-\left(\frac{1}{2}+x_3\right)\left(\rho_p^2+\rho_n^2\right)\right] \\
&-\frac{W_o}{2}\left(\rho\overrightarrow{\nabla}\mathbf{J}+\rho_p\overrightarrow{\nabla}\mathbf{J}_p+\rho_n\overrightarrow{\nabla}\mathbf{J}_n\right). \qquad \text{(A.73)}
\end{aligned}$$

# VITA

Au Kim Vuong was born in Da Nang, Viet Nam in 1975. He got a B.S. in physics from Hue University, Viet Nam in 1998. He moved to the Institute of Chemical and Physical Research (RIKEN), Japan in 1999 to work as a research assistant. Later, he came to Texas A&M University in 2001 to pursue his Ph.D. in physics. He received his Ph.D. in May 2007. He can be reached at RIKEN, Hirosawa, Wako, Saitama, Japan.

The typist for this dissertation was Au Kim Vuong.